Dispersion Controlled Natural Attenuation

The role of conservative plume characteristics in modelling reactive mixing processes

Dispersion Controlled Natural Attenuation

The role of conservative plume characteristics in modelling reactive mixing processes

Dispersie Gecontroleerde Natuurlijke Afbraak

De rol van conservatieve pluimkarakteristieken in het modelleren van reactieve mengprocessen
(met een samenvatting in het Nederlands)

PROEFSCHRIFT

ter verkrijging van de graad van doctor aan de Universiteit Utrecht op gezag van de rector magnificus, prof. dr. W.H. Gispen, ingevolge het besluit van het college voor promoties in het openbaar te verdedigen op maandag 1 mei 2006 des middags te 4.15 uur door

Philip Andrew Sison Ham

geboren op 27 oktober 1978 te Rochdale, Verenigde Koninkrijk.

Promotor: Prof. dr. ir. S.M. Hassanizadeh

Co-promotor: Dr. R.J. Schotting

Dit proefschrift werd (mede) mogelijk gemaakt met financiële steun van NWO.

Samenstelling promotiecommissie:

Rector Magnificus	voorzitter
Prof. dr. ir. S.M. Hassanizadeh,	Universiteit Utrecht, promotor
Dr. R.J. Schotting,	Universiteit Utrecht, toegevoegd promotor
Prof. dr. D.N. Lerner,	University of Sheffield
Prof. dr. P. Grathwohl,	University of Tuebingen
Prof. dr. ir. S.E.A.T.M. van der Zee,	Wageningen Universiteit
Dr. ir. H. Prommer,	CSIRO
Dr. ir. T. Heimovaara,	Groundwater Technology BV

Author email: ham@geo.uu.nl

"I may be drunk, Miss, but in the morning I will be sober and you will still be ugly."

Sir Winston Churchill

Contents

Chapter 1

Introduction

Foreword. This thesis is a hydrogeological study of dispersion controlled reactive solute transport in porous media. In this Introduction, the background topic within the context of the thesis is briefly discussed, along with this subject's relevance to society. It concludes with the research questions addressed by this thesis and an outline of the chapters which follow.

1.1 Background

Groundwater saturates permeable geological formations, called aquifers, and supplies wells and springs where it can be extracted and purified for consumption or used in industrial processes. Groundwater can easily become contaminated through an inexhaustible list of sources; most commonly through waste disposal, discharge of effluents, agricultural and industrial practices, etc. For example, a drinking water supply might become contaminated by a 'plume' of petroleum hydrocarbons, which have leaked into the subsurface from underground storage tanks at a nearby petrol station (see Figure 1.1).

Since, globally, environmental issues are of increasing importance it is not surprising that groundwater pollution is a focus of concern. Unfortunately the term 'contamination' is ambiguous at best, since environmental regulations differ from country to country. In this way, it is the role of independent environmental authorities to determine if groundwater and aquifers are contaminated and, if so, whether the sites should be remediated. The need for remediation is determined by the risk a polluted site poses, or could pose, to the local population, which is

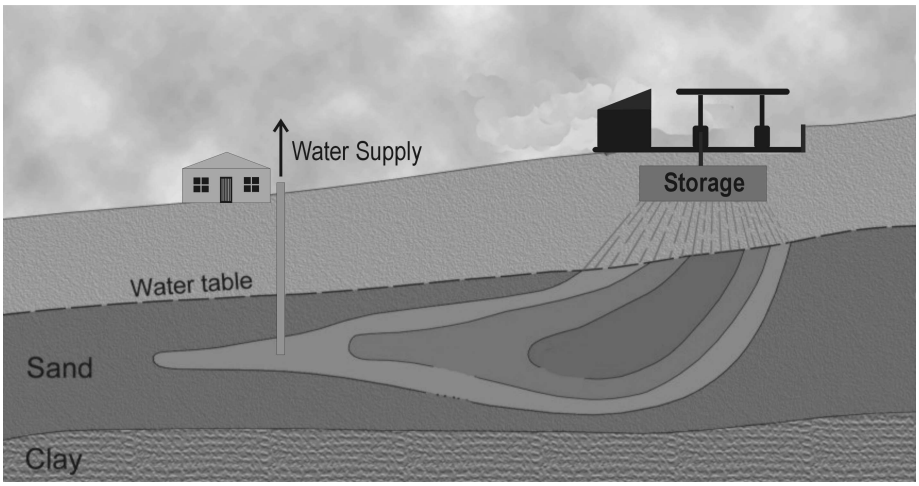

Figure 1.1: *Schematic of a water supply contaminated by a hydrocarbon plume originating from leaking underground storage tanks.*

typically a question concerning the possibility of amounts of specific elements or molecular compounds exceeding acceptable or safe limits. The threat of groundwater contamination and the remediation of already polluted aquifers, along with the need for a generic policy for tackling groundwater remediation, is therefore an important issue that can only be adequately addressed through better scientific understanding of geochemical processes and hydrological (transport) mechanisms.

The focus of many hydrogeology studies, therefore, is upon aquifer remediation, or 'attenuation', by describing transport and (reactive) mixing of solutes in aquifers, or other porous media. A porous medium can be defined as a solid matrix containing pores; normally, it refers to interconnected pores that can transmit the flow of (multiple) fluid and/or air phases. Some examples of *natural* porous media are sand, clay and rock, however, in a laboratory environment a porous medium maybe constructed experimentally using, say, inert silica glass beads. Applying water flow then allows one to simulate and observe the transport and mixing of solutes which might occur naturally. Alternatively numerical modelling techniques using, for example, mathematical descriptions of solute transport can be employed to study the same phenomenon.

In this thesis, mathematical (analytical and numerical) techniques along with laboratory and field-scale data are combined to describe the fate and interactions of reactive solutes in porous media. In particular, the focus is upon hydrodynamic

dispersion mechanisms, which can be a controlling factor in the attenuation of contaminated hydrocarbon plumes. Ultimately, this thesis aims to gain a better fundamental understanding into competing mixing processes involved in natural and enhanced attenuation.

1.2 Relevance to Society

Groundwater restoration has become increasingly important in the industrialised world. The first large-scale attempts to restore contaminated sites began in the early 1980's, after a number of environmental incidents led to legislation requiring the cleanup of abandoned waste sites. Perhaps the most notable of these incidents was the ecological disaster at the Love Canal, New York, where residents living on a former chemical landfill site suffered a range of human biologic hazards. This gave rise to early legislation, advocating the use of active remediation techniques, e.g., groundwater pump-and-treat or excavation, as a method of tackling groundwater pollution. The application of such techniques come at a high financial cost, typically because of the manpower required and the necessary means of waste disposal. Therefore, there has been an ever increasing focus on in-situ methods of groundwater remediation in recent years which, in comparison, are seen as cost effective strategies.

In-situ remediation includes active and passive techniques, both of which make use of natural attenuation processes. Active remediation techniques generally involve the injection or emplacement of particular chemicals and/or micro-organisms into the subsurface to enhance remediation. One example of active remediation is through the use of "bioscreens", i.e., permeable reactive barriers artificially created in the subsurface to enhance natural remediation. Conversely, natural attenuation alone is purely the monitoring of groundwater remediation, where it is believed that the ambient biogeochemical composition of a contaminated aquifer is sufficient to degrade contaminants over time. To this extent, natural attenuation is not only a collective term for naturally occurring biological and geochemical processes but it is also a risk-based engineering strategy for aquifer restoration. It is the term 'risk-based' which leads to uncertainty and, therefore, only through a thorough understanding of the fundamental processes governing attenuation, is it possible to accurately quantify risks of implementing such strategies.

1.3 Groundwater Flow, Diffusion and Dispersion

Groundwater flow occurs as a result of pressure or head gradients, i.e., groundwater flows from areas of high pressure to areas of low pressure. Take for example the hydrological cycle, where groundwater accumulating from precipitation moves from the hills down to the sea. Contaminated groundwater moves in the same way. Aqueous solutes, for example petroleum hydrocarbons leaking from underground storage tanks, mix with fresh groundwater forming toxic groundwater 'plumes' which migrate from the contaminant source zone in the direction of flowing groundwater (see Figure 1.1).

Mathematically, groundwater flow is a result of two main mechanisms: *advection* and *hydrodynamic dispersion*. Advection refers to the migration of groundwater in the principal flow direction whilst hydrodynamic dispersion is the mechanism by which groundwater spreads about the principal flow direction. The latter is a combination of two fundamental processes: *molecular diffusion* and *mechanical dispersion*. Molecular diffusion is driven by concentration gradients - solutes move from areas of high concentration to areas of low concentration. This process is only dependent on the migrating solutes, with different solutes being able to diffuse at different rates depending on their chemical and physical properties. Mechanical dispersion however is dependent on the structure of the porous medium and is based on the probability of individual solute particles choosing a particular pathway through the intricate matrix of pore spaces. These pathways are a summation of lateral (or transverse) and longitudinal movements around the principal groundwater flow direction. It is diffusive and dispersive processes which are of most importance in contaminant hydrology because they control mixing between polluted and fresh groundwater. Without mixing, zones where biological reactions occur cannot develop and contaminant plumes will not attenuate naturally.

1.4 Research Questions

In this study, the following research questions are addressed:

- Is there theoretical evidence to support the statement that transversal dispersion is the controlling dispersion parameter in cases of natural attenuation?
- If natural attenuation is an interplay between physical and biological processes, how is 'effective' transversal dispersion influenced by other natural attenuation processes, e.g., biodegradation?
- Theoretically, transversal dispersivity is a unique property of the porous medium, however literature suggests dispersivity values for non-reactive and reactive solute transport differ. Is there a link between these 'apparent' dispersivities and theoretical values?
- Is it possible to apply simple (mathematical) models to field-scale data to predict the natural attenuation capacity of aquifers?

1.5 Thesis Outline

This thesis consists of eight chapters. **Chapter 2** consists of a literature review of previous works; in particular the most important theories underpinning this thesis. **Chapters 3-7** provide the main results of this thesis, which have been prepared in the 'article' style. **Chapter 3** uses analytical techniques to explore the effects of longitudinal and transversal dispersivity on lengths of contaminant plumes where an instantaneous reaction occurs between two mixing solutes at the plume fringe. **Chapter 4** extends this approach to include plume core degradation. **Chapter 5** considers the case when reactions between mixing solutes are kinetically controlled, and presents a numerical model to study the effects of microbial activity on the size of the fringe of a contaminant plume. **Chapter 6** studies laboratory scale experiments where a non-classical form of the dispersion tensor is required to model reactive transport of mixing solutes. **Chapter 7** demonstrates the applicability of a three-dimensional extension of the model presented in Chapter 3, using high-resolution field data. Finally, there is a **Summary** of the previous chapters, which addresses the research questions posed in **Chapter 1**. This is available in both English and Dutch.

Chapter 2

General Theory

Foreword. In this chapter, an up-to-date historical overview into the theory surrounding the topic of hydrodynamic (transversal) dispersion is presented, a topic which has increased immensely in importance over the last 20 years largely due to the increased interest in bioremediation of polluted sites. Whilst this section attempts to be inclusive of the fundamental intricacies related to the understanding and quantification of transversal dispersion, it is impossible of course to compact all the many years of detailed scientific work into one document. The intention is, therefore, to present the underlying theories relevant in the context of this thesis.

2.1 Hydrodynamic Dispersion

The spreading phenomena of a tracer volume in a porous medium parallel and perpendicular to flow, is referred to as hydrodynamic dispersion. The concept of hydrodynamic dispersion is represented in Figure 2.1. It is a non-steady, irreversible process and consists of two main mechanisms: *mechanical dispersion* and *molecular diffusion*. Although ostensibly similar, dispersion should not be confused with diffusion. Mathematically, as will be demonstrated later, the hydrodynamic dispersion tensor is expressed in three dimensions as

$$D_{11} = D_l = D_m + \alpha_l |v|, \tag{2.1}$$

$$D_{22} = D_{th} = D_m + \alpha_{th} |v|, \tag{2.2}$$

$$D_{33} = D_{tv} = D_m + \alpha_{tv} |v|, \tag{2.3}$$

provided that the principal axes of the tensor coincide with the axes of the cartesian coordinate system. In equations (2.1-2.3), D_m is the molecular diffusion coefficient, D_l, D_{th} and D_{tv} are the longitudinal, transversal horizontal and transversal vertical dispersion coefficients, α_l, α_{th} and α_{tv} are the corresponding dispersivities, and v is the average linear *average linear velocity* in the $x-$direction (i.e. parallel to flow). It is generally accepted that molecular diffusion and mechanical dispersion

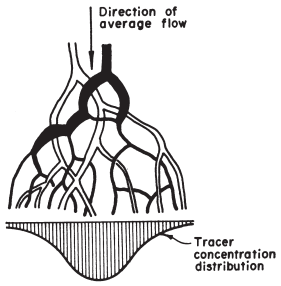

Figure 2.1: *Concept of hydrodynamic dispersion*

contribute most strongly to the degree of hydrodynamic dispersion. In fact, Bear (1972) lists in total six origins of hydrodynamic dispersion, inclusive of these main two main phenomena, including:

1. External forces acting on the liquid;

2. Microscopic geometry of the pore network;

3. Molecular diffusion;

4. Variations in liquid properties, e.g., density;

5. Changes in tracer concentrations due to chemical/physical processes; and,

6. Interactions between liquid and solid phases, e.g., sorption.

This introduction limits itself to a description of the processes of molecular diffusion and mechanical diffusion, as these concepts are central to understanding the theory surrounding our main topic of hydrodynamic (transversal) dispersion.

2.2 Molecular Diffusion

Molecular diffusion is the most fundamental process to hydrodynamic dispersion and can be defined as the movement of a tracer volume in a fluid due to concentration gradients, i.e., from an area of high concentration to an area of low concentration. Molecular diffusion is independent of the flow of the fluid - indeed it is this property that makes hydrodynamic dispersion an irreversible process. In fact molecular diffusion is a result of random oscillatory motions (random walk) of tiny molecules, or *Brownian Motion*.

2.2.1 Historical overview

In 1827 Robert Brown, a botanist, suspended some pollen grains in water and examined them closely, only to see them "filled with particles" that were "very evidently in motion". He was soon satisfied that the movement "arose neither from currents in the fluid, nor from its gradual evaporation, but belonged to the particle itself" (Brown, 1828; Ford, 1992). At first Brown believed that only organic materials exhibited such movements but soon extended his observations to inorganic materials. He concluded that any solid mineral, in a sufficiently fine powdery form, would reveal this phenomenon. However, at this time, much controversy surrounded Brown's observations and his revolutionary explanation of this natural phenomenon.

In the years that followed, physicists were split in their beliefs of the unifying concepts of physical science. The minority, including most notably amongst others Maxwell, Clausius, Boltzmann and Einstein, believed physics was unified on the foundation of mechanics. Mechanics assumes that all matter consists of atoms (or molecules) and that heat is nothing but the energy of motion, or kinetic energy, of the atoms. At this time, the atom was a hypothetical concept.

The majority of theoretical physicists sought unity in one of two non-mechanical alternatives: the so-called *energetic* and *electromagnetic* points of view. These alternatives arose from nineteenth-century challenges to the mechanical program in studies of heat and electromagnetism. The study of thermodynamics had culminated in two fundamental laws regarding heat. The first law related heat, energy, and useful work to each other in thermal processes and could be understood in terms of the motions and collisions of Newtonian atoms. The second law could not. According to the second law, the transport of heat in natural processes, such as the

melting of an ice cube, is always irreversible; that is, heat will not naturally flow of its own accord in the opposite direction - a melted ice cube at room temperature will not refreeze by itself. How could this be accounted for in mechanical terms? In light of this paradox, scientists such as Ernst Mach and Wilhelm Ostwald chose to deny the very existence of material atoms.

It was not until 1905 that Albert Einstein developed a statistical molecular theory of liquids. Furthermore he applied the molecular theory of heat to liquids in obtaining an explanation of what had been, unknown to Einstein, Brown's observed particle movements: the phenomenon now referred to as *Brownian Motion*. Although the concept of the atom was still open to objection in 1905, Einstein predicted that the random motions of molecules in a liquid impacting on larger suspended particles (such as pollen seeds) would result in irregular, random motions of the particles, which could be directly observed under a microscope (Einstein, 1905a). This predicted motion corresponded precisely with the controversial Brownian motion. From this motion, Einstein could accurately determine the dimensions of the hypothetical molecules and along with the work of Perrin (1909), the evidence was so compelling that by 1909 molecules could no longer be considered hypothetical.

Although Einstein's work proved mechanics to be the basis of physical science, and that Brownian motion did exist, Brown's original work received continued criticism. Well into the 20th Century various scientists questioned whether Brown, with his primitive microscopes of the day, could have possibly observed such particle movements and whether he in fact observed some alternative hydrodynamic effect attributed to such a closed system (e.g., Deutsch (1991)). Years of speculation were put to rest in 1992, when after a reconstruction of Brown's original microscope (Ford, 1982) and the experiments he undertook, scientists concluded that there was no question of extraneous hydrodynamic phenomena in such a closed system (Ford, 1992) and Robert Brown's claims, 165 years prior, were clearly no exaggeration.

2.2.2 Mathematical overview

Brownian motion of a particle is a thermodynamic effect, resulting from the bombardment of the particle by thermally excited molecules in a fluid. Under the assumption that interactions between other moving particles in the fluid are neglected, a particle moving under Brownian motion will follow a random walk, i.e.

a stochastic process where movements (in both $x-$, $y-$, and $z-$directions) are independent normal random variables. If each movement of a random walk is a random event, i.e., if the direction after each collision is random, then the mean square distance travelled by a particle is proportional to time; the central limit theorem applies to calculate the statistical properties of the random walk (Bear, 1972). Mathematically, Brownian motion is a stochastic process such that, if the position p of a particle at time t is known, then the particle's position at a subsequent time $t+dt$ is a normally distributed random variable with a mean of $p+\mu dt$ and a variance of $\sigma^2 dt$; the parameter μ is the linear drift, and the parameter σ^2 is the power of the noise.

Brownian motion forms the basic physical concept for understanding molecular diffusion of particles in a gas or fluid. However it was Einstein's formula for diffusivity, and not his derivation of the diffusion equation, which was his most significant contribution to this subject. From this formula for diffusivity, Perrin was able to determine the Avagadro number. Furthermore, Einstein (1905a) reasoned that if a specie is a spherical solute molecule in a solvent made up of much smaller molecules, then the *molecular diffusivity* D^* of a particle can be modelled by

$$D^* = \frac{kT}{6\pi\mu R} \tag{2.4}$$

where k is the Boltzman constant, T is the absolute temperature, μ is the viscosity of the solvent and R is the radius of the solute. Equation (2.4) is referred to as the *Stokes-Einstein Model* because Einstein used Stokes' Law (Stokes, 1950) to calculate the coefficient of friction.

Whilst Einstein provided a derivation of the diffusion equation, based upon random particle displacements, the relationship between the net flux of a species (crossing a unit area per unit time) due to dispersive processes and the concentration of a species was first considered by Graham (1850). In that paper, it was concluded that the flux caused by diffusion is proportional to the concentration difference of the species in solution. In his first publication (Fick, 1855a), Adolf Fick confirmed Grahams's original observations using qualitative theories and quantitative experiments. Then, inspired by Fourier's law of heat flow (Fourier, 1822), Fick developed the 1^{st} law of diffusion (Fick, 1855b); that diffusion of a species at a point x in time t can be represented, in three dimensions, as

$$\mathbf{J} = -D^* \cdot \nabla C(\bar{x}, t); \quad < \bar{x} = x_1, x_2, x_3 >, \tag{2.5}$$

where **J** is the diffusive flux and C is the concentration of the species at a point in time. Combining Fick's law for molecular diffusion with the equation for mass conservation yields

$$\frac{\partial C(\bar{x},t)}{\partial t} = \nabla \mathbf{J}, \tag{2.6}$$

and hence we obtain the standard diffusion equation, often referred to as Fick's second law

$$\frac{\partial C(\bar{x},t)}{\partial t} = D^* \cdot \nabla^2 C(\bar{x},t). \tag{2.7}$$

Equation (2.7) refers only to the aqueous diffusion of particles. In the case of *porous media*, Fick's laws must be modified to account for *porosity*, *tortuosity* and *electrical effects*. The most important effects are porosity and tortuosity. Tortuosity, as will be shown later, is related to the porosity of the medium. Extending equation (2.7) to include defining properties of the porous medium yields

$$\phi\frac{\partial C(\bar{x},t)}{\partial t} = \phi D^* \cdot \nabla^2 C(\bar{x},t), \tag{2.8}$$

where ϕ is the porosity of the medium. Note that if $\phi \to 1$ then equation (2.8) reduces to equation (2.7). The porosity term in equation (2.8) represents the reduction in volume that a species C has available to diffuse. Therefore, the presence of a porous medium means that the path length, over which a species C can diffuse, increases (Figure 2.2). This decrease in the available volume and

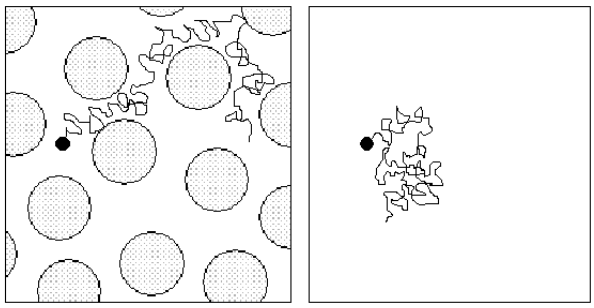

Figure 2.2: *Diffusion in a porous medium (Equation 2.8) compared to standard diffusion in a fluid (Equation 2.7).*

increase in the path length, or tortuosity τ, over which a particle can diffuse, is

represented by the *formation factor*

$$F = \frac{\tau}{\phi} \quad \Rightarrow \quad \frac{\partial C(\bar{x},t)}{\partial t} = \frac{D^*}{\tau} \cdot \nabla^2 C(\bar{x},t). \tag{2.9}$$

If the diffusivity in equation (2.7), or the ϕD^* value in equation (2.8) is constant, i.e. the equations are linear, then solutions can be obtained for equations of this form. Take for example the case of diffusion in one dimension, where D^* is assumed constant and $\phi = 1$. In this case the standard diffusion equation (2.8) reduces to

$$\frac{\partial C(x,t)}{\partial t} = D^* \frac{\partial^2 C(x,t)}{\partial x^2}. \tag{2.10}$$

The fundamental solution to equation (2.10) for a finite mass M of a tracer species concentrated on a plane at x = 0 at time t = 0 takes the form:

$$C(x,t) = \frac{M_{(species)}}{2\sqrt{2\pi D^* t}} exp\left(\frac{-x^2}{4D^* t}\right) \text{ for } t \geq 0, \tag{2.11}$$

and is shown graphically in Figure 2.3. It is clear from solution (2.11) that

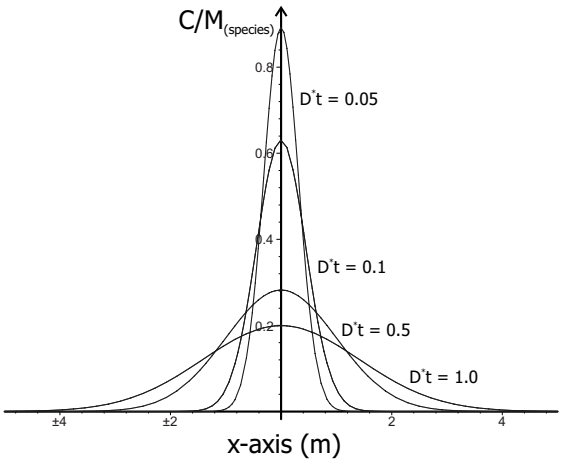

Figure 2.3: *Concentration - distance curves for an instantaneous planar source.*

$C(x,t) \to 0$ in the limit $x \to \infty$ and $C(x,t) \to \infty$ when $t \to 0$. Solution (2.11) can be easily extended to account for two and three dimensionality or problems involving, for example, linear equilibrium sorption or simple reactions. A fully detailed discussion of the diffusion equation and solutions thereof can be best found in Crank (1964) and Carslaw & Jaeger (1986). Solutions of the form (2.11) agree

with the statistical approach (Einstein, 1905a,b) to the derivation of the diffusion equation, which demonstrates that the dispersive spreading of molecules is analogous to a Gaussian normal distribution, i.e.,

$$P_x = \frac{1}{\sigma\sqrt{2\pi}} exp\left(\frac{-x^2}{2\sigma^2}\right), \tag{2.12}$$

where P_x is the probability and σ is the standard deviation.

2.3 Mechanical Dispersion

In the case of aqueous solutes moving through porous media, the theory of solute transport must also consider convective processes in addition to molecular diffusion. Local velocity variations due to micro-scale heterogeneities in permeability and porosity of the porous medium result in enhanced spreading of the solute front. This effect is called mechanical dispersion and a number of theories exist which describe this process. Some of these theories are described here.

2.3.1 Taylor's deterministic approach

The *deterministic* work carried out by Taylor (1953) considered the movement of a tracer in laminar Newtonian flow in long capillary tubes. The idea was thus (see Figure 2.4): a tracer displaces a resident fluid in a capillary tube of circular cross sectional area πR^2. If molecular diffusion D_m is zero, then the tracer moves with a

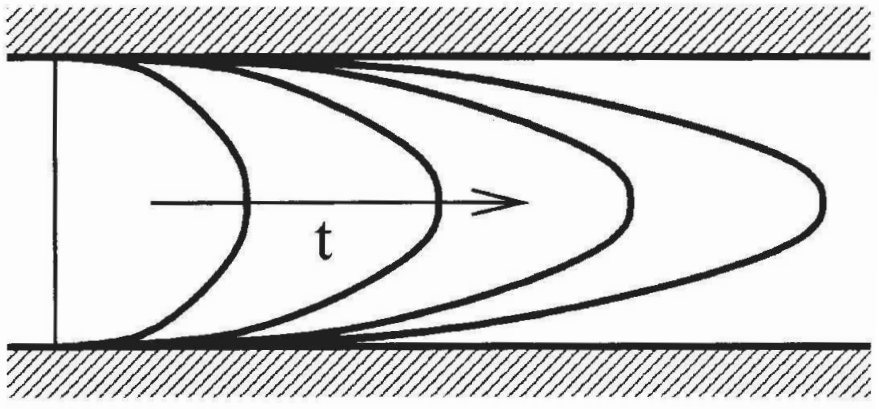

Figure 2.4: *Flow in a capillary tube.*

constant velocity; the interface between the tracer species and fluid is parabolic and the concentration distribution takes the form of a sharp step indifferent wave. If $D_m > 0$, then the sharp concentration interface is smeared. Taylor's theory states that if molecular diffusion D_m and the capillary length L are large in comparison to the the product of the average velocity v and the square of the capillary radius R, then the mixing zone will travel with the same mean speed of the injected fluid and would be dispersed as if there were a constant longitudinal dispersion coefficient. In this circumstance, the longitudinal dispersion coefficient D_l is given by

$$D_l = D_m + \frac{v^2 R^2}{48 D_m}. \tag{2.13}$$

Dispersion of this nature is called *Taylor dispersion*. It is important to remember that there is of course no transversal dispersion - only longitudinal dispersion and molecular diffusion in the transversal direction - because the walls of the tube limit the square-width of any tracer distribution to be less or equal to R^2, thus there is no lateral spreading of the tracer. It is also important to remember that the value for the longitudinal dispersion coefficient only becomes valid after a sufficiently long time has elapsed from the injection of the tracer particles. Aris (1956) later extended this approach to capillaries of any cross section.

Taylor (1953) only analysed flow in a single capillary tube but we can extend this idea and visualise a porous medium as a number, or network, of uniform capillary tubes connected together by pore throats. If a tracer is injected in only one of these capillaries, at the boundary of a domain, then we have not only longitudinal but also transversal, i.e., perpendicular to the direction of flow, components of dispersion. Concentrations of the tracer species in adjoining capillary tubes then meet and mix in the pore throats before exiting into another capillary.

An estimate for the dispersion coefficient D based on the similarity of diffusion processes and the Gauss distribution is obtained by measuring the mean squared (Gaussian) displacement σ a tracer fluid undergoes in one dimension during a time interval t, which yields

$$D = \frac{\bar{\sigma}^2}{2t}, \tag{2.14}$$

or in 3D by

$$D = \frac{\bar{\sigma}^2}{k2t}, \quad (k = 1, 2, 3). \tag{2.15}$$

Longitudinal dispersion occurs primarily in the capillaries, thus the coefficient of

longitudinal dispersion can be estimated by approximating the average capillary distance d over which the tracer fluid travels before mixing, where the travel time is equal to $\frac{d}{|v|}$, where d is the average particle diameter and v is the interstitial velocity. Hence, equation (2.14) yields

$$D_l = \frac{d|v|}{2} \tag{2.16}$$

as an estimate for the coefficient of longitudinal mechanical dispersion. Transversal mechanical dispersion is largely a result of the tracer fluid streams splitting when they exit the pore after mixing. This motion can be visualised as the tracer fluid moving laterally by a distance of $\frac{d}{2}$ before entering a new capillary tube. Consequently, the time t for this to occur is the time taken while the fluid moves one particle diameter d. Thus

$$D_t = \frac{d|v|}{8} \tag{2.17}$$

Equations (2.16) and (2.17) show a clear dependence on the structure of the porous medium - a combination of the average grain size and velocity through the medium. Similarly, the equations derived earlier for the molecular diffusion coefficient also show a dependence on the porous structure. Theory assumes that the effects of molecular diffusion are independent from one another and in combination these two processes make up what we commonly refer to as hydrodynamic dispersion. Therefore, a value for a hydrodynamic dispersion coefficient in the longitudinal and transversal directions can be yielded through the simple addition of the molecular diffusion coefficient to equations (2.16) and (2.17), i.e.

$$D_l = \frac{D_m}{\phi F} + \frac{d|v|}{2}, \tag{2.18}$$

and

$$D_t = \frac{D_m}{\phi F} + \frac{d|v|}{8}. \tag{2.19}$$

In dimensionless form, equations (2.18) and (2.19) become

$$\frac{D_l}{D_m} = \frac{1}{\phi F} + \frac{d|v|}{2D_m}, \tag{2.20}$$

and

$$\frac{D_t}{D_m} = \frac{1}{\phi F} + \frac{d|v|}{8D_m}. \tag{2.21}$$

The dimensionless expression on the right hand side of (2.20) and (2.21) is called the *microscopic Peclet number of molecular diffusion*, a ratio between the convective mixing and molecular diffusion or

$$Pe = \frac{|v|d}{D_m} \tag{2.22}$$

where d is the average grain size.

In comparison to the deterministic model of Taylor (1953), there has been much work to represent dispersion through statistical models. The idea behind a statistical approach is that it is impossible to describe mathematically the motion of a single tracer particle in a fluid but it is possible to attribute probabilities to predict the distribution of many tracer particles at a certain time t, that were initially in close proximity to each other at time t_o. Statistical approaches therefore employ (Gaussian) probability distributions to describe the velocities (and motion) of particles in a porous medium. In short: Over large enough time periods, using the *law of large numbers*, the time-averaged velocity characteristics of a single particle can be used in place of the averages taken over the whole group of particles; thus the problem reduces to that of the random motion of a single particle (Bear, 1972).

2.3.2 Scheidegger's random walk theory

Scheidegger (1954) employed the theory of a random walk to describe dispersion in three dimensional space. This work assumes the movement of a particle, under laminar flow conditions, through a homogeneous isotropic porous medium comprising systems of capillaries with identical macroscopic characteristics. Such a system is referred to as *periodic* or in this case *spatially periodic*, i.e., the model is analogous with a system comprising different types of porous media which are macroscopically similar. The underlying assumption is that a particle with a sufficiently long path length in a specific system will experience all the conditions encountered in the ensemble of systems, and hence a temporal average over a single path equally representative of a spatial average over an ensemble of path lengths in different systems. Scheidegger (1954) also assumed that molecular diffu-

sion is absent and that if a particle is given a large enough number of displacement periods, a Gaussian distribution is obtained in the form

$$p(x,y,z,t) = (4\pi Dt)^{\frac{3}{2}}\ exp\left(-\frac{[(x-\bar{x})^2+(y-\bar{y})^2+(z-\bar{z})^2]}{4Dt}\right), \tag{2.23}$$

where $D = \frac{N\sigma^2}{2t} \Rightarrow \frac{\sigma^2}{2\Delta t}$ and N is the number of intervals $\Delta t = \frac{t}{n}$ in each of which a particle undergoes a displacement; $\bar{x} = v_x t$, $\bar{y} = v_y t$, $\bar{z} = v_z t$ where v_x, v_y and v_z are components of the uniform velocity field.

Solution (2.23) assumes that the porous medium is isotropic and as such the probability distribution is the same in both the $x-$, $y-$ and $z-$directions, i.e., parallel and perpendicular to the uniform flow direction. Thus the value for the dispersion coefficient makes no distinction between longitudinal and transverse spreading of a tracer.

2.3.3 De Josselin de Jong's statistical approach

De Josselin de Jong (1958) employs a statistical approach for obtaining estimates of both longitudinal and transversal dispersion coefficients as separate, albeit coupled, processes. In both de Josselin de Jong (1958) and Saffman (1959), the approach is based on a more realistic visualisation of the porous structure than in models presented by Taylor (1953) and Scheidegger (1954). Instead of uniformly distributed particles, de Josselin de Jong (1958) visualises a porous medium as a series of interconnected straight channels of equal length, orientated at random, uniformly distributed in all directions, in which average uniform flow takes place (Figure 2.5). Such a geometric matrix is commonly referred to as *random porous media*. Considering just one of these capillaries, the pressure gradient can be seen as being proportional to $\cos\theta$, where θ is the angle between the direction z of the channel and of the uniform flow. Within each channel it is assumed that a tracer particle moves with a mean velocity v with a radial diffusion pattern. The residence time t_j of a particle in a capillary of radius r is therefore

$$t_j = \frac{r}{v\cos\theta}. \tag{2.24}$$

In spherical co-ordinates, components of the j^{th} displacement are

$$x_j = r\sin\theta_j\cos\phi_j;\quad x_j = r\sin\theta_j\sin\phi_j;\quad z_j = r\cos\theta_j, \tag{2.25}$$

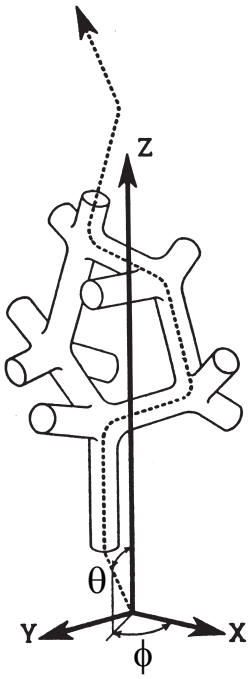

Figure 2.5: *Path of particles through a random porous medium, courtesy of G. de Josselin de Jong.*

where θ and ϕ are angles in the spherical co-ordinate system.

The probability $P(\theta, \phi)$ that a tracer particle chooses a direction defined by the angular interval $(\theta, \theta + \Delta\theta)$ and $(\phi, \phi + \Delta\phi)$ is proportional to discharge $Q(\theta, \phi)$ in that direction and total discharge Q, i.e. $P(\theta, \phi) = Q(\theta, \phi)/Q$. The assumptions here are different to the assumptions made in the random walk theory. That is,

1. If the velocity in a channel is $v \cos\phi$, then during $\Delta t < \frac{r}{v \cos\phi}$ a particle moves a distance $d = \Delta t v \cos\theta$.

2. Particles entering a junction will be distributed radially, which means that particles reach the end of channels at different times and are confronted with new choices. Hence each particle will undergo a different number of displacements in a the same given time interval. Compare this with the theory of Scheidegger (1954), where it is assumed that each displacement has the same duration.

Markov's method is used to predict the probability of a particle arriving at a given point p after a given time t, after many displacements. The result of dispersion from a point injection is a Gaussian distribution in three-dimensional space, from which standard deviations in the longitudinal σ_l and transversal σ_t are obtained. The diffusion constants obtained from the standard deviations are

$$D_l = \frac{{\sigma_l}^2}{2T_o} = \frac{vl(\lambda + \frac{3}{4} - \ln\gamma)}{6}, \tag{2.26}$$

$$D_t = \frac{{\sigma_t}^2}{2T_o} = \frac{3vl}{16}, \tag{2.27}$$

where T_o is the arrival time of a maximum number of particles after a given time, travelling in elementary canals of length l. λ is a function of the distance travelled Z_o, i.e., the distance travelled in the direction of the mean flow. The ratio of the coefficients of longitudinal (D_l) and transversal (D_t) dispersion fall between $6 \rightarrow 10$. Variations on the work by de Josselin de Jong (1958) yield other, albeit similar, results. In all of these studies in a porous matrix it is concluded that the value of D_l, and therefore D_t, is not only proportional to the mean velocity but also to the length l of the elementary canals, which is of the order of grain size d. Whilst D_l in equation (2.26) is dependent on the travel distance in the direction of mean flow, D_t is obviously not. It must be concluded therefore that the ratio between D_l and D_t increases as the mean distance of travel increases.

This contradicts the work of Blackwell (1959), which states that the ratio of D_l to D_t is dependent on the mean velocity only and independent of the distance travelled by the tracer.

2.3.4 Saffman's statistical approach

Saffman (1959) studied a similar geometric porous structure as that of de Josselin de Jong (1958), in which capillaries are orientated randomly. However, Saffman (1959) concludes that at high Peclet numbers, dispersion never becomes purely mechanical. Instead, because the flow of a tracer fluid at the side of a capillary is zero; in the presence of no molecular diffusion to release this tracer from the system the effective diffusivity increases at a rate equal to $Pe \ln Pe$. This implies that under such a regime the time required for a tracer to flow through a capillary becomes infinite. Therefore, Saffman (1959) introduces molecular diffusion into the model. In comparison with the work of de de Josselin de Jong (1958), the probability function for a tracer flowing through a random porous in Saffman (1959) accounts not only for the probability of a particle choosing a capillary of orientation $(\theta, \theta+\Delta\theta)$ and $(\phi, \phi+\Delta\phi)$, but also for the velocity distribution within a capillary, i.e., the probability that a particle chooses a streamline $(r, r+\Delta r)$ in that capillary. Similar to de Josselin de Jong (1958), values for longitudinal and transversal dispersion are based on Darcy velocity v, capillary length l, molecular diffusion D_m and at a time t from an instantaneous point source injection

$$D_l = \frac{1}{2t}(x-vt)^2 = \frac{1}{2}vlS^2; \quad S^2 = ln\frac{3v\tau_o}{l} - \frac{1}{12}; \quad \tau_o = \frac{l^2}{2D_m}. \tag{2.28}$$

After a sufficient number of displacements N, so that the total displacement of individual tracer particles become statistically independent, equation (2.28) reduces to the conclusion (2.27) of de Josselin de Jong (1958)

$$\frac{v\tau_o}{l} \ll \left[N \ln\left(\frac{3v\tau_o}{l}\right)\right]^{1/2} \quad \Rightarrow \quad D_t = \frac{1}{2t}y^2 = \frac{3}{16}vl. \tag{2.29}$$

2.4 Molecular Diffusion vs. Mechanical Dispersion

Theoretical studies consider the coefficient of hydrodynamic dispersion $D_{hydrodynamic} = D_{molecular} + D_{mechanical}$ to be dependent on basic properties or characteristics of the

porous medium. Both diffusion and dispersion are scale dependent mechanisms. Diffusion is primarily important on the microscopic scale. It is the diffusive process that brings reacting species into contact with each other and transports chemicals across boundaries. In contrast, mechanical dispersion is an effect of the variation of velocities within the porous matrix, resulting from inhomogeneity, which causes enhanced mixing and spreading of the solute front. On the macroscopic scale diffusion is extremely slow and, due to the increased variations in heterogeneity, typically gives way to dispersion.

Where hydrodynamic dispersion models consider the combined effect of velocity distribution in a channel and transverse molecular diffusion,

$$D \propto v^2 \tag{2.30}$$

where D is the dispersion coefficient (Scheidegger, 1954). Where only the average velocity in the channel is considered (Bear & Todd, 1960), i.e. in a porous medium, then

$$D \propto v \tag{2.31}$$

Considering the combined effect of molecular diffusion coupled with mechanical dispersion, from equation (2.22), and considering one-dimensional flow (so only longitudinal dispersion) experimental results allow the relationship between molecular diffusion and convective (longitudinal) dispersion to be plotted. In Figure 2.6 molecular diffusion dominates when the Peclet number Pe is small compared to unity and conversely convective dispersion dominates when the Pe is large compared to unity. Moreover, Figure 2.6(B) shows that:

- In **zone I** molecular diffusion dominates.
- In **zone II** the effect of molecular diffusion is of the same order as mechanical dispersion. Typically $Pe \approx 0.4 \rightarrow 5$.
- In **zone III** dispersion is caused from mechanical dispersion combined with transversal molecular diffusion. It follows experimentally that

$$\frac{D_L}{D_m} = \alpha(Pe)^m; \;\; \alpha \approx 0.5; \;\; 1 < m < 1.2 \tag{2.32}$$

  and m is the slope of the curve.

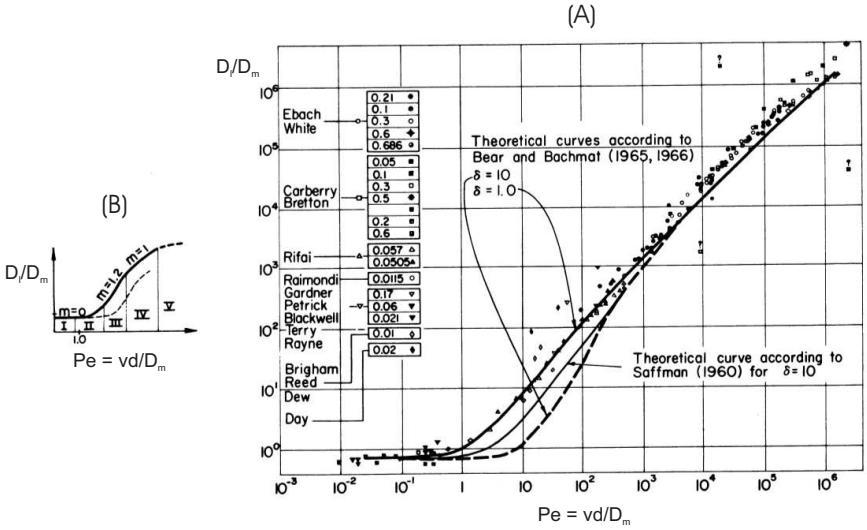

Figure 2.6: *Relationship between molecular diffusion and convective dispersion, along with selected data from experimental studies, from Bear (1972).*

- **Zone IV** is the region of dominant mechanical dispersion where

$$\frac{D_L}{D_m} = \beta Pe; \quad \beta \approx 1.8. \tag{2.33}$$

- **Zone V** is also dominated by mechanical dispersion, but also largely influenced by turbulence. Here the slope of the curve m is less than 1.

Such an experimental description of the relationship between longitudinal dispersion and molecular diffusion encouraged the idea that a similar relationship could exist for the transversal dispersion. The work of Scheidegger (1954) was based on the assumption that the porous medium was isotropic, thus values for longitudinal and transversal dispersion would be the same. Conversely, de Josselin de Jong (1958) showed for the first time a distinct difference between longitudinal and transverse components of mechanical dispersion. In the years that followed these first theories about dispersion, scientists have learned that indeed the relationships/ratios between longitudinal and transversal dispersion differ widely. These relationships are discussed in Section 2.7.1.

2.5 Advection-Diffusion Equation

It is impossible to give an overview of dispersion without considering convective processes. In cases where there is fast mass transfer of concentrated solutions, diffusion itself causes convective flow and, of course, in many practical problems, both diffusion and convection occur. There are many excellent reference books which cover the origins of flow in porous media in greater detail (e.g., Bear (1972); Freeze & Cherry (1979); Fetter (1993)) and it is not the object of this work to discuss these issues in depth. In most practical cases, flow in porous media is sufficiently slow and close to solid boundaries for the inertia terms in the Navier-Stokes equations to become negligible; thus flow is considered incompressible and can be modelled by the Stokes equations for momentum conservation. The Stokes equations can be derived from the Navier-Stokes equations when the Reynolds number is small (i.e., laminar flow). Darcy's law (Darcy, 1856) follows from the Stokes equations where specific discharge q from a porous media is proportional to the head gradient $\nabla\varphi$ across it. From the perspective of hydrology, Darcy's law can be expressed as

$$q = -K \cdot \nabla\varphi \tag{2.34}$$

where K is the hydraulic conductivity of the porous medium. Through Darcy's law, the standard diffusion equation (2.7) coupled to the convection equation yields the general form of the advection-diffusion equation (ADE), a linear partial differential equation.

2.5.1 ADE for non-reactive tracers

In three dimensions, the spreading of a tracer solute in porous media is described as

$$\frac{\partial c^k}{\partial t}(x,t) = \nabla \cdot (D \cdot \nabla c^k(x,t)) - v(x) \cdot \nabla c^k(x,t),\ \bar{x} =< x_1, x_2, x_3 >, \tag{2.35}$$

where c is the concentration of species k, D is the hydrodynamic dispersion tensor, and v is the average pore water velocity through the medium. The components of the hydrodynamic dispersion tensor, according to classical theory, were presented in (2.1)-(2.3).

It is not difficult to see that the advection and dispersion phenomena of a tracer fluid in a porous medium are coupled processes, i.e., one cannot solve one

without solving the other. In most cases we solve such problems by considering the influence of advection on dispersion. Indeed, it may be expected that the cross influence of dispersion upon flow is only of secondary importance; dispersion will lead to a more gradual transition between a tracer concentration and the fluid it travels in, but it is conjectured that this will negligibly change the velocities.

2.5.2 ADE for reactive species

In the case of a species undergoing a reaction the ADE takes the form

$$\frac{\partial c^k}{\partial t}(x,t) = \nabla \cdot (D \cdot \nabla c^k(x,t)) - v(x) \cdot \nabla c^k(x,t) + R_{c^k},\ \bar{x} =< x_1, x_2, x_3 >, \quad (2.36)$$

where R_c is the reaction term. The reaction term can take many forms, of which some are listed in Table 2.1 and are discussed below. Specific (geochemical) reactions are considered in the subsequent Chapters of this thesis.

Reaction	*Term* R_{c^k}
Linear equilibrium sorption	$-k_d c$
First-order decay	$-\lambda\theta c;\ \ \lambda = \frac{(ln2)}{t_{(1/2)}}$
Instantaneous bimolecular	$r_{AB} = -r_A = -r_B$
Monod kinetics	$\frac{\partial c_A}{\partial t} = k_m \frac{c_A}{(k_A + c_A)} \frac{c_B}{(k_B + c_B)}$

Table 2.1: *Types of reaction (R_{c^k}) and corresponding mathematical terms.*

Linear equilibrium sorption

Sorption refers to the mass transfer process between the contaminants dissolved in the aqueous phase and the contaminants sorbed on the solid phase. The functional relationship between the dissolved and sorbed concentrations under a constant temperature is referred to as the sorption isotherm which can be linear and non-linear. The simplest form of the sorption isotherm for linear sorption is listed in Table 2.1, where k_d is the distribution coefficient. The local equilibrium assumption (LEA) is often applied to the various sorption processes when it can be assumed that the sorption process is sufficiently fast enough compared to the transport time scale, i.e., groundwater velocities. In this case LEA can be represented by a

retardation factor

$$R = 1 + \frac{\rho_b}{\theta} k_d, \tag{2.37}$$

where ρ_b and θ are the bulk density and porosity of the porous medium respectively. In addition, Freundlich and Langmuir isotherms can be used to represent equilibrium controlled non-linear sorption, whilst non-equilibrium sorption is typically represented by first-order reversible kinetic reactions.

First-order decay

The first-order irreversible rate reaction term included in Table 2.1 represents the mass loss from the dissolved phase, where λ is a first order reaction rate for the dissolved phase and $t_{(1/2)}$ is the half-life of the biodegradable (or radioactive) material. A similar expression can be included for the sorbed phase if this is considered important, although for biodegradation, however, it has been observed that certain reactions occur only in the dissolved phase.

Instantaneous bimolecular reaction

If two reactants A and B mix together to form a product AB, $r_{AB} = -r_A = -r_B$ expresses the rate of production of AB equal to the rate of loss of each reactant. The instantaneous reaction model is considered to be an efficient alternative to more complex multispecies reactive models, e.g., Monod kinetics, when reaction rates are sufficiently fast in relation to groundwater velocities.

Monod kinetically controlled reaction

Only in cases where high flow velocities occur, such as with some enhanced remediation technologies, might a kinetic modelling approach be necessary. Kinetics of biodegradation reactions between species can be described for example by the Michaelis-Menten model (Michaelis & Menten, 1913) listed in Table 2.1. Here, k_m is a reaction rate constant, c_A and c_B are the concentrations of species A and B, and k_A and k_B are the half saturation constants for the A and B.

2.5.3 Solutions of the ADE

Analytical solutions of linear partial differential equations, like the ADE, (where both the dispersion coefficient and velocity are constant) typically take the form of exponential functions or error functions (integrals of exponential functions). They depend strongly on the shape of the volume in which diffusion occurs and the initial and boundary conditions imposed on the system. Explicit analytical solutions to the ADE can be obtained for a variety of scenarios, where simplifying assumptions, often in terms of imposed boundary conditions, are applicable to the case in question. Crank (1964) and Carslaw & Jaeger (1986) both give detailed descriptions and methodologies for solving such problems. Where simplifying assumptions are not valid, as is often the case with complex geochemical and heterogeneous systems, numerical models must be used to give the required solutions.

A number of pre-existing numerical codes are available which typically use, in order of mathematical complexity and elegance, finite difference, finite volume or finite element methods to approximate the ADE over a specified domain or grid (Vermolen, 2005). In this thesis, only finite difference methods, based on the classical Newton derivative, have been used to predict the movement and distribution of contaminant species. A comprehensive overview of these types of codes is given by Prommer (2002).

In the following chapters of this thesis, appropriate analytical and numerical models are used to quantify non-reactive and reactive solute mixing.

2.6 Reactive Mixing

In the context of multi-component reactive transport, reactive mixing is the term used to describe plumes of different reactive species which, after initially being separated, overlap one another and react together to form new compounds. When species are non-sorbing, mixing is caused solely by dilution which is a direct result of the mechanism of diffusion. In this way, and as is shown below, mixing and dilution are very closely related to each other (Cirpka *et al.*, 1999). However, if one or all of the species considered are sorbing, or undergo other mass transfer processes, then plumes can overlap and species can mix without dilution. The following mixing processes are therefore of interest in hydrogeology.

2.6.1 Dilution

Dilution is caused by diffusion. For example, high concentrations within a contaminant plume decrease with time and travel distance due to diffusive processes and, in turn, mass conservation results in an increase of the volume occupied by the dissolved contaminant species. The significance of dilution is illustrated in Figures 2.7 and 2.8. In these graphical representations, the distributions of two non-sorbing species (A and B) with an initial concentration C, introduced simultaneously into a one dimensional domain at different locations, are considered.

Figure 2.7 demonstrates only advective transport in a heterogeneous medium.

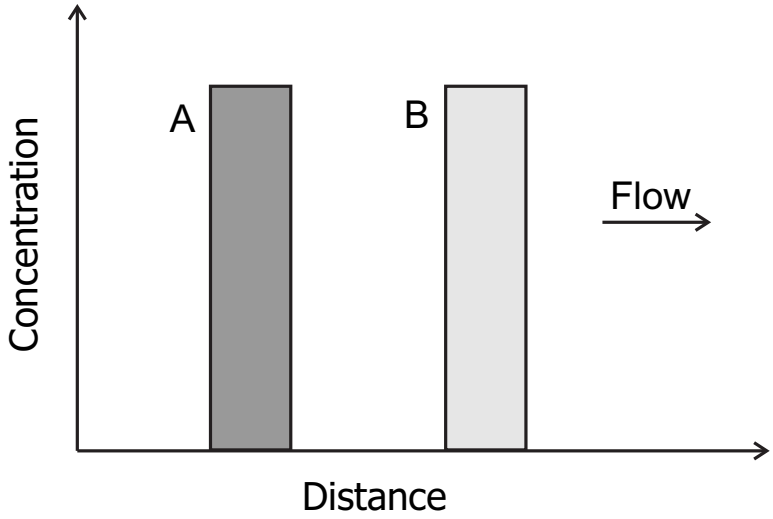

Figure 2.7: *Advective flow.*

Since there is no diffusive process occurring, the plumes do not overlap and the peak concentrations of the species do not decrease. In Figure 2.8, macrodispersion in addition to advection is considered in a homogeneous medium. In this case both of the plumes are Gaussian, and overlap each other. If the species considered in Figure 2.8 were reactive, then mixing and reaction rates between the species would be overestimated (Cirpka *et al.*, 1999). Conversely, if Figure 2.8 were to show the effects of advection and local-scale dispersion, this time in a heterogeneous medium, the overlapping would be far less than that predicted by the macrodispersion model. In this case, peak concentrations would remain high at the plume core, with sharp concentration gradients at the plume fringes and, in the case of reactive species, mixing would be confined to a much narrower transition zone between the species.

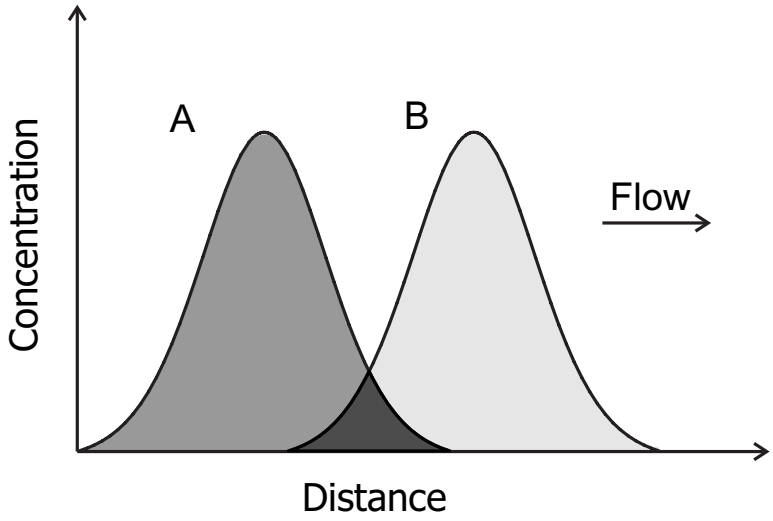

Figure 2.8: *Advective and dispersive flow.*

2.6.2 Chromatographic mixing

Chromatographic mixing, or advective mixing (Oya & Valocchi, 1998), occurs when species with different mobilities are introduced into the same domain. A more mobile species may overlap a less mobile species and cause mixing (e.g., if species B in Figure 2.7 were sorbing). Chromatographic mixing is common when considering the biodegradation of contaminant plumes because typically contaminants can be strongly sorbing, whereas electron acceptors (e.g., oxygen, nitrogen) are not.

2.6.3 Kinetic mass transfer

Kinetic mass transfer from the immobile phases into the aqueous mobile phase can cause mixing due to the delayed response of immobile phase concentrations to concentration changes in the aqueous phase.

2.7 Effective (Transversal) Dispersion

Transversal dispersion, as has already been identified, can be seen as a complementary process to longitudinal dispersion. To some extent it is impossible to explain transversal dispersion without some reference to longitudinal dispersion. A tracer fluid flowing through a homogeneous porous system will experience dispersion; the

dispersion tensor D based on additive values of molecular diffusion and mechanical dispersion in longitudinal and transversal directions. To date, there have been many publications concerning longitudinal dispersion, but far fewer over transversal dispersion. Part of the reason for this is the rule-of-thumb approach: that transversal dispersion is typically a factor of ten less in order than longitudinal dispersion. Such an attitude comes from those earlier works covering hydrodynamic dispersion mechanisms, where the relevance of transversal dispersion was not well understood. At the field-scale such an approach may be, to a certain extent, valid, however in the rest of this chapter, it is demonstrated that in situations where dispersion is a governing factor, i.e., in many natural attenuation problems, it is important to consider transversal dispersion as a process in it's own right.

Note that care should be taken to consider any factors which may effect dispersive processes, which might lead to anomalous results in place of those predicted by theories alone. Factors such as particle size distribution, particle shape and packing, or heterogeneities in permeability, viscosity ratios, gravity forces, amount of turbulence, and effect of an immobile phase should not be overlooked (Fried & Combarnous, 1971). If any of these factors are significant to a particular flow regime, then resulting dispersion coefficients may be termed 'effective', as they represent a compound of individual processes which affect dispersion mechanisms.

Under certain flow conditions, when the transport of a tracer is controlled mainly by advection, then we assume that dispersion through molecular diffusion is small in comparison to mechanical dispersion. It has been experimentally determined that molecular diffusion only becomes significant at Peclet numbers less than 10^{-3} (see Figure 2.6) (Bear, 1972). Therefore in many field-scale problems, interest is often limited to cases where advection and mechanical dispersion are the dominant transport mechanisms. Also, under such conditions, it is usually feasible to negate the effects of longitudinal mechanical dispersion. Transverse mixing is usually more important than longitudinal mixing because, for a plume of a long length, the fringe mixing area is much larger than the frontal mixing area (Cirpka *et al.*, 1999). In addition, it is typical that we envisage a contaminant plume as an ideal 'cigar-shaped' mass (Figure 2.9a), when in reality the influence of heterogeneity makes it is more realistic to imagine a plume made up of a number of 'fingers' (Figure 2.9b). In this way, we see that the fringe area is much larger than might otherwise be predicted, and thus the influence of transversal mixing is much greater than that of longitudinal mixing. Our problem, therefore, typically

reduces to a study on the dispersion of solutes occurring perpendicular to the flow direction.

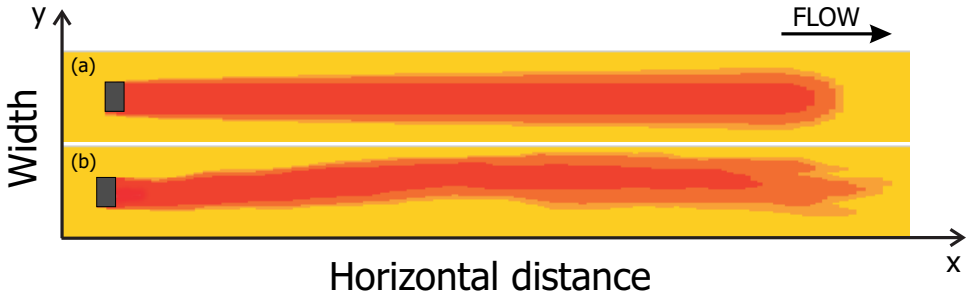

Figure 2.9: *Plan view of hypothetical plume development from a fixed source: (a) symmetrical plume shape, and (b) more realistic plume shape, resulting from heterogeneous conductivity field distribution.*

2.7.1 Transversal dispersivity and tracer transport

De Josselin de Jong (1958) proposed that the hydrodynamic transversal dispersion coefficient in a homogeneous medium is equal to the product of the average linear velocity and the transversal dispersivity, which is solely a property of the porous medium, equal in magnitude to 3/16 of the grain size (see equation (2.27)). This result has been validated through experimental observations using conservative tracers (e.g., Grane & Gardner (1961) and more recently by Person *et al.* (1996)).

However, there is also a large body of experimental data which challenges the classical formulation of the transversal dispersion coefficient. For example, Han *et al.* (1985) carried out laboratory measurements of the transversal dispersion coefficient using three different size distributions of glass beads, the results of which suggested that under steady-state conditions, lateral dispersivities showed no dependence on the particle size distribution. To some extent this is also in agreement with the earlier experimental works of Harleman & Rumer (1963) and Gunn & Pryce (1969), where transversal dispersion coefficients were measured at values of Peclet number (from 10 to 10^3) and a considerably different dependency of Peclet number on the lateral dispersivity was obtained. From their experimental work, Harleman & Rumer (1963) propose that the ratio of the coefficient of longitudinal dispersion to transversal dispersion for a tracer fluid is given by

$$\frac{D_l}{D_t} = \lambda \Re^n \tag{2.38}$$

where λ and n are dimensionless coefficients dependent on the geometry of the porous medium and $\Re$ is the Reynolds number. More recently Boving & Grathwohl (2001) and Klenk & Grathwohl (2002) have reported from laboratory findings that at high flow rates, there is an apparent decrease of transverse dispersivity with average linear velocity. This is confirmed by well-controlled experimental investigations conducted by Olsson (2005), which suggests a non-linear increase of the dispersion coefficient D_t across a range of seepage velocities from 0.37 m/d to 164 m/d, using a sand and glass bead porous medium. The empirical expression

$$\frac{D_t}{D_{aq}} = \frac{D_m}{D_{aq}} + 0.26(Pe)^{0.74}, \tag{2.39}$$

was proposed, where D_{aq} is the aqueous diffusion coefficient and Pe is the Peclet number of molecular diffusion equal to $|v|d/D_{aq}$. Expression (6.5) is valid for non-reactive tracers and comparison with existing data from literature demonstrates that the expression holds for all investigated Peclet numbers (from $Pe \approx 1$ to 6307).

These laboratory findings are just some examples which demonstrate the contradictions between theoretical derivations and laboratory findings as to the dependency of the (transversal) dispersion tensor on properties of the porous medium. Whilst theoretical relationships indicated that transversal dispersivity is only a property of the porous medium, laboratory investigations suggest that there are many situations when this is not the case and 'effective' or 'apparent' dispersivities should be adopted.

2.7.2 Transversal dispersivity and reactive solute transport

There are many examples of literature describing methods for modelling transport coupled with reactions though homogeneous porous media (e.g., Person *et al.* (1996); Steefel & MacQuarrie (1996)). Typically, such modelling assumes that dispersive processes, and therefore parameters such as coefficients of hydrodynamic dispersion, are the same for reactive and non-reactive species flowing through a porous medium. However, experimental data and theoretical work have shown that this approach leads to over-predictions of solute mixing. Gramling *et al.* (2002) performed one-dimensional experiments in homogeneous porous media where an instantaneous reaction occurred between two mixing solutes. Their laboratory

data showed the amount of reaction product predicted from an analytical solution of the ADE was overestimated by approximately 20%. The reason for this lies in the fact that dispersion, in terms of the ADE, is a Fickian process and concentrations are averaged over representative elementary volumes. The ADE is therefore a macroscopic equation, which assumes complete mixing at the pore-scale. Dispersion coefficients for tracers derived using the ADE will therefore be largely a function of mechanical dispersion (Gramling *et al.*, 2002). However, at the pore-scale, concentrations may be highly variable. As such, any reactions occurring between mixing solutes are governed by pore-scale molecular diffusion and not mechanical dispersion. Other investigations have also found similar differences between dispersivity values for non-reactive and reactive transport, e.g., Semprini & McCarty (1991); Ginn *et al.* (1995); Kemblowski *et al.* (1997); Kapoor *et al.* (1997); Miralles-Wilhelm *et al.* (1997) all suggest that the rate of mixing between reactive solutes is much smaller than predicted using (non-reactive) macroscopic dispersion parameters.

2.7.3 Transversal dispersion at different scales

Typically, measurements of transverse dispersivity taken on the field-scale are several orders of magnitude higher than those made at the laboratory scale (Pickens & Grisak, 1981a; Sudicky & Cherry, 1979). These earlier studies suggest that the dispersivity of a medium is not unique and depends on solute travel distance and the scale of observations/measurements taken and several efforts have been made to account for this. Most of the theories rely on the heterogeneous nature of the porous media. Stochastic theories (e.g., Gelhar *et al.* (1979); Dagan (1982, 1984); Gelhar & Axness (1983); Neuman *et al.* (1987)) relate macrodispersivity with the spatial correlation structure of the hydraulic conductivity of the porous media. According to stochastic models, macrodispersivity is a function of time initially and will reach an asymptotic constant value after all scales of variability have been experienced.

Moreover, dispersion processes at the field-scale maybe expected to be non-Fickian because the permeability fluctuations may extend over length scales comparable to the length scales of the transport processes (Hassanizadeh, 1996). Thus, by applying Fickian macrodispersion to reactive transport problems, mixing and spreading mechanisms are merged leading to overestimates of the rates of reactions actually taking place. Cirpka *et al.* (1999) also notes that macrodispersion, i.e.,

dispersion at the field-scale, which can be accurately predicted for conservative tracer studies, should not be applied to similar studies in reactive transport. This is because reactions take place at the (micro) scale (e.g., biodegradation), whereas macrodispersion describes the rate at which the second spatial moments of a large plume increase; the quantity therefore includes mixing of reactants on the local scale and spreading of the plume at the larger scale.

Furthermore, on the field-scale, values of transversal dispersivity are often over-predicted because typically we assume a plume as a 'cigar-shaped' mass with one fringe, when in fact it is more realistic to envisage it as a mass made up of a number of fingers, all with a fringe area. Hence, the values of transversal dispersivity taken from the field give an unrealistic impression of the physical structure of the plume. To some extent, this problem has been addressed through the use of high resolution sampling techniques (e.g., Davis *et al.* (1999)), which capture more intricacies of plume development. Unfortunately, this alone cannot bridge the gap between macro and microdispersion. In order to accurately model field-scale dispersion, macroscale 'effective' dispersivities, which account for pore scale heterogeneities, must be adopted (Cirpka & Attinger, 2003).

Bibliography

Aris, R., 1956. On the dispersion of a solute in a fluid flowing through a tube. Proc. R. Soc. London, Ser. A 235, 67-77.

Bear, J. Dynamics of Fluids in Porous Media. American Elsevier, New York, 1972.

Bear, J., Todd, D.K., 1960. The transition zone between fresh and salt waters in coastal aquifers. University of California, Water Resources Center Contrib. 29.

Blackwell, R.J., 1959. Experiments on mixing by fluid flow in porous media. Proceedings of Amer. Inst. Chem. Eng. and Soc. Petrol. Eng. 29.

Boving, T.B., Grathwohl, P., 2001. Tracer diffusion coefficients in sedimentary rocks: correlation to porosity and hydraulic conductivity. J. Contam. Hydrol. 53(1-2), 85-100.

Brown, R., 1828. A brief account of microscopical observations. Philos. Mag. 4, 161-173.

Carslaw and Jaeger (eds.), 1986. Conduction of Heat in Solids (Second Edition). Claredon Press, Oxford.

Cirpka, O.A., Frind, E.O., Helmig, R., 1999. Numerical simulation of biodegradation controlled by transverse mixing. J. Contam. Hydrol. 40, 159-182.

Cirpka, O.A., Attinger, S., 2003. Effective Dispersion in Heterogeneous Media under Random Transient Flow Conditions. Water Res. Res. 39(9), 1257.

Crank, J., 1964. The mathematics of diffusion (Third Edition). Clarendon Press, Oxford.

Dagan, G. 1982. Stochastic modeling of groundwater flow by unconditional and conditional probabilities 2: The solute transport. Water Resour. Res. 18, 835-848.

Dagan, G. 1984. Solute transport in heterogeneous porous formations. J. Fluid Mech. 145, 151-177.

Darcy, H., 1856. Les Fontaines Publiques de la Ville de Dijon. Victor Dalmont, Paris.

Davis, G.B., Barber, C., Power, T.R., Thierrin, J., Patterson, B.M., Rayner, J.L., Wu, Q., 1999. The variability and intrinsic remediation of a BTEX plume in anaerobic sulphate-rich groundwater. J. Contam. Hydrol. 36, 265-290.

de Josselin de Jong, G., 1958. Longitudinal and transverse diffusion in granular deposits. Transactions of the American Geophysical Union 39, 67-74.

Deutsch, D.H., 1991. Did Robert Brown observe Brownian Motion: probably not. Bulletin of the American Physical Society 36(4), 1374.

Einstein, A., 1905a. Zur Elektrodynamik bewegter Krper. Annalen der Physik 17, 37-65.

Einstein, A., 1905b. Does the Inertia of a Body Depend on its Energy Content?. Annalen der Physik 18, 639-641.

Fetter, C.W., 1993. Contaminant Hydrology. Macmillan Pub. Co., New York.

Fick, A., 1855. Ueber diffusion. Ann. Phys. Chem. 59.

Fick, A., On liquid diffusion, Philos. Mag. J. Sci. 10, 31.

Ford, B.J., 1982. The Restoration of Brown's first Botanical Microscope. Microscopy 34, 406-418.

Ford, B.J., 1992. Brownian movement in clarkia pollen: A reprise of the first observations. The Microscope 40(4), 235-241.

Ford, B.J., 1992. The Controversy of Robert Brown and Brownian Movement. Biologist 39(3), 82-83.

Fourier, J.B.J., 1822. Théorie Analytique de la Chaleur. F. Didot, Paris.

Freeze, R.A., Cherry, J.A., 1979. Groundwater. Prentice Hall, Inc.

Fried, J.J., Combarnous, M.A., 1971. Dispersion in Porous Media. Advances in Hydroscience 7, 169-282.

Gelhar, L.W., Gutjahr, A.L., Naff, R.L., 1979. Stochastic analysis of macrodispersion in a stratified aquifer. Water Resour. Res. 15, 1387-1397.

Gelhar, L.W., Axness, C.L., 1983. Three-dimensional stochastic analysis of macrodispersion in aquifers. Water Resour. Res. 19(2), 161-180.

Ginn, T.R., Simmons, C.S., Wood, B.D., 1995. Stochastic-convective transport with nonlinear reaction: Biodegradation with microbial growth. Water Resour. Res. 31(11), 26892700.

Graham, T., 1850. On the Diffusion of Liquids. Philosophical Transactions of the Royal Society 140, 146.

Gramling, C.M., Harvey, C.F., Meigs, L.C., 2002. Reactive transport in porous media: A comparison of model prediction with laboratory visualization. Environmental Science and Technology 36(11), 2508-2514.

Grane, F.E., Gardner, G.H.F., 1961. Measurements of transverse dispersion in granular media. J. Chem. Eng. Data 6(2), 283-287.

Gunn, D.J., Pryce, C, 1969. Dispersion in packed beds Trans. Int. Chem. Engrs. 47, 341-350.

Han, N., Bhakta, J., Carbonell, R.G., 1985. Longitudinal and Lateral Dispersion in Packed Beds: Effect ofColumn Length and Particle Size Distribution. AIChE Journal 31, 277-288.

Harleman, D.R.F., Rumer, R.R., 1963. Longitudinal and lateral dispersion in an isotropic porous medium. J. Fluid Mech. 16, 385-394.

Hassanizadeh, S.M., 1996. On the Transient Non-Fickian Dispersion Theory. Transport in Porous Media 23, 107-124.

Huang, W.E., 2002. The role of transverse mixing of electron acceptors and carbon substrates in natural attenuation. PhD thesis, University of Sheffield, Sheffield.

Kapoor, V., Gelhar, L.W. , Miralles-Wilhelm, F., 1997. Bimolecular second order reactions in spatially varying flows: Segregation induced scale-dependent transformation rates. Water Resour. Res. 33(4), 527-536.

Kemblowski, M.W., Chang, C.M., Kamil, I., 1997. A mean behavior model of aerobic biodegradation in heterogeneous formation. Stochastic Hydrol. Hydraul. 11, 255-266.

Klenk, I.D., Grathwohl, P, 2002. Transverse vertical dispersion in groundwater and the capillary fringe. J. Contam. Hydrol. 58, 111-128.

Michaelis, L., Menton, M.M.L., 1913. Die Kinetik der Invertinwerkung. Biochemische Zeitschrift 49.

Miralles-Wilhelm, F., Gelhar L.W., Kapoor, V., 1997. Stochastic analysis of oxygen-limited biodegradation in three-dimensionally heterogeneous aquifers. Water Resour. Res. 33(6), 1251-1263.

Neuman, S.P., Winter, C.L., Neuman, C.N., 1987. Stochastic theory of field scale Fickian dispersion in anisotropic porous media. Water Res. Resour. 23(3), 453-466.

Olsson, Å.H., 2005. Investigation and modelling of dispersion-reaction processes in natural attenuation groundwater. PhD thesis, Eberhard-Karls Universität of Tübingen, Tübingen.

Oya, S., Valocchi, A.J., 1998. Analytical approximation of biodegradation rate for in situ bioremediation of groundwater under ideal radial flow conditions. J. Cont. Hydrol. 31, 275-293.

Perrin, J.B., 1909. Mouvement brownien et réalité moléculaire. Annales de Chimie et de Physique 18, 5-114.

Person, M., Raffensperger, J.P., Garven, G., 1996. Basin-scale hydrogeologic modeling. Reviews in Geophysics 34, 61.

Pickens, J.F., Grisak, G.E., 1981a. Scale-dependent dispersion in a stratifiedgranular aquifer. Water Resour. Res. 17(4), 1191-1211.

Prommer, H., 2002. PHT3D: A Reactive Multicomponent Transport Model for Saturated Porous Media, User's Manual Version 1.0. Contaminated Land Assessment and Remediation Research Centre, The University of Edinburgh.

Saffman, P.G., 1959. A theory of dispersion in a porous medium. Journal of Fluid Mechanics 6(3), 321349.

Scheidegger, A.E., 1954. Statistical hydrodynamics in porous media. J. Appl. Phys. 25(8), 994-1001.

Semprini, L. McCarty, P.L., 1991. Comparsion between model simulation on field results for in-situ biorestoration of chlorinated aliphatics: Part 1. Biostimulation of the methanotrophic bacteria. Groundwater 29(3), 365-374.

Steefel, C.L., MacQuarrie, K.T.B., 1996. Approaches to modelling of reactive transport in porous media. In Reactive Transport in Porous Media, Reviews in Mineralogy 34, 83-129.

Stokes, R.H., 1950. An Improved Diaphragm-Cell for Diffusion Studies, and some Tests of the Method. J. Amer. Chem. Soc. 72(1), 763-767.

Sudicky, E.A., Cherry, J.A., 1979. Field observations of tracer dispersion under-natural flow conditions in an unconfined sandy aquifer. Water Pollut. Res. Can. 14, 1-17.

Taylor, G., 1953. Dispersion of soluble matter in solvent flowing slowly through a tube. Proc. R. Soc. Ser. A 219, 186-203.

Vermolen, F., 2005. Introduction into Numerical Modelling: The Finite Element Method, Delft University of Technology.

Chapter 3

Effects of Hydrodynamic Dispersion on Plume Lengths for Instantaneous Bimolecular Reactions [1]

Abstract. In this article a new two-dimensional analytical model is presented, which explores the effects of longitudinal (α_l) and transverse (α_t) dispersivity on the transient and steady-state length of a plume undergoing an instantaneous bimolecular reaction. A solute B is injected into a steady, uniform flow field in a homogeneous porous medium initially filled with a solute A. Mixing of the solutes occurs only through longitudinal and transversal dispersion and reaction between the solutes is assumed to occur where both solutes are simultaneously present. Explicit steady-state solutions (in the limit $t \rightarrow \infty$) are presented, which describe the distributions of reactants and products in $x - y$ space in the form of the modified Bessel function of zero order and second kind. When $\alpha_t \leq \alpha_l \leq 10\ \alpha_t$, i.e., limits typically used in practical engineering scenarios, the steady-state length of a contaminant plume is obtained as a simple algebraic expression including α_t; the influence of α_l upon plume length being negligible. This phenomenon has been observed experimentally and in numerical simulations. The analysis provided in this paper proves that this behavior follows directly from the governing equations. In addition, the effects of hydrodynamic dispersion on the transient plume development are investigated. The assumption that α_l is only important

[1] Ham, P.A.S., Schotting, R.J., Prommer, H., Davis, G.B., 2004. *Advances in Water Resources Research.* 27, 803-813.

for the transient development of the plume is verified through the use of a numerical solution.

3.1 Introduction

Transversal mixing of reactants through dispersion and diffusion is thought to be the controlling process for natural attenuation and also for enhanced attenuation of organic and other contaminants (Cirpka *et al.*, 1999). After an initial phase during which a contaminant plume develops and expands, the plume length stabilises once the overall mass removal rate through biodegradation matches the rate of contaminant release at the source. When this occurs, transversal mixing through hydrodynamic dispersion appears to be the dominant mechanism for the supply of electron acceptors, or growth limiting nutrients, to plumes of biodegradable, oxidisable organic compounds (Grathwohl *et al.*, 2000; Klenk & Grathwohl, 2002). Laboratory-scale experimental studies involving two reacting solutes clearly suggest the existence of an empirical relationship between plume length and transversal dispersivity (Grathwohl *et al.*, 2001). Conversely, longitudinal dispersion seems to have little effect on overall mass removal rates (Borden & Bedient, 1986).

Both analytical and numerical models are available and are routinely used to mathematically describe the coupled transport and reactive processes of contaminant plumes (Barry *et al.*, 2002), depending on the complexity of the underlying hydrogeochemical and/or hydrogeological conceptual model. Practical applications of such models, in particular of the BIOPLUME code (Borden & Bedient, 1986; Borden *et al.*, 1986) but also the RT3D code (Clement, 2002; Lu *et al.*, 1999) and, for more complex geochemical settings, the PHT3D code (Prommer *et al.*, 2003, 2002) have been most commonly devoted to cases where aromatic hydrocarbons, acting as electron donors (ED), biodegrade in the presence of one or more electron acceptors (EA).

The kinetics of the biodegradation reaction between ED and EA can be described for example by the Michaelis-Menten model (Michaelis & Menten, 1913)

$$\frac{\partial C_{ED}}{\partial t} = k_m \frac{C_{ED}}{(K_{ED} + C_{ED})} \frac{C_{EA}}{(K_{EA} + C_{EA})}, \tag{3.1}$$

where k_m is a reaction rate constant, C_{ED} and C_{EA} are the concentrations of the ED and EA, and K_{ED} and K_{EA} are the half saturation constants for the ED

and EA. However, if the above reaction is assumed to proceed rapidly (compared to transport), the so-called instantaneous reaction model is considered to be an efficient alternative (Barry *et al.*, 2002; Borden & Bedient, 1986), i.e.,

$$\begin{aligned}
\frac{\partial C_{EA}}{\partial t} &= -\frac{Y_{EA}}{Y_{ED}}\frac{C_{ED}}{\Delta t} \quad \text{for} \quad C_{ED} \leq \frac{Y_{ED}}{Y_{EA}} C_{EA}, \\
\frac{\partial C_{EA}}{\partial t} &= -\frac{C_{EA}}{\Delta t} \quad \text{for} \quad C_{ED} > \frac{Y_{ED}}{Y_{EA}} C_{EA}; \\
\frac{\partial C_{ED}}{\partial t} &= -\frac{C_{ED}}{\Delta t} \quad \text{for} \quad C_{ED} \leq \frac{Y_{ED}}{Y_{EA}} C_{EA}, \\
\frac{\partial C_{ED}}{\partial t} &= -\frac{Y_{ED}}{Y_{EA}}\frac{C_{ED}}{\Delta t} \quad \text{for} \quad C_{ED} > \frac{Y_{ED}}{Y_{EA}} C_{EA},
\end{aligned} \tag{3.2}$$

where Y_{EA} and Y_{ED} are the stoichiometric coefficients for the EA and ED respectively and Δt is a timestep length.

To determine the range of validity of the instantaneous reaction model in comparison with a kinetic model, Koussis *et al.* (2003) have conducted a detailed theoretical and numerical analysis. The work concludes that generally the application of the instantaneous reaction assumption is appropriate, and significant differences can only be expected (i) in the initial period of contaminant plume development, and (ii) close to the contamination source. Thus, the necessity of applying a kinetic modelling approach might be limited to cases where high flow velocities occur, such as with some enhanced remediation technologies. Huang *et al.* (2003) came to similar conclusions, based on their numerical analysis of an experiment where a constant acetate (point) source was degraded aerobically.

With respect to analytical models, closed form solutions have been traditionally employed to solve the governing advection-diffusion equation, sometimes including sorption and/or biodegradation (i.e., decay) terms, e.g. Bear (1972); Wilson & Miller (1976); Domenico (1987), to list but a few. Those solutions can be used to describe the transport and reaction of a single ED. However, such solutions always neglect the dependency of the ED removal rate on the presence of other reactants, in particular of EA concentrations. In the absence of an analytical solution, Borden *et al.* (1986) used a superposition of the independent solutions for non-reactive transport of each solute (EA and ED) to determine concentrations of the reactants. This however can become a cumbersome approach when used to determine the distance (i.e., plume length) at which pre-defined concentration

levels are reached. Despite the attention that this type of problem has received and despite its practical relevance, there is no evidence in the literature of the derivation of an analytical solution. The analysis of the governing equations in this article provides the 'missing' mathematical proof.

3.2 Problem Statement

A bimolecular chemical reaction is considered between two aqueous species that goes to completion, i.e.,

$$Y_1 A + Y_2 B \rightarrow A_{Y_1} B_{Y_2}, \tag{3.3}$$

where Y_1 and Y_2 are stoichiometric coefficients. For simplicity, the bimolecular reaction (3.3) is initially considered to be stoichiometrically equivalent, i.e., $Y_1 = Y_2 = 1$. At time $t = 0$ the two dimensional domain Ω (infinite in x and y) contains only solute A which has a constant concentration C_A throughout the domain. At a point (x_0, y_0), solute B is injected into the flow domain with constant mass flow rate $Q * {C_B}^o$, where Q $[L^2T^{-1}]$ is the injection flow rate and ${C_B}^o$ $[ML^{-2}]$ denotes the concentration of injected solute B. The flow field in Ω is constant and uniform, such that $\mathbf{q} = (q_x, 0)$, where q_x $[LT^{-1}]$ denotes the specific discharge in the positive $x-$direction. Figure 3.1(A) is a schematic representation of the problem definition. Figure 3.1(B) represents qualitatively the expected concentration contours of solute B, whereby concentrations decrease with increasing distance from the injection point (x_0, y_0). For the bimolecular reaction considered here, the rate

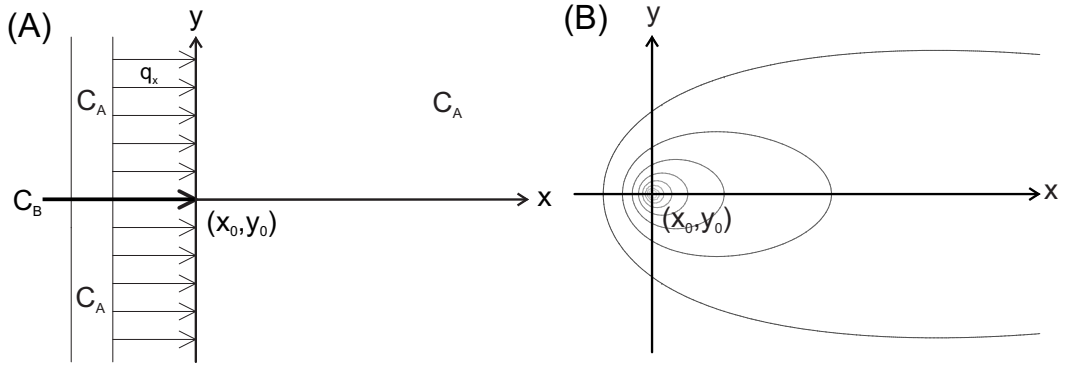

Figure 3.1: *Domain Ω: (A) Problem definition, and (B) Expected contour distributions of solute B.*

of production of AB (r_{AB}) at any point in the flow domain is equal to the rate of loss of each reactant (r_A, r_B), implying

$$r_{AB} = -r_A = -r_B. \tag{3.4}$$

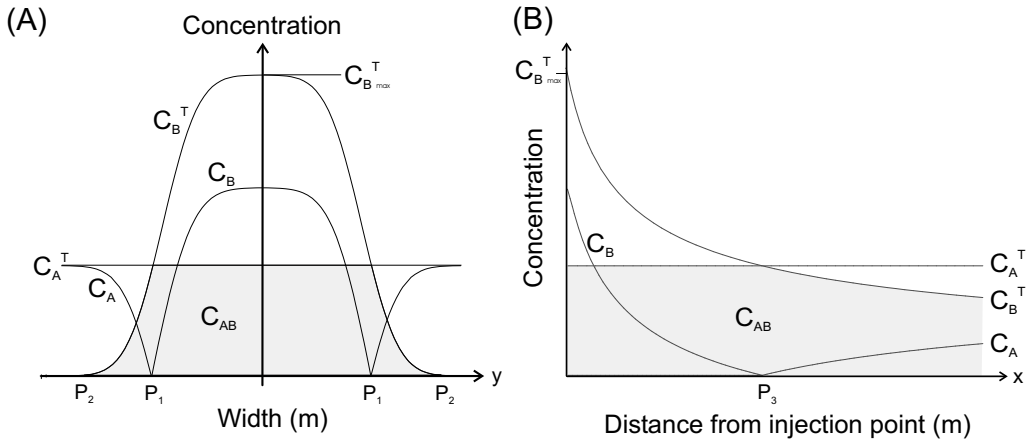

Figure 3.2: *Idealised profiles of components and species across the reactive fringe for a cross section, (A) across the plume down gradient of the source, and (B) along the plume.* ${C_A}^T$ *and* ${C_B}^T$ *denote the total aqueous component concentration of A and B respectively,* C_A, C_B *and* C_{AB} *denote the concentrations of species A, B and AB; points* P_1 *and* P_2 *denote the inner and outer boundaries of the plume fringe in the* $y-$*direction and point* P_3 *denotes the inner boundary in the* $x-$*direction respectively.* ${C_B}^T{}_{max}$ *is the concentration a small distance from the source where* ${C_B}^T$ *is assumed to be at a maximum.*

In accordance with the instantaneous reaction model (3.2), and consistent with the work of Gramling *et al.* (2002), the reaction (3.3) is assumed to occur at all locations where both solutes A and B coexist. In Figure 3.2 the profiles through an idealised cross-section along both the x- and y-axis for this problem are considered. As illustrated, either reactant A or B is the limiting reactant depending on the location at which the reaction is taking place, typically in this case on the plume fringe. From Figure 3.2(A), $C_{AB} = {C_A}^T$ for $|y| < P_1$ and $C_{AB} = {C_B}^T$ for $|y| > P_1$. Note also that the point P_1 is the inner boundary of the plume fringe, where the concentrations of C_A and C_B are identically zero. In Figure 3.2(A), P_2 represents the outer boundary of the fringe, i.e., where ${C_B}^T \approx 0$ and $C_A \approx {C_A}^T$.

3.3 Model Equations, Boundary and Initial Conditions

The mass-balance equations for species A and B are given by

$$n\frac{\partial C_A}{\partial t} + q_x\frac{\partial C_A}{\partial x} - \alpha_l q_x\frac{\partial^2 C_A}{\partial x^2} - \alpha_t q_x\frac{\partial^2 C_A}{\partial y^2} + r_{AB} = 0, \tag{3.5}$$

$$n\frac{\partial C_B}{\partial t} + q_x\frac{\partial C_B}{\partial x} - \alpha_l q_x\frac{\partial^2 C_B}{\partial x^2} - \alpha_t q_x\frac{\partial^2 C_B}{\partial y^2} + r_{AB} = 0, \tag{3.6}$$

and for product AB

$$n\frac{\partial C_{AB}}{\partial t} + q_x\frac{\partial C_{AB}}{\partial x} - \alpha_l q_x\frac{\partial^2 C_{AB}}{\partial x^2} - \alpha_t q_x\frac{\partial^2 C_{AB}}{\partial y^2} - r_{AB} = 0. \tag{3.7}$$

Here, n denotes porosity and α_l and α_t are the longitudinal and transversal dispersion lengths (or dispersivities) respectively; assumed constant and equal for all species present in the uniform flow field. Equations (3.5-3.7) assume that both transversal and longitudinal dispersion can be modelled as a product of the specific discharge q_x and the appropriate dispersion length (α_l or α_t). Adding the mass balance equations (3.6) and (3.7) yields

$$n\frac{\partial {C_B}^T}{\partial t} + q_x\frac{\partial {C_B}^T}{\partial x} - \alpha_l q_x\frac{\partial^2 {C_B}^T}{\partial x^2} - \alpha_t q_x\frac{\partial^2 {C_B}^T}{\partial y^2} = 0, \tag{3.8}$$

where ${C_B}^T = {C_B}^T(x,y,t) = C_B(x,y,t) + C_{AB}(x,y,t)$ denotes the combined concentrations of species B and AB, i.e., the total aqueous concentration of species B in domain Ω.

Introducing the dimensionless parameters

$$x^* = \frac{x}{\alpha_l}, \;\; y^* = \frac{y}{\alpha_l}, \;\; \text{and} \;\; q^* = \frac{q_x}{q_o}, \tag{3.9}$$

and substituting these into (3.8) gives

$$n\frac{\partial {C_B}^T}{\partial t} + \frac{q_o q^*}{\alpha_l}\frac{\partial {C_B}^T}{\partial x^*} - \frac{q_o q^*}{\alpha_l}\frac{\partial^2 {C_B}^T}{\partial x^{*2}} - \frac{q_o q^* \alpha_t}{{\alpha_l}^2}\frac{\partial^2 {C_B}^T}{\partial y^{*2}} = 0. \tag{3.10}$$

Multiplying (3.10) by α_l/q_o, introducing the dimensionless parameter $t^* = tq_o/n\alpha_l$ and the new variable $\beta = \alpha_t/\alpha_l$, and dropping the * notation for convenience yields

$$\frac{\partial {C_B}^T}{\partial t} + q\frac{\partial {C_B}^T}{\partial x} - q\frac{\partial^2 {C_B}^T}{\partial x^2} - \beta q\frac{\partial^2 {C_B}^T}{\partial y^2} = 0, \tag{3.11}$$

i.e., the mass balance equation for ${C_B}^T$ in dimensionless notation. The uniform flow field infers $q_o = q_x$, implying $q^* = 1$. Introducing the moving coordinate $s(x,t) = x - t$ such that ${C_B}^T(x,y,t) = {C_B}^T(s(x,t),y,t)$ gives

$$\frac{\partial {C_B}^T}{\partial t} = \frac{\partial^2 {C_B}^T}{\partial s^2} + \beta\frac{\partial^2 {C_B}^T}{\partial y^2}, \tag{3.12}$$

which will be the starting point for further analysis.

The initial condition is given by

$${C_B}^T(s,y,0) = 0 \text{ for all } (s,y) \in \mathbf{R}, \tag{3.13}$$

implying

$${C_A}^T(s,y,0) = C_A(s,y,0) = C_o \text{ for all } (s,y) \in \mathbf{R}. \tag{3.14}$$

At a point (x_0, y_0) reactant B is continuously injected, such that

$$M = M(t) = \int_0^t Q{C_B}^o \, dt, \tag{3.15}$$

where M $[M]$ denotes the injected mass of solute ${C_B}^o$ and Q is the injection flow rate. Introducing the parameter $\bar{M} = \frac{M}{(\alpha_l)^2}$, substituting in (3.15), and rewriting using dimensionless time, yields

$$\bar{M} = \bar{M}(t) = \int_0^{t^*} Q{C_B}^o \cdot \frac{n}{\alpha_l q_0} \, dt^* = \int_0^{t^*} Q^*{C_B}^o \, dt^*, \tag{3.16}$$

which implies $Q^* = \frac{Qn}{\alpha_l q_0}$.

3.4 Solution Procedure

First consider instantaneous injection of a constant mass $\bar{M}$ at the origin $(0,0)$. In this case the fundamental solution of (3.12), using dimensionless notation, is given by Crank (1964) *Eqn. 3.4*

$$C_B{}^T(s,y,t) = \frac{\bar{M}}{4\pi\sqrt{\beta}}\frac{1}{t}e^{-\frac{s^2}{4t}-\frac{y^2}{4\beta t}}. \tag{3.17}$$

Next consider continuous injection at the origin, such that

$$d\bar{M} = Q^* C_B{}^o \, dt. \tag{3.18}$$

The change in concentration due to the instantaneous injection of an infinitesimally small mass $d\bar{M}$ follows directly from (3.17), yielding

$$dC_B{}^T(s,y,t) = \frac{d\bar{M}}{4\pi\sqrt{\beta}}\frac{1}{t}e^{-\frac{s^2}{4t}-\frac{y^2}{4\beta t}}. \tag{3.19}$$

For continuous injection over the time interval $(0,t)$, (3.18) can be substituted into (3.19) and integrated to give

$$C_B{}^T(s,y,t) = \frac{C_B{}^o Q^*}{4\pi\sqrt{\beta}}\int_0^t \frac{1}{(t-\tau)}e^{-\frac{s^2}{4(t-\tau)}-\frac{y^2}{4\beta(t-\tau)}}d\tau, \tag{3.20}$$

where τ is the integration variable. Next, set $\xi = t-\tau$. The integral (3.20) can be recast as

$$C_B{}^T(x,y,t) = -\frac{C_B{}^o Q^*}{4\pi\sqrt{\beta}}\, e^{\frac{x}{2}} \int_0^t \frac{1}{\xi}e^{-\frac{A_1(s,y)}{\xi}-B_1\xi}\, d\xi, \tag{3.21}$$

where $A_1(x,y)$ and B_1 are respectively given by

$$A_1(x,y) = \frac{\beta x^2 + y^2}{4\beta} \quad \text{and} \quad B_1 = \frac{1}{4}. \tag{3.22}$$

Equation (3.21) becomes

$$C_B{}^T = -\frac{F}{2\sqrt{\beta}}\, e^{\frac{x}{2}} \int_0^t \frac{1}{\xi}e^{-\frac{A_1(s,y)}{\xi}-B_1\xi}\, d\xi, \tag{3.23}$$

where one obtains $F = \frac{nC_B{}^oQ}{2\pi q_o \alpha_l}$. In the limit $t \to \infty$, (3.23) reduces to the stationary concentration distribution, given by Gradshteyn & Ryzhik (1979) *Eqn. 3.471(9)*,

$$C_B{}^T = \frac{F}{\sqrt{\beta}} e^{\frac{x}{2}} K_0(2\sqrt{A_1 B_1}), \tag{3.24}$$

where K_0 denotes the modified Bessel function of zero order and second kind. Using the original dimensionless variables

$$C_B{}^T(x^*, y^*, \infty) = \frac{F}{\sqrt{\beta}} e^{\frac{x^*}{2}} K_0 \left(\frac{1}{2} \sqrt{\left(x^{*2} + \frac{y^{*2}}{\beta} \right)} \right). \tag{3.25}$$

The solution procedure implies that an infinite concentration of component B ($C_B{}^T$) is located at the point of injection. Physically this is unrealistic, however mathematically the assumption of a finite mass (although an infinite concentration at the origin) allows the derivation of an explicit solution (3.25) to the problem using the fundamental solution. The solution (3.25) of $C_B{}^T$ is therefore not representative of a physical situation, as $(x, y) \longrightarrow (0, 0), C_B{}^T \longrightarrow \infty$. However these non-physical effects occur only in close proximity to the origin, not at other parts of the domain. Clearly, further solutions of (3.12) can be obtained by differentiating or integrating the fundamental solution with respect to either x or t (Carslaw & Jaeger, 1986).

3.5 Concentration Distributions and Profiles

In this section it is, through the use of an example, demonstrated how concentration distributions and profiles of the non-reactive solutes, reactive solutes and products can be obtained. It follows, as previously stated, from mass balance (see also Figure 3.2) that

$$\begin{aligned} C_{AB} &= C_B{}^T \ \text{ for } \ P_3 \leq x < \infty, \\ C_{AB} &= C_A{}^T \ \text{ for } \ 0 \leq x \leq P_3; \end{aligned} \tag{3.26}$$

$$\begin{aligned} C_A &= C_A{}^T - C_{AB} \ \text{ for } \ P_3 \leq x < \infty, \\ C_B &= C_B{}^T - C_{AB} \ \text{ for } \ 0 \leq x \leq P_3. \end{aligned} \tag{3.27}$$

Since ${C_B}^T/{C_B}^T{}_{max}$ is not well defined close to the origin $(0,0)$, the solution is manipulated to disregard these non-physical effects, i.e., profiles of ${C_B}^T(x,0,\infty)/$ ${C_B}^T{}_{max} > 1$ are ignored. Selecting the parameter values $n = 0.3$, $q_0 = 1\ m/d$, $\alpha_l = \alpha_t = 0.05\ m$, ${C_A}^T = 0.0003\ mol/l$, $Q = 1\ m^2/d$ and ${C_B}^o = 0.002\ mol/l$, substituting them into equation (3.25), and applying conditions (3.26-3.27) gives the results displayed in Figure 3.3. Note that ${C_B}^T$ rapidly declines within a short distance downstream of the point source. The product AB is found wherever ${C_B}^T$ and ${C_A}^T$ are simultaneously present, i.e., the concentration profile of $C_{AB}(x,0,\infty) = {C_B}^T(x,0,\infty)$ for $P_3 \leq x < \infty$ in Figure 3.3. The distance from the origin to the point P_4, where ${C_B}^T(x,0,\infty)/\ {C_B}^T{}_{max} = 1$, is for the present example given by

$$P_4 \approx 1.57\ m.$$

Therefore, in this profile, interest is limited to solutions of ${C_B}^T(x,0,\infty)$ for values of $x \geq P_4 \approx 1.57\ m$. The value of ${C_B}^T$ for $x \leq P_4 \approx 1.57\ m$ is taken to be $0.002\ mol/l$. The nature of the instantaneous reaction means that there is instant degradation of species B at $x = 0$. Therefore the value of C_B for $x \leq P_4 \approx 1.57\ m$ is easily calculated to be $0.00017\ mol/l$ $({C_B}^T - {C_A}^T)$. Likewise, point P_3, where reactants B and A are zero, can be determined by solving equation (3.26), i.e., obtaining the solution in x for ${C_B}^T(x,0,\infty) = {C_A}^T(x,0,\infty)$. This represents the length of the plume, after which species B has been completely degraded. It follows from evaluation of (3.25) that the value of P_3

$$P_3 \approx 70.70\ m.$$

In order to validate these results, a comparison was undertaken with PHT3D (Prommer *et al.*, 2003), a verified reactive transport model. PHT3D combines the transport simulator MT3DMS (Zheng & Wang, 1999) with the geochemical model PHREEQC-2 (Parkhurst & Appelo, 1999) to simulate reactive transport in saturated porous media. The reaction (3.3) was included into the reaction database as a complexation between A and B ($\log K$ =20). The domain in the numerical model consists of 5500 grid cells and has an extension of 190 m (in flow direction) by 25 m. A discretisation perpendicular to the flow Δy of 1 m and a varying discretisation in the direction of the flow Δx ($\Delta x_{min} = 0.1\ m$, $\Delta x_{max} = 1\ m$), was used in conjunction with the afore selected hydrological parameters. A steady-

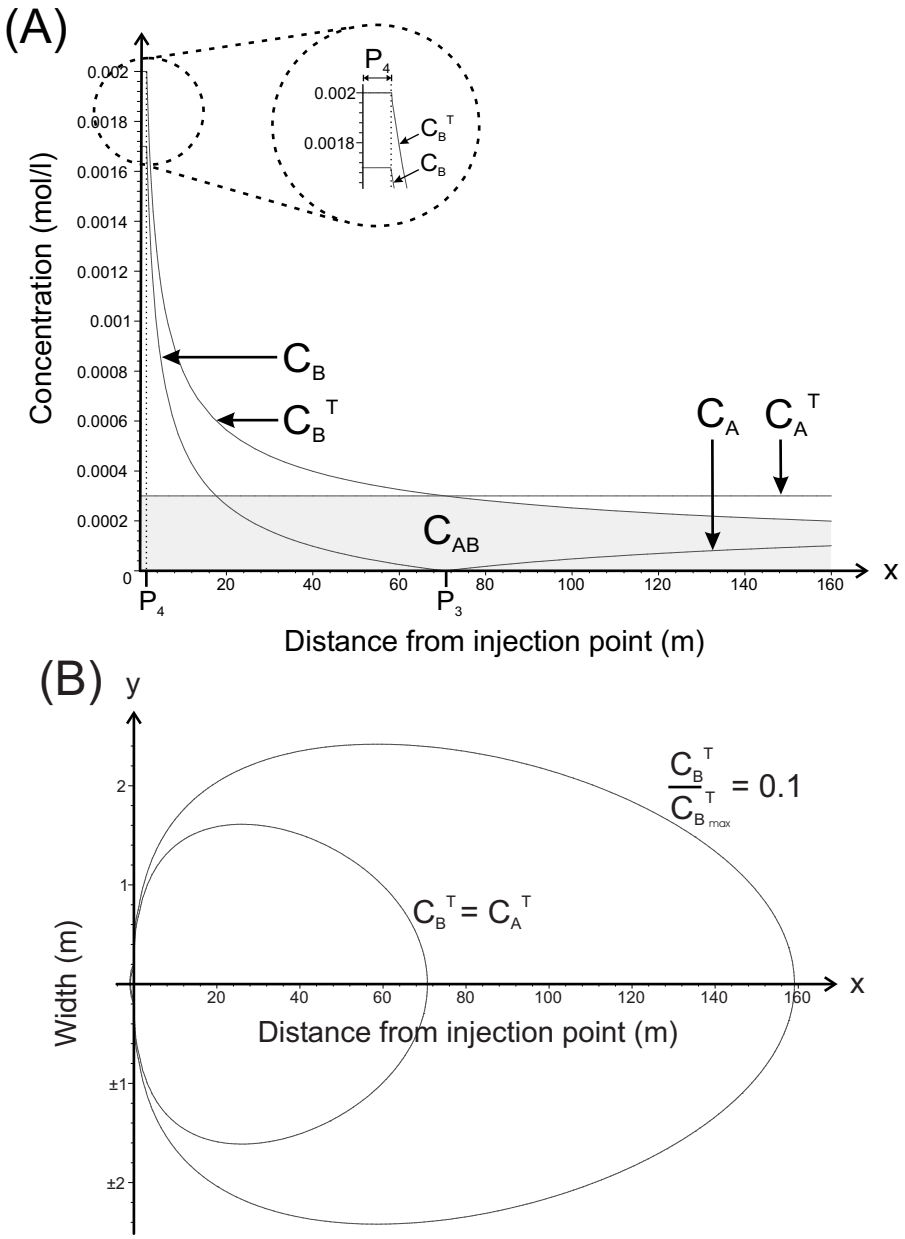

Figure 3.3: *(A) Profiles of non-reactive and reactive species along $x-$axis, and (B) Distribution of non reactive species B ($C_B{}^T(x, y, \infty) = C_A{}^T$ and $C_B{}^T(x, y, \infty)/C_B{}^T{}_{max} = 0.1$) in domain Ω.*

state flow field was induced in the model using a *Neumann* boundary condition at the upstream boundary and fixed head cells (*Dirichlet* boundary condition) at the downstream boundary. A mass transfer rate equal to $Q * {C_B}^o$ $[MT^{-1}]$ was realised through the use of the mass-loading feature of the transport model (Zheng & Wang, 1999) to mimic the injection of solute B into the flow domain without disturbance of the parallel flow. The concentration of solute A was selected to be ${C_A}^T = 0.0003$ mol/l throughout the domain. The TVD scheme (Leonard, 1988) was used to solve the advective transport problem and the model was run for a simulation period of 100 *days*, during which steady-state concentration profiles were reached. Figure 3.4 shows block-centered results obtained from the numerical simulation. Comparison of results for $C_B(x, y, \infty)$ shows that the numerical model generates plumes that are only marginally larger than those produced analytically. Figure 3.4 illustrates that discrepancies are largely confined to the source zone, as one might expect.

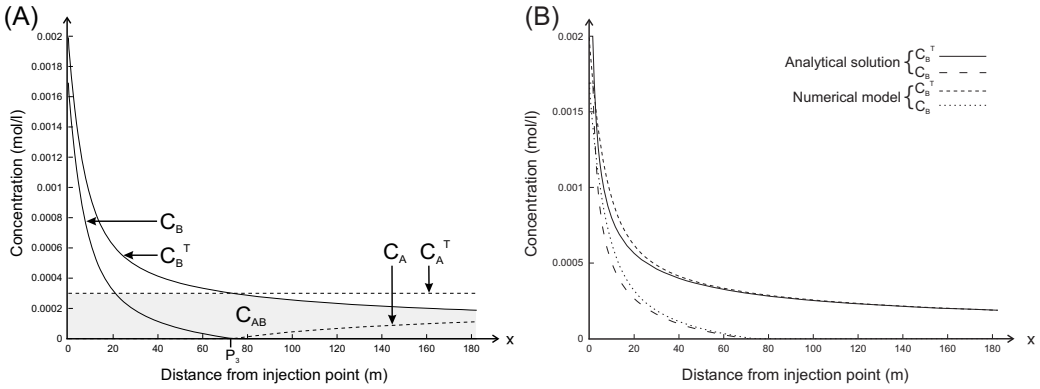

Figure 3.4: *(A) Numerically generated profiles for non-reactive and reactive species along the x-axis, and (B) Comparison of numerical and analytical profiles for component and species B.*

3.6 Plume Length

Generally plume length L might be arbitrarily defined as the length of the plume measured along the x-axis from the origin to a certain concentration contour. In this article the length of the plume is defined as the contour line where all of the species B is degraded, i.e., $C_B(x, y, \infty) = 0$. The nature of the instantaneous reaction means that this point coincides with the solution of ${C_B}^T(L^*, 0, \infty) =$

${C_A}^T(L^*, 0, \infty)$, which leads to the implicit expression

$$ {C_B}^T(L^*, 0, \infty) = \frac{F}{\sqrt{\beta}}\, e^{\frac{L^*}{2}} K_0\left(\frac{L^*}{2}\right) = {C_A}^T(L^*, 0, \infty) = C_o. \tag{3.28} $$

Note that expression (3.28) implicitly defines the relation between plume length L^* and the two dispersion lengths, i.e., $L^* = L^*(\alpha_l, \alpha_t)$. In most cases the argument of the Bessel function in (3.28) will be large, typically because $\alpha_l << L^*$, therefore $K_0(z)$ can be approximated for $2 \leq z < +\infty$ by the series expansion, Abromowitz & Stegun (1964) *Eqn. 9.7.2*,

$$ z^{\frac{1}{2}}\, e^z\, K_0(z) \sim \sqrt{\frac{\pi}{2}} \left(1 - \frac{1}{8z} + \frac{9}{128z^2} + \varepsilon\right), \tag{3.29} $$

where $|\varepsilon| < \frac{75}{1024z^3}$. As a first approximation only the first term on the right-hand side of the series expansion is considered, i.e.,

$$ z^{\frac{1}{2}}\, e^z\, K_0(z) \approx \sqrt{\frac{\pi}{2}}. \tag{3.30} $$

Substitution of this approximation in (3.28) yields

$$ L^* = \frac{L}{\alpha_l} \approx 2 \left(\frac{F}{C_o}\right)^2 \frac{\pi}{2} \cdot \frac{1}{\beta} = \frac{\pi F^2}{{C_o}^2} \cdot \frac{1}{\beta}. \tag{3.31} $$

Simplifying (3.31) gives

$$ L = \frac{n^2 {C_B}^{o2} Q^2}{4\pi {C_o}^2 q_o^2} \cdot \frac{1}{\alpha_t}. \tag{3.32} $$

Note that in this approximation, the plume length L is solely a function of α_t, i.e., independent of the longitudinal dispersion length α_l. The notation β^n is used to represent the ratio of α_t/α_l, where the superscript n represents the value of α_t. Figure 3.5 shows plume length and concentration distributions, as obtained from the exact solution (3.28), for different values of $\beta^{0.05} = \alpha_t/\alpha_l$, using the example previously defined in Section 3.5. In the limit $0.1 \leq \beta^{0.05} \leq 1$, the concentration distributions ${C_B}^T(x, y, \infty) = C_o$ are very similar. In terms of the example used in this paper, plume length is calculated from the exact solution (3.28) $L^{exact} \approx 70.70$ m compared to $L^{zero} \approx 70.73$ m from the zero order solution (3.32). This difference

is illustrated further in Figure 3.6.

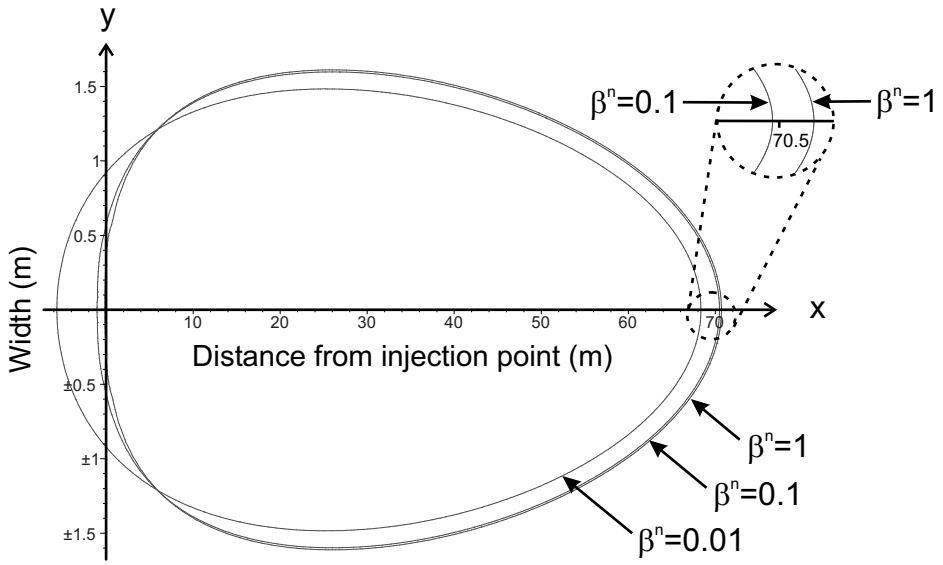

Figure 3.5: ${C_B}^T(x, y, \infty) = C_o$ *contourplots of the exact solution for* $\beta^{0.05} = 1, 0.1$ *and* 0.01.

As a next, more accurate approximation, the second term at the right-hand side of the series expansion for K_0 is included, i.e.,

$$z^{\frac{1}{2}}\, e^z\, K_0(z) \approx \sqrt{\frac{\pi}{2}} \left(1 - \frac{1}{8z}\right). \tag{3.33}$$

Substitution of this approximation into (3.28) gives

$$\frac{\sqrt{\beta} C_o}{F} \left(\frac{L^*}{2}\right)^{\frac{1}{2}} \approx \sqrt{\frac{\pi}{2}} \left(1 - \frac{1}{4L^*}\right), \tag{3.34}$$

or

$$\frac{\beta {C_o}^2}{F^2 \pi}\, L^* - 1 \, + \frac{1}{2L^*} - \frac{1}{16 {L^*}^2} \approx 0. \tag{3.35}$$

Therefore, keeping only the first two terms of the series expansion (i.e., discarding the term in L^2) and multiplying by L^* gives

$$\frac{\beta {C_o}^2}{F^2 \pi}\, {L^*}^2 - L^* \, + \frac{1}{2} = 0. \tag{3.36}$$

The solution of (3.36), i.e., a quadratic algebraic equation, yields

$$L^* = \frac{L}{\alpha_l} = \frac{F^2\pi}{2\beta {C_o}^2}\left\{1 \pm \sqrt{1 - \frac{2\beta {C_o}^2}{F^2\pi}}\right\} \tag{3.37}$$

and explicitly defines $L = L(\alpha_l, \alpha_t)$. Figure 3.6 represents both the zero and first order approximations, together with the exact (Bessel) solution. For values of $0.1 \leq \beta^{0.05} \leq 1$ the zero order approximation (3.32) satisfactorily predicts plume lengths. For $\beta^{0.05} < 0.1$, the difference between the zero order approximation and the exact solution becomes significant and the first order approximation (3.37) provides an excellent estimate of plume length, the difference between the results is barely visible in Figure 3.6; $|\varepsilon| < \frac{9}{128z^2}$. In both the exact solution and first order approximation, as $\beta^{0.05} \to 0, L \to 0$.

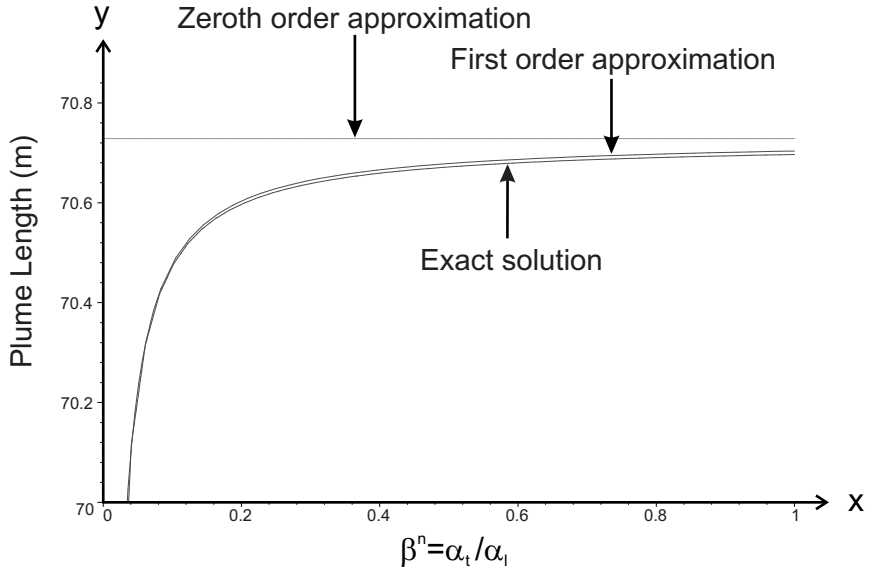

Figure 3.6: *Effect of ratio $\beta^{0.05}$ on plume length.*

3.7 Transient Development of Plume Length

At values of $\beta^{0.05}$ close to 1, the length of a steady-state plume is almost independent of α_l. The assumption therefore is that α_l is only important for the transient development of the plume. In order to verify this assumption, the transient plume is analysed; the starting point for the analysis is the expression that relates $L^*(t)$,

i.e., the length of the plume measured from the injection point at $x = 0$ along the $x-$axis to the ${C_B}^T(L^*(t), 0, t)) = {C_A}^T(L^*(t), 0, t)) = C_o$ concentration contour. This is given by

$$ {C_B}^T(L^*(t), 0, t) = \frac{F}{2 * \sqrt{\beta}} e^{\frac{L^*(t)}{2}} \int_0^t \frac{1}{\xi} e^{-\frac{B_1 {L^*(t)}^2}{\xi} - B_1 \xi} d\xi = C_o. \tag{3.38} $$

This problem can be solved numerically as follows. Equation (3.38) is rewritten as

$$ \int_0^t \frac{1}{\xi} e^{-\frac{B_1 L(t)^2}{\alpha_l^2 \xi} - B_1 \xi} d\xi = \frac{2 C_o \sqrt{\beta}}{F e^{\frac{L(t)}{2\alpha_l}}}. \tag{3.39} $$

The *right hand side* (RHS) of equation (3.39) is simply an algebraic expression and can be solved directly by specifying an appropriate plume length. However, the integral that forms the *left hand side* (LHS) of equation (3.39) is more complicated. Thus, as a first step, the RHS is solved for a segment of size $j * \Delta L$. For the same $j * \Delta L$ the LHS is solved iteratively for small time steps (Δt) and approximated using the trapezium rule. When the LHS is approximately equal to the RHS, the time ($i * \Delta t$) taken to reach the length $j * \Delta L$ is known. Consecutive solutions in this manner can be plotted to produce the transient solution. Figure 3.7 is a schematic representation of this procedure.

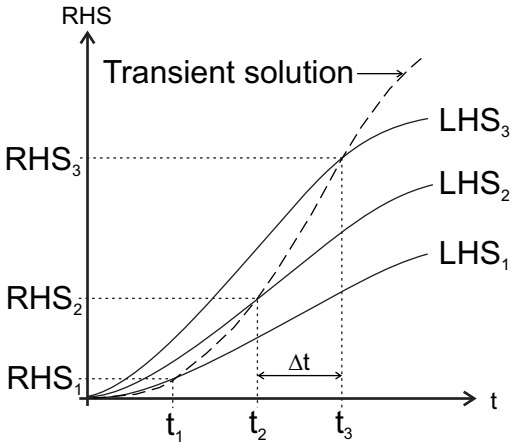

Figure 3.7: *Solution procedure to approximate the transient solution.*

Again, the example outlined in Section 3.5 is used. Equation (3.39) was calculated for $\beta^{0.05} = 1$, 0.1 and 0.01. Figure 3.8 represents the transient development

of the plume. For $1 \geq \beta^{0.05} \geq 0.1$ plume length develops rapidly to an asymptotic

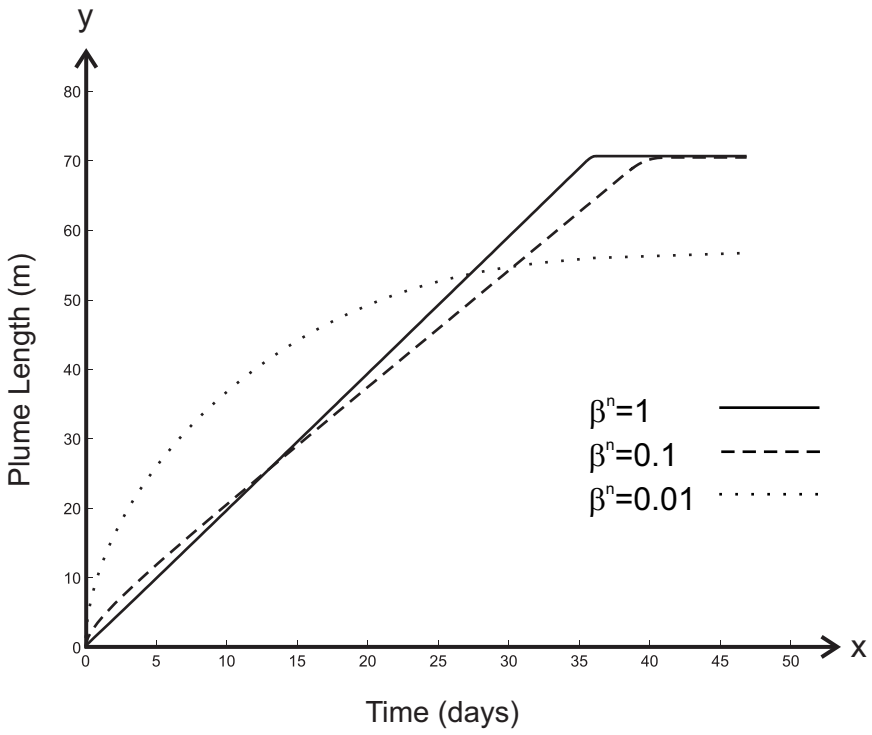

Figure 3.8: *Transient development of plume; results for* $\beta^{0.05} = 1, 0.1$ *and* 0.01.

value; for values of $\beta^{0.05}$ close to unity the initial growth in plume length is almost linear. For smaller values of $\beta^{0.05}$, i.e., $\beta^{0.05} < 0.1$, steady-state plume development is considerably slower. In these cases α_l plays a much more important role and delays the development of the steady-state plume. Note that the asymptotic values, as one might expect, are identical to the results for plume lengths obtained in Section 3.6.

3.8 Sorption

Sorption is a process that effects the transient development of concentration profiles. Sorption of one or more aqueous species results in a retardation of those species and perhaps the reaction products. At steady-state, when the adsorption rate equals the desorption rate at any location within the domain, the effects of sorption cannot be seen. Since it is only possible to derive an explicit analytical solution at steady-state, the numerical model is again used to study the effect of

sorption. Accounting for linear equilibrium sorption, in the mass balance equations yields

$$n\frac{\partial C_A}{\partial t} + \frac{q_x}{R_A}\frac{\partial C_A}{\partial x} - \frac{\alpha_l q_x}{R_A}\frac{\partial^2 C_A}{\partial x^2} - \frac{\alpha_t q_x}{R_A}\frac{\partial^2 C_A}{\partial y^2} + r_{AB} = 0, \tag{3.40}$$

$$n\frac{\partial C_B}{\partial t} + \frac{q_x}{R_B}\frac{\partial C_B}{\partial x} - \frac{\alpha_l q_x}{R_B}\frac{\partial^2 C_B}{\partial x^2} - \frac{\alpha_t q_x}{R_B}\frac{\partial^2 C_B}{\partial y^2} + r_{AB} = 0, \tag{3.41}$$

and for product AB

$$n\frac{\partial C_{AB}}{\partial t} + \frac{q_x}{R_{AB}}\frac{\partial C_{AB}}{\partial x} - \frac{\alpha_l q_x}{R_{AB}}\frac{\partial^2 C_{AB}}{\partial x^2} - \frac{\alpha_t q_x}{R_{AB}}\frac{\partial^2 C_{AB}}{\partial y^2} - r_{AB} = 0, \tag{3.42}$$

where R_A, R_B and R_{AB} are the retardation coefficients of solute A, B and product AB respectively. Only under the assumption that $R_B = R_{AB}$ can a transient solution similar to that presented in (3.23) be produced. Where $R_A \neq R_B \neq R_{AB}$, which would typically be the case, the method presented in Section 3.5 is no longer valid.

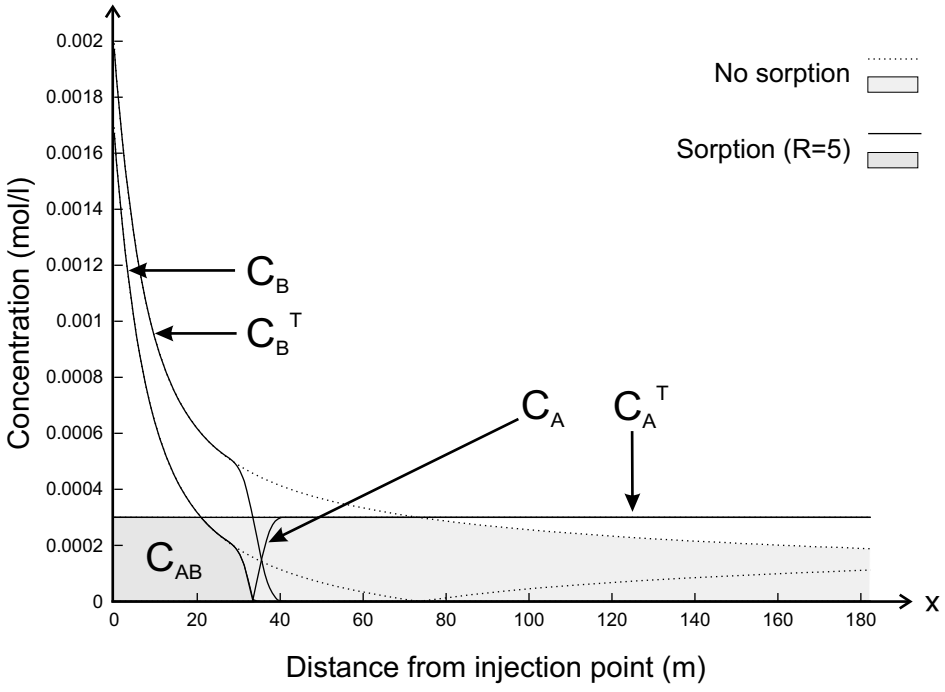

Figure 3.9: *Effect of sorption on concentration profiles*

Figure 3.9 compares the simulated plume development, computed with PHT3D, for sorbing solutes, based on the example outlined in Section 3.5. The solution at steady-state (dotted lines) is shown, the profiles at steady-state being the same for non-sorbing and sorbing cases when $t \rightarrow \infty$. Also presented in Figure 3.9 is a solution for $t = 50$ *days* when the reactive solutes were considered sorbing (continuous lines). A retardation factor $R_{solute} = 5$ was used in the example. The two cases considered were: Solute B only sorbs; both solutes A and B sorb. Note, the solutions at this timestep are still transient, and the plumes have developed approximately 30 m horizontally in both cases. At $x < 30$ m, the solutions are already at the steady-state.

Figure 3.9 demonstrates that if only solute B sorbs, species A is consequently consumed less quickly. The profile ${C_B}^T$ and consequently C_B and C_A, are therefore retarded by $1/R$. Where both solutes A and B sorb, both profiles ${C_A}^T$ and ${C_B}^T$ are retarded by $1/R$. The profile for ${C_A}^T$ appears unaffected of course, the conceptual model stipulating ${C_A}^T$ is constant in time throughout the whole domain. In the numerical simulation, product AB is modelled as a complex of components A and B, and can only form where both ${C_A}^T$ and ${C_B}^T$ are simultaneously present. There is no evidence here that sorption increases/decreases the rate of the bimolecular reaction, only that the reaction front is hindered by the least sorbing solute. The transient development of a sorbing reactant plume can be plotted in the same fashion as that demonstrated in Section 3.7 by simply multiplying the time taken to reach a certain plume length by R_{solute}.

3.9 A Note on β^n

Since β is defined as α_t/α_l, a β value of 1 implies that $\alpha_t = \alpha_l$ and neither the exact value of α_l or α_t is known. The superscript n was introduced to clarify this ratio, but little has been said with respect to its relevance. Figure 3.10 shows the variation of plume length at the stationary condition against values of the transversal dispersivity α_t, using the example previously defined. Figure 3.10 clearly demonstrates that steady-state plume length is much more dependent on α_t than α_l, but also that the plume length is not the same for all β^n values. When $\alpha_t \leq \alpha_l \leq 10\ \alpha_t$, the difference in plume length is minor for all sensible values of n.

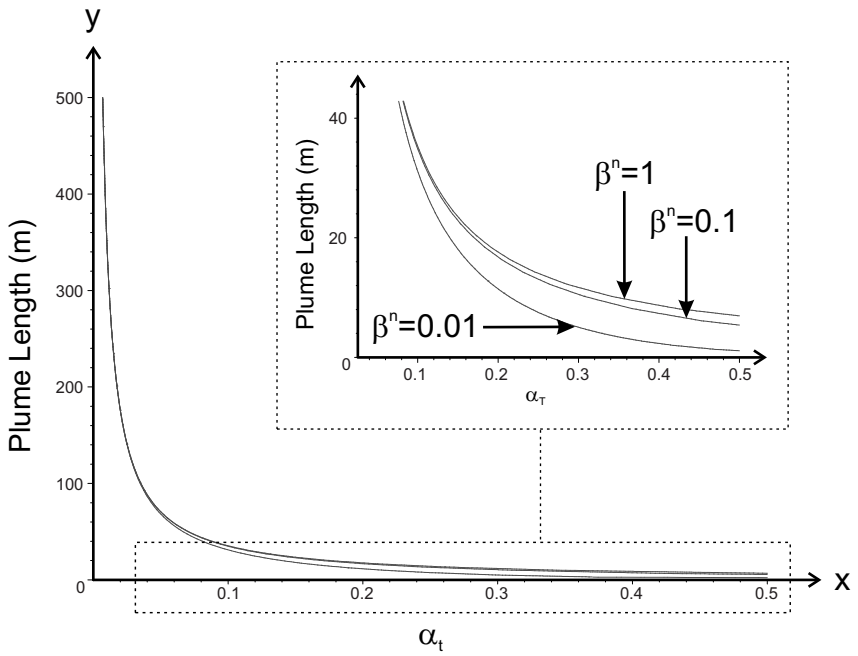

Figure 3.10: *Variation of plume length with value of* α_t.

3.10 Extension for Arbitrary Stoichiometries

So far, the bimolecular reaction (3.3) has been considered to be stoichiometrically equivalent, i.e., $Y_1 = Y_2 = 1$. To be useful for practical cases it is necessary to be able to consider arbitrary stoichiometric relationships. For example in the case of a toluene plume that degrades under sulfate-reducing conditions (Davis *et al.* , 1999; Prommer *et al.*, 2002), the reaction

$$C_7H_8 + 4.5{SO_4}^{2-} + 3H_2O + 2H^+ \rightarrow 7{HCO_3}^- + 4.5H_2S \tag{3.43}$$

delivers $Y_1 = 4.5$ for the EA (sulphate) and $Y_2 = 1$ for the ED (toluene). Addressing this case with the analytical solution presented here is a simple matter of scaling the solution in accordance with the reaction stoichiometry. Therefore, if 4.5 moles of sulphate are required to degrade one mole of toluene, the 'base' solution (3.25) must be scaled by dividing ${C_A}^T$ by 4.5. In this way 4.5 moles of EA are used to degrade every mole of the ED. In terms of the base solution (3.25), the effective molar concentration of the EA is therefore 4.5 times smaller.

3.11 Conclusions

Concentration distributions of reactants and products involved in the simple bimolecular reaction (3.3) anywhere in a two dimensional domain can be modelled using the solution (3.25) of the modified Bessel function. Moreover the solution (3.25) can be applied to any case where suitably fast reactions occur between two reactive solutes. Arbitrary stoichiometric reactions can be addressed through scaling the results of the base case (where $Y_1 = Y_2 = 1$).

Plume length L can be defined as the distance from the origin to an arbitrary concentration contour, and solved for (3.28). In this study ${C_B}^T(x, 0, \infty) = {C_A}^T(x, 0, \infty) = C_o$ was chosen, which defines the length of a contaminant plume, i.e., the maximum extent of the contaminant before it is totally degraded. However any other concentration level can be substituted where desired. In the limit where $0.1 \leq \beta^n \leq 1$ and $\alpha_l << 1$, the plume length L can be expressed as a zero order approximation (3.32) consisting of a few hydrological parameters including α_t but independent of α_l. This confirms the findings made by previous experimental and numerical studies (Borden & Bedient, 1986; Cirpka *et al.*, 1999; Grathwohl *et al.*, 2000, 2001; Klenk & Grathwohl, 2002), where it is suggested that α_t, and not α_l, dictates steady-state plume length development and concentration distributions. This study provides the mathematical proof of these effects. The use of a zero order approximation (3.32) to equation (3.28) should serve accurately to quantify the length of a plume in common situations where the conceptual model of an instantaneous reaction between two solutes applies. When $\beta^1 < 0.1$, a first order approximation (3.37) provides an excellent approximation for L, which depends both on α_t and α_l.

Results from numerical simulations show that the longitudinal dispersion α_l affects transient plume development, especially when $\alpha_l >> \alpha_t$. Transient plume development is also affected by sorption, and was considered in this paper for linear equilibrium sorption. When sorption plays a role, an analytical solution of the transient problem similar to that presented in (3.23) only exists when $R_B = R_{AB}$, which in practise is rarely the case. For the multi-species reaction considered here, results produced using the numerical model indicate that sorption only hinders the propagation of the reaction front but has no influence on the steady-state solution.

The focus of this article is on macro-scale dispersion; the governing flow and transport equations define advective and dispersive processes over representative elementary volumes. However, it is well understood that in the context of biodegra-

dation, the relevant scale of mixing is the pore scale (Bear, 1972; Cirpka *et al.*, 1999). It is therefore important to remind the reader that the mechanisms of dispersion are scale-dependent (Dykaar & Kitanidis, 1996) and the assumption here is that local-scale mixing/dispersion be similar to plume-scale/macro-scale dispersion. This is valid in the case of uniform flow through a homogeneous domain. Homogeneous here means that the spatial scale of any heterogeneity, physical or chemical, is small compared to the scale of the contaminant (electron donor) plume. Note that in practice there might be many situations where this assumption does not apply, as for example discussed by Trefry *et al.* (2003) but, moreover, the reader should be aware that understanding scale issues is critical to understanding dispersive processes.

Bibliography

Abramowitz, M., Stegun, I.S.(eds.), 1964. Handbook of Mathematical Functions. With fomulas, graphs and mathematical tables. Dover Publications Inc., New York.

Bear, J., 1972. Dynamics of Fluids in Porous Media. American Elsevier, New York.

Barry, D.A., Prommer, H., Miller, C.T., 2002. Engesgaard, P., Zheng, C. Modelling the fate of oxidizable organic contaminants in groundwater. Adv. Water Resources 25, 899-937.

Borden, R.C., Bedient, P.B., 1986. Transport of dissolved hydrocarbons influenced by oxygen-limited biodegradation: 1. Theoretical development. Water Resour. Res. 13, 1973-1982.

Borden, R.C., Bedient, P.B., Lee, M.D., Ward, C.H., Wilson, J.T., 1986. Transport of dissolved hydrocarbons influenced by oxygen-limited biodegradation: 2. Field application. Water Resour. Res. 13, 1983-1990.

Carslaw and Jaeger (eds.), 1986. Conduction of Heat in Solids (Second Edition). Claredon Press, Oxford.

Cirpka, O.A., Frind, E.O., Helmig, R., 1999. Numerical simulation of biodegradation controlled by transverse mixing. J. Contam. Hydrol. 40, 159-182.

Clement, P.T., 2002. A modular computer code for simulating reactive multi-species transport in 3-dimensional groundwater aquifers. Technical Report PNNL-SA-28967, Battelle Pacific Northwest National Laboratory Research Report, Richlands, Washington.

Crank, J., 1964. The mathematics of diffusion (Third Edition). Clarendon Press, Oxford.

Davis, G.B., Barber, C., Power, T.R., Thierrin, J., Patterson, B.M., Rayner, J.L., Wu, Q., 1999. The variability and intrinsic remediation of a BTEX plume in anaerobic sulphate-rich groundwater. J. Contam. Hydrol. 36, 265-290.

Domenico, P.A., 1987. An analytical model for multidimensional transport of a decaying contaminant species. J. Hydrol. 91, 49-58.

Dykaar, B.B., Kitanidis, P.K., 1996. Macrotransport of a biologically reacting solute through porous media. Water Resour. Res. 32(2), 307-320.

Gradshteyn, I.S., Ryzhik, I.M., 1979. Table of integrals, series and products (Twelfth Printing). Academic Pres Inc., New York.

Gramling, C.M., Harvey, C.F., Meigs, L.C., 2002. Reactive Transport in Porous Media: A Comparison of Model Prediction with Laboratory Visualization. Environ. Sci. Technol. 36, 2508-2514.

Grathwohl, P., Klenk, I.D., EBerhardt, C., Maier, U., 2000. Steady state plumes: mechanisms of transverse mixing in aquifers. Contaminant Site Remediation: From Source Zones to Ecosystems. Proc. CRSC, Melbourne, Vic., 4-8 Dec., Centre for Groundwater Studies, CSIRO, Perth, Western Australia, 459-466.

Grathwohl, P., Klenk, I.D., Eberhardt, C., Maier, U., 2001. Steady State Plumes: Mechanisms of Transverse Mixing in Aquifers. In Seiler and Wohnlich (eds): New Approaches Characterizing Groundwater Flow, Proceedings IAH congress, 89-94.

Huang, W.E., Oswald, S.E., Lerner, D.N., Smith, C.C., Zheng C., 2003. Dissolved oxygen imaging in a porous medium to investigate biodegradation in a plume with limited electron acceptor supply. Environ. Sci. Technol. 37, 1905-1911.

Klenk, I.D., Grathwohl, P., 2002. Transverse vertical dispersion in groundwater and the capillary fringe. J. Contam. Hydrol. 58, 111-128.

Koussis, A.D., Pesmajoglou, S., Syriopoulou, D., 2003. Modelling biodegradation of hydrocarbons: when is the use of the instantaneous reaction approximation justified? J. Contam. Hydrol. 60, 287-305.

Leonard, B.P., 1998. Universal limiter for transient interpolation modeling of the advective transport equations: The ULTIMATE conservative difference scheme, NASA Technical Memorandum 100916 ICOMP-88-11, Washington, DC.

Lu, G., Clement, T.P., Zheng, C., Wiedemeier, T.H., 1999. Natural attenuation of BTEX compounds, model development and field-scale application, Ground Water 37(5), 707-717.

Michaelis, L., Menton, M.M.L., 1913. Die Kinetik der Invertinwerkung. Biochemische Zeitschrift 49.

Parkhurst, D.L., Appelo, C.A.J., 1999. User's guide to PHREEQC (Version 2)-A computer program for speciation, batch-reaction , one-dimensional transport, and inverse geochemical calculations. U.S. Geological Survey Water-Resources Investigations Report 99-4259.

Prommer, H., Barry, D.A., Zheng, C., 2003. MODFLOW/MT3DMS-based reactive multicomponent transport modelling. J. Ground Water 41(2), 247-257.

Prommer, H., Davis, G.B., Barry, D.A., 2002. Modelling of physical and reactive processes during biodegradation of a hydrocarbon plume under transient groundwater flow conditions. J. Cont. Hydrol. 59, 113-131.

Trefry, M.G., Ruan, F.P., McLaughlin, D., 2003. Numerical simulations of preasymptotic transport in heterogeneous porous media: Departures from the Gaussian limit. Water Resour. Res. 39(3):10.1029/2001WR001101.

Wilson, J.L., Miller, P.J., 1976. Two-dimensional plume in uniform ground-water flow. Journal of the Hydraulics Division, ASCE 104; HY4, 503-512.

Zheng, C., Wang, P.P., 1999. MT3DMS: A modular three-dimensional multispecies model for simulation of advection, dispersion and chemical reactions of contaminants in groundwater systems; Documentation and User's Guide. Contract Report SERDP-99-1, U.S. Army Engineer Research and Development Center, Vicksburg, MS.

Chapter 4

Analytical Modelling as a Basis for Monitored Natural Attenuation studies [2]

Abstract. In this paper, an analytical approach to modelling simultaneous fringe and core degradation of a contaminant plume is presented. Explicit steady-state solutions are derived in three-dimensions using a well-known analytical solution for a continuous planar source problem, combined with instantaneous and first-order reaction terms. These solutions provide rapid methods to evaluate the risk of subsurface pollution by contaminated groundwater plumes at field sites, particulary in terms of maximum potential plume lengths.

The resulting fringe-core degradation model suggests the controlling parameters of natural attenuation are (i) the size of the contaminant source, (ii) electron acceptor to electron donor ratio, (iii) transverse dispersivities, and (iv) the term (λ/ν). This term provides a simple check on the relative weights of transport to core degradation and can be used to estimate the importance of core degradation in overall plume attenuation. The developed method is applied to data from a well-known field site to demonstrate the applicability of the new model in NA studies where both fringe and core degradation occur. The results demonstrate that only through the consideration of both of these degradation processes, can the maximum length of the steady-state plume be accurately approximated.

[2]Excerpts from Gutierrez-Neri, M., Ham, P.A.S., Schotting, R.J., Lerner, D.N. In preparation for submission to *Ground Water*.

4.1 Introduction

Monitored natural attenuation (MNA) can be an acceptable remediation option for managing subsurface contamination, particularly, by organic pollutants (Weidemeier *et al.*, 1999; Kao & Wang, 2000; Suarez & Rifai, 2002). Increasingly, MNA employs mathematical modelling techniques in the analysis of environmental systems and, in particular, in the quantification of natural attenuation processes (Cirpka *et al.*, 1999; Mayer *et al.*, 2000; Prommer *et al.*, 2002).

One method of analysis is through the use of analytical models derived from the governing flow and transport equations. Through making simplifying assumptions about environmental systems, closed-form expressions can be obtained to quantify the migration of contaminants from a source zone. Moreover, simple reactions which occur between mixing solutes can also be included (Borden & Bedient, 1986; Ham *et al.*, 2004). Since MNA is a 'risk-based' engineering strategy, the question most frequently posed is: *To what extent will a contaminant plume develop before it reaches a steady-state?* Therefore, the preliminary assessment of field-scale MNA scenarios typically focuses on steady-state plume behavior (e.g. in terms of plume lengths, concentration profiles). Indeed, in field cases where subsurface conditions can be considered relatively homogeneous, analytical solutions may even provide sufficient results in order to decide if MNA is a suitable option for aquifer restoration.

The effectiveness of natural attenuation relies heavily on naturally occurring hydrological and biogeochemical processes. In terms of aquifer remediation, the most important process is biodegradation. Biodegradation can be divided into two categories depending on the location at which it occurs within the plume: degradation occurring at the plume fringes, and degradation occurring in the interior (core) of the plume (Lerner *et al.*, 2005). For example, consider the degradation of oxidisable organic contaminants. In this case, core degradation is an anaerobic process resulting from interactions between contaminants and available sediment-bound electron acceptors in the aquifer matrix (Christensen *et al.*, 2000a; Essaid *et al.*, 1995). It may also be the result of sulphate reduction and methane fermentation processes (Thornton *et al.*, 2001b). The large content of such electron acceptors compared to dissolved oxygen, often causes anaerobic processes to be important mechanisms for overall plume degradation (Essaid *et al.*, 2003). Conversely, fringe degradation is often controlled by mechanisms of hydrodynamic dispersion which induces mixing and reactions between the contaminant species (electron donor)

and the electron acceptors in the background groundwater, resulting in the degradation of the contaminant species (Cirpka *et al.*, 1999; Klenk & Grathwohl, 2002; Thornton *et al.*, 2001a; Huang *et al.*, 2003).

A number of analytical solutions exist that consider degradation using first-order kinetics, e.g., (Bear, 1972; Hunt, 1978; Domenico, 1987). In these models, degradation processes are represented using uniform first-order decay over the whole plume volume, which is referred to as the core-style degradation model. Other models consider degradation as a process limited by electron acceptor mixing. These include, most recently, Ham *et al.* (2004); Chu *et al.* (2005); Dietrich *et al.* (In press). In these models, degradation is assumed to occur as an instantaneous reaction between the electron donor and the electron acceptor. We shall refer to this as the fringe-style degradation model.

Given that existing analytical solutions assume that biodegradation follows either a fringe- or core-style degradation model, in this article, an approach is presented which represents a combination of both fringe and core degradation. This approach utilises the analytical solution from Domenico & Robbins (1985), applying and extending the methodology already presented in Ham *et al.* (2004) (Chapter 3 of this thesis). The resulting model is then applied to a well-known field-scale problem described by Essaid *et al.* (2003).

4.2 Problem Description

This analysis considers an extension to the problem considered by Ham *et al.* (2004). At time $t = 0$, the three-dimensional domain Ω, contains only species A, which has a constant concentration C_A throughout the domain. Species B with a constant concentration ${C_B}^0$, is continuously injected into the flow domain. The flow field in Ω is considered steady and uniform. Mixing through dispersion causes an aerobic bimolecular reaction to occur between the A and B. This reaction is assumed to be instantaneous and stoichiometrically equal, producing an inert reaction product (AB), i.e. $A + B = AB$. Moreover, species B is also subject to anaerobic degradation, which is assumed to follow a first-order kinetic process, leading to the decay of the B species. These assumptions imply that the instantaneous reaction is confined to the plume fringe, whilst the decay of species B occurs throughout the entire plume. Figure 4.1 is a schematic representation of the problem description.

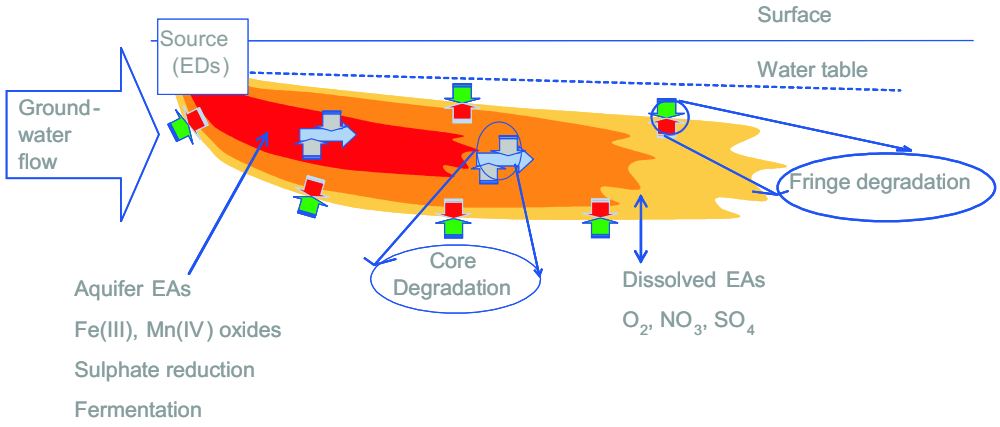

Figure 4.1: *Schematic representation of fringe and core processes occurring in a contaminant plume omitted from a continuous source, adapted from Lerner et al. (2005).*

4.3 Analytical Approach

4.3.1 Non-reactive transport

The three-dimensional transport equation of a non-sorbing, conservative species, under the assumtion that molecular diffusion is negligible compared to mechanical dispersion, is given by

$$\frac{\partial C(k)}{\partial t} = \alpha_l \nu \frac{\partial^2 C(k)}{\partial x^2} + \alpha_{th} \nu \frac{\partial^2 C(k)}{\partial y^2} + \alpha_{tv} \nu \frac{\partial^2 C(k)}{\partial z^2} - \nu \frac{\partial C(k)}{\partial x}, \tag{4.1}$$

where C denotes the concentration of species k, t is the time, ν is the effective velocity, α_l, α_{th} and α_{tv} are the longitudinal, transversal horizontal and transversal vertical dispersivities respectively. Closed-form solutions techniques have been employed to solve equation (4.1). In some cases these solutions can be written as the product of three one-dimensional solutions (e.g., Hunt (1978); Domenico & Robbins (1985); Leij *et al.* (2000)), i.e.,

$$C_B{}^T(x, y, z, t) = S \cdot F_1(x, \alpha_l, t) \cdot F_2(\alpha_{th}, y) \cdot F_3(\alpha_{tv}, z), \tag{4.2}$$

where $C_B{}^T$ denotes the concentration of the conservative species B^T, S denotes the source term, F_1 is the function in the $x-$direction that accounts for advection

and longitudinal dispersion and F_2 and F_3 are the solution functions in $y-$ and $z-$directions that account for transverse dispersion. Using the analytical solution from Domenico & Robbins (1985) for three-dimensional conservative transport, equation (4.2) takes the form

$$\begin{aligned} S &= \frac{{C_B}^0}{8}, \\ F_1 &= \left[\operatorname{erfc}\left(\frac{x-vt}{2\sqrt{\alpha_l vt}}\right)\right], \\ F_2 &= \left[\operatorname{erf}\left(\frac{y+Y/2}{2\sqrt{\alpha_{th}x}}\right) - \operatorname{erf}\left(\frac{y-Y/2}{2\sqrt{\alpha_{th}x}}\right)\right], \\ F_3 &= \left[\operatorname{erf}\left(\frac{z+Z/2}{2\sqrt{\alpha_{tv}x}}\right) - \operatorname{erf}\left(\frac{z-Z/2}{2\sqrt{\alpha_{tv}x}}\right)\right], \end{aligned} \tag{4.3}$$

where ${C_B}^0$ is the initial concentration and Y is the source width and Z is the source height. At steady-state, the solution reduces to

$$\begin{aligned} S &= \frac{{C_B}^0}{4}, \\ F_2 &= \left[\operatorname{erf}\left(\frac{y+Y/2}{2\sqrt{\alpha_{th}x}}\right) - \operatorname{erf}\left(\frac{y-Y/2}{2\sqrt{\alpha_{th}x}}\right)\right], \\ F_3 &= \left[\operatorname{erf}\left(\frac{z+Z/2}{2\sqrt{\alpha_{tv}x}}\right) - \operatorname{erf}\left(\frac{z-Z/2}{2\sqrt{\alpha_{tv}x}}\right)\right]. \end{aligned} \tag{4.4}$$

4.3.2 Reactive transport

In the case of simultaneous transport and biodegradation of a species, the addition of a reaction term to the governing equation (4.1) yields

$$\frac{\partial C(k)}{\partial t} = \alpha_l \nu \frac{\partial^2 C(k)}{\partial x^2} + \alpha_{th} \nu \frac{\partial^2 C(k)}{\partial y^2} + \alpha_{tv} \nu \frac{\partial^2 C(k)}{\partial z^2} - \nu \frac{\partial C(k)}{\partial x} - r^{C(k)}, \tag{4.5}$$

where r is the reaction rate.

Core degradation model

If biodegradation is assumed to follow a first-order kinetic law (i.e. decay), r is defined by

$$r^B = \lambda \cdot C_B, \tag{4.6}$$

where the decay constant

$$\lambda = \frac{\ln(2)}{t^{1/2}}, \tag{4.7}$$

and $(t^{1/2})$ is the half-life of the biodegradable species. Analytical solutions to the advection-dispersion equation, including species decay, can be generalised in the form

$$C_B = {C_B}^T \cdot K(\lambda), \tag{4.8}$$

where K is a function that accounts for first-order decay. The analytical solution provided by Domenico (1987) defines K as

$$K(\lambda) \;=\; \exp\left[\left(\frac{x}{2\alpha_l}\right)\left(1-\sqrt{1+\frac{4\lambda\alpha_l}{\nu}}\right)\right]. \tag{4.9}$$

Other analytical solutions to transport and decay include works by Baetsle (1969); Hunt (1978) and Bear (1972). We refer to equation (4.8) as the core degradation model.

Fringe degradation model

It follows from Ham *et al.* (2004) that the general solution for the transport of species undergoing an instantaneous reaction is given by

$$C_B \;=\; {C_B}^T - {C_A}^0, \tag{4.10}$$

where ${C_A}^0$ denotes the initial concentration of species A. We refer to equation (4.10) as the fringe degradation model.

Combined degradation model

Here, a solution to equation (4.5), where the reaction term accounts for both the decay of species (following first-order kinetics) and the instantaneous reaction, is obtained through the combination of the two independent solutions for fringe degradation and core degradation. The combined degradation model can be mathematically represented by

$$C_B = {C_B}^T \cdot \quad K(\lambda) - {C_A}^0. \tag{4.11}$$

The procedure proposed in equation (4.11) implies that the degradation of the electron donor is two-fold: first occurring throughout the entire plume following a first-order decay law, and subsequently as a instantaneous fringe reaction with species A in the ambient groundwater. It follows from equation (4.11) that if $\lambda = 0$, equation (4.11) reduces to solutions for fringe degradation, i.e., equation (4.10). If ${C_A}^0$ is small, solutions are reduced to core degradation, i.e., equation (4.8). In addition, if $\lambda = 0$ and ${C_A}^0$ are both small, solutions reduce to equation 4.2 for non-reactive transport, i.e., as given by equation (4.3). Implementing the combined degradation model in the steady-state form of the analytical solution by Domenico & Robbins (1985), equation (4.4), the analytical solution takes the form

$$C_B(x, y, z) \quad = \quad S \cdot F_2(\alpha_{th}, y) \cdot F_3(\alpha_{tv}, z) \cdot K(\lambda) - {C_A}^0, \tag{4.12}$$

with all the terms being the same as previously defined.

Plume length

As in Ham *et al.* (2004), plume length is defined as the distance measured along the centreline to where all of the species B is completely exhausted, i.e., $C_B = 0$. It follows that the maximum plume length $L(x)$, in three dimensions, is given by the solution to

$$\frac{{C_A}^0}{{C_B}^0} = \operatorname{erf}\left(\frac{Y}{4\sqrt{\alpha_{th} L(x)}}\right) \operatorname{erf}\left(\frac{Z}{4\sqrt{\alpha_{tv} L(x)}}\right) \exp\left[\frac{L(x)}{2\alpha_l}\left(1 - \sqrt{1 + \frac{4\lambda\alpha_l}{\nu}}\right)\right] \tag{4.13}$$

An iterative numerical method has to be used to solve for the exact value of $L(x)$. Equation (4.13) implicitly suggests that the controlling parameters on plume

length are (i) size of contaminant source, (ii) ratio of A to B, (iii) longitudinal and transversal dispersivities, and (iv) the dimensionless group $(\alpha_l \lambda/\nu)$ contained within the exponential term. The latter term is a form of the Damkohler number and is defined as the (bio)degradation rate relative to advective transport

$$Da = \frac{\lambda \alpha_l}{\nu}, \tag{4.14}$$

with the longitudinal dispersion length, α_l, as the characteristic length. The exponential term can be recast as

$$\exp\left[\frac{L}{2\alpha_l}\left(1 - \sqrt{1 + 4Da}\right)\right]. \tag{4.15}$$

Figure 4.2 is an example plot of plume length $L(x)$ obtained from the exact solution (4.13) against Da. It can be seen that for values of $Da >> 0.1$, the length of the steady-state plume is virtually independent of Da. Therefore, if $Da \ll 1$, the

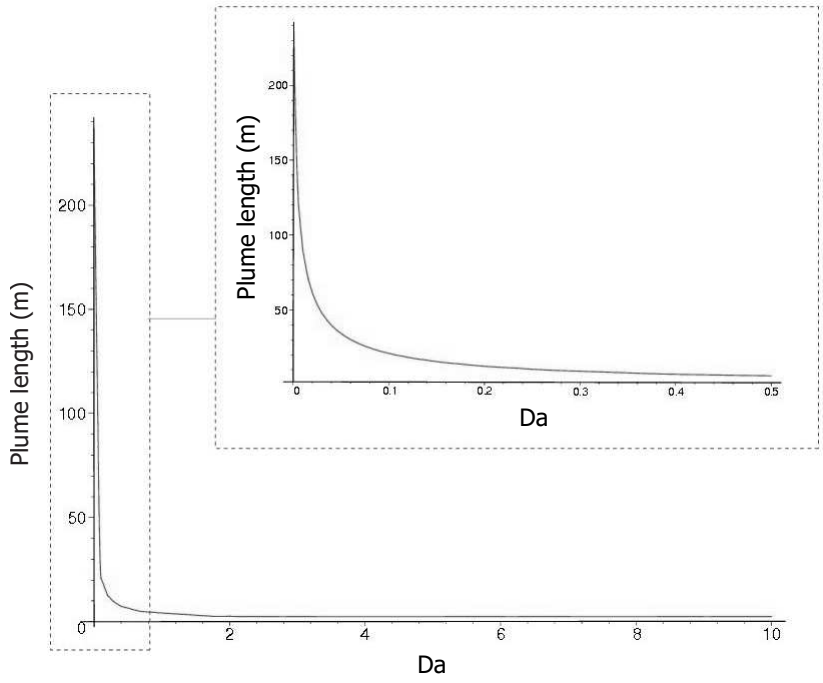

Figure 4.2: *Variation of plume length with value of Da. Parameter values used:* $Y = 5m$, $Z = 2m$, $\alpha_l = 1\ m$, $\alpha_{th} = 0.1\ m$, $\alpha_{tv} = 0.01\ m$, ${C_B}^0 = 10\ meq/L$, ${C_A}^0 = 1\ meq/L$.

exponential term can be written

$$\exp\left(\frac{-L\,\lambda}{\nu}\right), \tag{4.16}$$

and equation (4.13) reduces to

$$\frac{{C_A}^0}{{C_B}^0} = \operatorname{erf}\left(\frac{Y}{4\sqrt{\alpha_{th}L}}\right)\operatorname{erf}\left(\frac{Z}{4\sqrt{\alpha_{tv}L}}\right)\exp\left(\frac{-L\,\lambda}{\nu}\right). \tag{4.17}$$

This approximation implies that plume length is only a function of the transversal dispersivities α_{th} and α_{tv}, i.e., independent of longitudinal dispersivity α_l. This condition was observed previously in experimental studies (e.g., Grathwohl *et al.* (2000); Huang *et al.* (2003)) and was demonstrated mathematically in two-dimensions by Ham *et al.* (2004) and Cirpka & Valocchi (In press). Figure 4.3 illustrates this phenomenon using the same parameter values as in Figure 4.2, where $\alpha_l = 0.001$ and $100\ m$. Note the differences between the centreline concentration profiles are very small. An explicit expression for the plume length $L(x)$ can

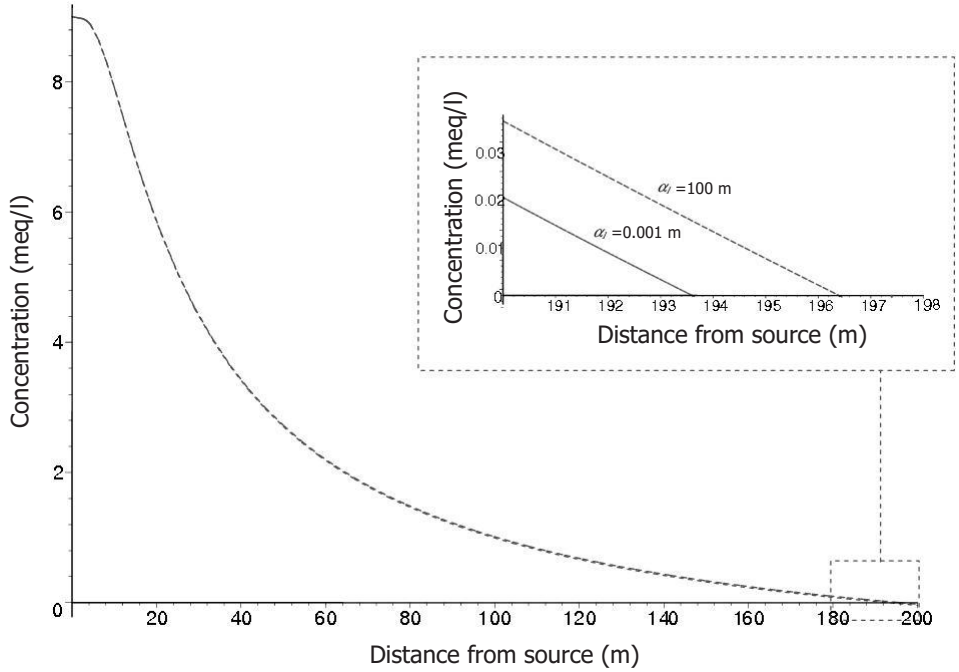

Figure 4.3: *Centreline concentration profiles for species B for values of* $\alpha_l = 0.001$ *and* $100\ m$.

be obtained if the error function and the exponential functions are approximated by their respective series expansion (Beyer, 1987), i.e.

$$\mathrm{erf}(\beta) = \frac{1}{\sqrt{\pi}}\left(2\beta - \frac{2}{3}\beta^3 + \frac{1}{5}\beta^5 - \frac{1}{21}\beta^7 ...\right), \tag{4.18}$$

and

$$\exp^x = 1 + \frac{x}{1!} + \frac{x^2}{2!} + \frac{x^3}{3!} + ... \tag{4.19}$$

If only the first term on the right-hand side of the series expansions is considered, a first approximation for the plume length L(x) yields

$$L(x) \approx \frac{Y\ Z}{4\pi\sqrt{\alpha_{th}\ \alpha_{tv}}\ \frac{{C_A}^0}{{C_B}^0}\ +\ Y\ Z\ \frac{\lambda}{\nu}}. \tag{4.20}$$

Again, equation (4.20) shows the main controlling variables for the steady-state plume length are (i) size of the contaminant source, (ii) ratio of species A to species B, (iii) transversal dispersivities, and (iv) the ratio λ/ν. A comparison of the approximation solution and the exact solution for different values of λ/ν is represented in Figure 4.4. For values of $\lambda/\nu \ll 0.1$, i.e., typical values for field sites, the plume length predicted by equation (4.20) approaches the exact solution given by equation (4.13).

4.3.3 Comparison of degradation models

In this section, a comparison of plume length predicted by the combined and simplified models, i.e. core degradation and fringe degradation, is undertaken. Figure 4.5 is a plot of plume length against λ/ν, where different ratios of ${C_A}^0/{C_B}^0$ are also considered. The relative importance of core degradation in the overall plume degradation can be assessed by λ/ν. Small values of λ/ν mean that the the half-life ($t^{1/2}$) of the degrading species B increases, $\lambda = ln(2)/t^{1/2}$ decreases, λ/ν decreases and in turn the exponential term in equation (4.13) approaches the value of 1. In this case, a solution is similar to that given by the fringe degradation model, i.e., equation(4.10). That is, a small λ/ν number means the mass of species B in the plume core is migrating faster relative to the decay rate making core degradation ineffective. Conversely, for short half-lives λ is relatively

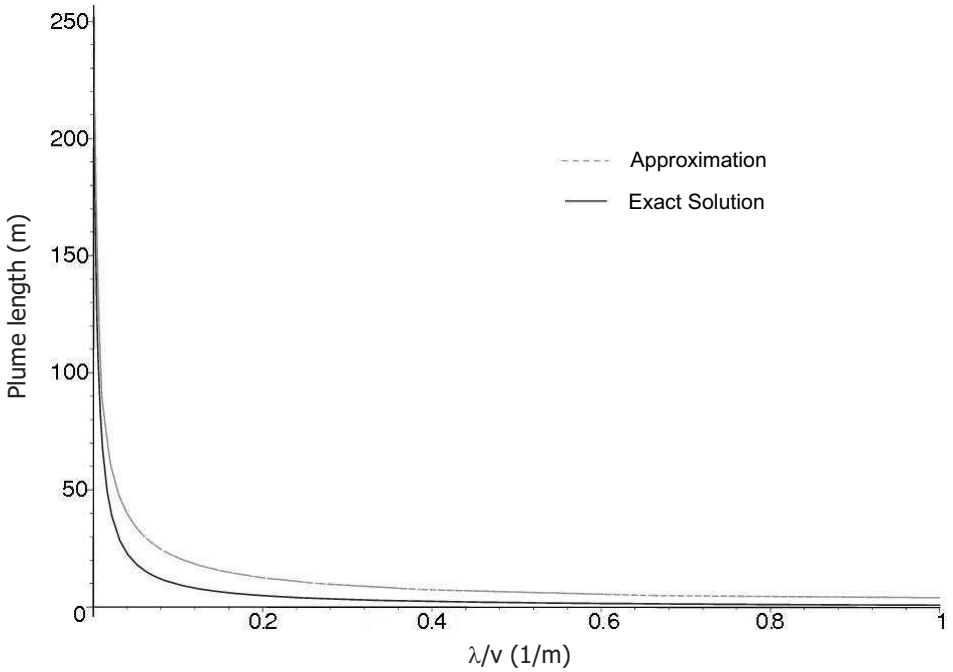

Figure 4.4: *Variation of plume length with values of ratio λ/ν.*

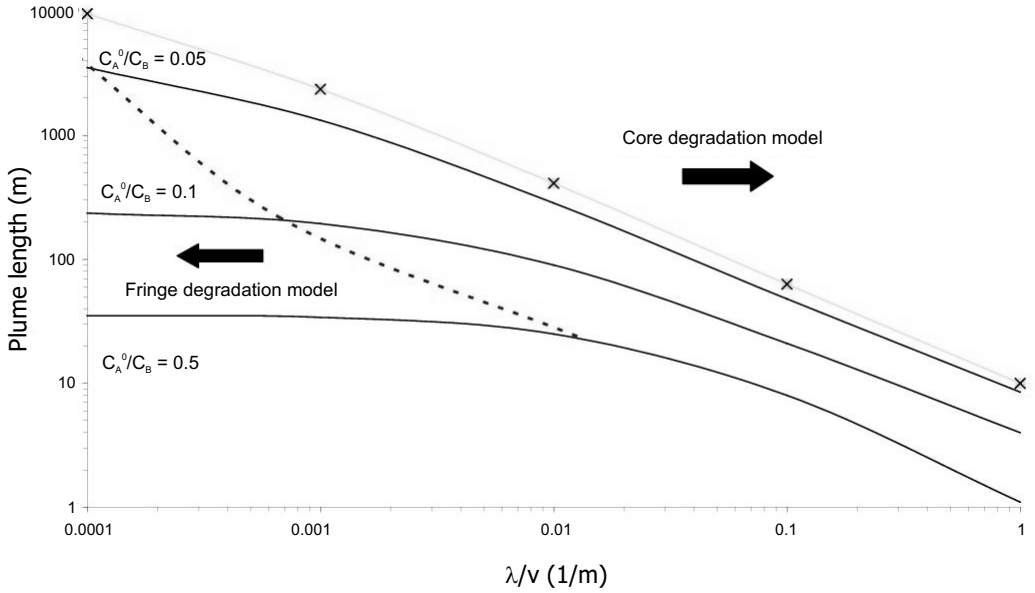

Figure 4.5: *Variation of plume length with values of λ/ν for different values of ratio ${C_A}^0/{C_B}^0$. The line with X-marker denotes the core degradation model, and the solid line denotes the combined model. The dashed line denotes the limit where the combined degradation model approximates the result of the fringe degradation model.*

large, implying that λ/ν increases and core degradation accounts for most of the concentration decrease of species B. In this case, the mass of species B in the plume core decays much faster than it can be transported, which makes fringe degradation insignificant.

The fringe degradation model is independent of λ/ν but dependant on the ratio ${C_A}^0/{C_B}^0$. If the ratio ${C_A}^0/{C_B}^0$ equals 0.5 (see Fig 4.5), it can be seen that for λ/ν values of less than 0.01, the plume length predicted by the combined degradation model approximates the fringe degradation model; core degradation becomes insignificant as λ/ν decreases. For λ/ν values greater than 0.001 the combined degradation model should yield better predictions for plume length than the core degradation model. This is because fringe degradation is significant at this ratio. However, if the ratio ${C_A}^0/{C_B}^0$ exceeds 0.05, results from the combined degradation model are comparable to the core degradation model. Figure 4.5 also illustrates that the applicability of the combined model should fall within the region bounded by the dashed lines. To the left- and right-hand side of that region, simpler models, i.e., fringe or core degradation can be employed.

4.4 Application to Field-Scale Natural Attenuation Studies

In this section the combined fringe-core model is applied to a suitable field-case. Moreover, the combined model is compared to the fringe and core models to demonstrate the differences between them. The field-case, discussed in detail in Essaid *et al.* (1995, 2003), relates to the attenuation of a plume of petroleum hydrocarbons.

Background

In 1979 a buried oil pipeline located in a pitted and dissected glacial outwash plain near Bemidji, Minnesota, spilled approximately 11,000 barrels of crude oil resulting in the formation of a BTEX plume. The plume developed anaerobic conditions in the interior and was subject to aerobic degradation at the plume fringes due to mixing with oxygen present in the background water. Concentration, first-order degradation rates for the individual hydrocarbon compounds as well as transport parameters have been reported. These parameter values are listed in Table 1. Two-dimensional vertical contour plots constructed from data analyses are available and

Parameter	Measurement
Y	2.5m
ν	0.06 m day^{-1}
α_l	1 m
$\alpha_t v$	0.036 m
λ	0.00065 day^{-1}
C_B^0	10 meq/L
C_A^0	0.5meq/L
Plume Length	180m

Table 4.1: *Predicted Parameter values and plume characteristics, obtained from Essaid et al. (1995, 2003).*

previous field estimates and numerical modelling efforts indicate the length of the plume to be approximately $180m$ (Essaid *et al.*, 1995, 2003). Furthermore, the modelling results indicated that it is necessary to consider both fringe and core processes in order to accurately quantify the fate of the hydrocarbon plume. A simple assessment to test whether this is true is to check the λ/ν values. In this case, the plume λ/ν value of 0.012 and a ratio ${C_A}^0/{C_B}^0 = 0.05$ suggests the suitability of the field site to be better modelled by the combined degradation model.

Analysis

The modelling exercise was limited to the consideration of centreline profiles of hydrocarbons and electron acceptors and the determination of the maximum plume length. It should be noted that for this case, the maximum plume length will be given by the concentrations of the benzene compound, which in this particular case is the less attenuated compound. The combined, core, and fringe models, in two-dimensional form, were applied using the parameter values in Table 4.1 and Figure 4.6 shows the resulting centerline profiles for all three models. As illustrated in Figure 4.6, in order to better match the reported plume length, consideration of both fringe and core processes is indeed necessary. If only fringe degradation, i.e., aerobic degradation, is considered, the plume length is estimated to be approx 4km (not shown in plot). Furthermore, consideration of core degradation alone is not enough to account for the plume attenuation reported.

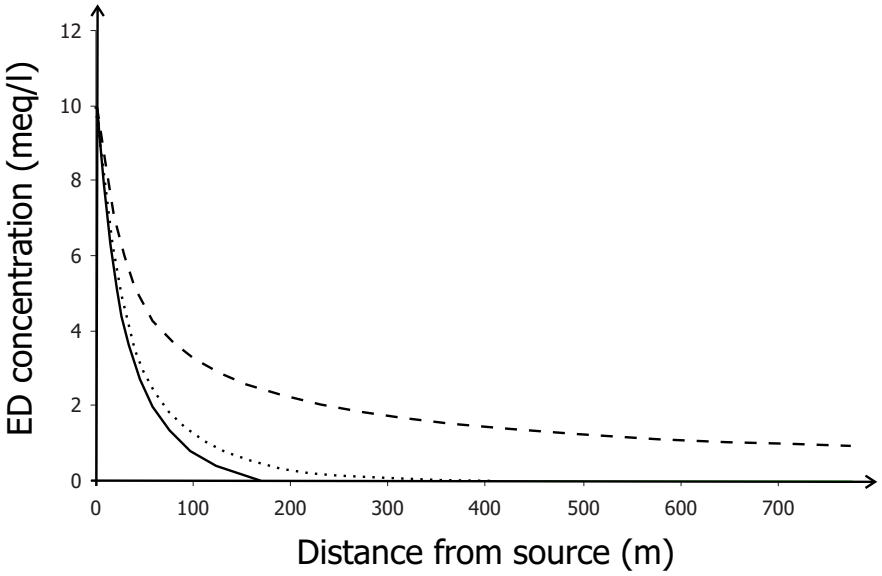

Figure 4.6: *BTEX plume centreline concentration as predicted by the three models. The dashed line denotes the fringe-only degradation model, the dotted line denotes the core-only degradation model, the solid line denotes the combined model.*

4.5 Summary and Conclusions

The degradation of a contaminant plume can be characterised by processes occurring in the core and at the fringe. Within the context of MNA, core degradation is typically considered to be a slow anaerobic process, whilst fringe mixing can usually be considered a fast (instantaneous) process whereby reactions between EA and ED (here represented by species A and B respectively) occur and new reaction products are formed. However, depending on the rates of anaerobic degradation and the availability of EA, i.e., relatively high degradation rates and/or relatively low EA availability, it can be necessary to model both core and fringe degradation processes in order to accurately quantify plume attenuation.

An analytical approach to model fringe and core degradation was proposed using a combination of instantaneous and first-order reactions. Already established analytical solutions were used to provide a closed-form expression to evaluate plume behaviour, in particular steady-state length of a contaminant plume emitted from a continuous planar source. This expression shows the main controlling variables for the steady-state plume length are (i) size of the contaminant source, (ii) ratio of species A to species B, (iii) transversal dispersivities, and (iv)

the ratio λ/ν. The last term can be used to quickly attain the relative importance of both fringe and core degradation processes at a field site. Where λ/ν is small, fringe processes control contaminant degradation whilst large values of λ/ν indicate core mechanisms to be the dominant means of attenuation. In any other cases, aquifer remediation will be governed by a combination of reactions occurring in the plume fringe and core.

This steady-state solution provides a rapid method to evaluate risk at field sites, in terms of the potential maximum plume length, in cases where both fringe and core degradation processes are important. This was demonstrated through a comparison of the analytical model to field data obtained from a two-dimensional field-scale natural attenuation study. In that case, excellent agreement between modelled and predicted (from data) plume lengths was found. In comparison the both the fringe model and the core model failed to accurately predict the plume length.

Bibliography

Baetsle, L.H., 1969. Migration of radionuclides in porous media. Progress in Nuclear Energy Series XII, Health Physics, ed. A. M. F. Duhamel: Elmsford, N.Y., Pergamon Press, 707-730.

Bear, J., (1972). Dynamics of Fluids in Porous Media. Elsevier Science, New York.

Beyer, W.H., 1987. CRC Standard Mathematical Tables, 28th ed. Boca Raton, FL: CRC Press, pp. 299-300.

Borden, R.C., Bedient, P.B., 1986. Transport of dissolved hydrocarbons influenced by oxygen-limited biodegradation: 1. Theoretical development. Water Resour. Res.,13, 1973-1982.

Cirpka, O.A., Frind, E.O., Helmig, R., 1999. Numerical simulation of biodegradation controlled by transverse mixing. J. Contam. Hydrol. 40, 159-182.

Cirpka, O.A., Valocchi, A.J., 2004. Two-dimensional concentration distribution for mixing-controlled bioreactive transport in steady state. Adv. Water Resour. Res.

Christensen, T.H., Bjerg, P.L., Banwart, S.A., Jakobsen, J., Heron, G., Albrechtsen, H., 2000a. Characterisation of redox conditions in groundwater contaminant plumes. J. Contam. Hydrol., 45(3-4), 165-241.

Chu, M., Kitanidis, P.K., McCarty, P.L., 2005. Modeling microbial reactions at the plume fringe subject to transverse mixing in porous media: When can the rates of microbial reaction be assumed to be instantaneous?, Water Resour. Res., 41, 1-15.

Domenico, P.A., 1987. An analytical model for multidimensional transport of a decaying contaminant species, J. Hydrol., 91(1-2), 49-58.

Domenico, P.A., Robbins, G., 1985. A new method of contaminant plume analysis, Ground Water 23(4), 476-485.

Essaid H.I., Bekins, B.A., Godsy, E.M., Warren, E., Baedecker, M.J., Cozzarelli, I.M., 1995. Simulation of aerobic and anaerobic biodegradation processes at a crude oil spill site, Water Resour. Res. 31(12), 3309-3327.

Essaid H.I., Cozzarelli, I.M., Eganhouse, R.P., Herkelrath, W.N., Bekins, B.A., Delin, G.N., 2003. Inverse modelling of BTEX dissolution and biodegradation at the Bemidji, MN crude-oil spill site, J. Contam. Hydrol. 67, 269-299.

Grathwohl, P., Klenk, I.D., Ederhardt, C., Maier, U., 2000. Steady state plumes: mechanisms of transverse mixing in aquifers. In C.D. Johnston: Contaminant Site Remediation: From Source Zones to Ecosystems, Proc. CRSC, Melbourne, Vic., 4-8 Dec., Centre for Groundwater Studies, CSIRO, Perth, Western Australia, pp.459-466.

Gutierrez-Neri, M., Ham, P.A.S., Schotting, R.J., Lerner, D.L. Analytical modelling of fringe and core biodegradation in groundwater plumes. Article in preparation for submission to Ground Water.

Ham, P.A.S., Schotting, R.J., Prommer, H, Davis, G.B., 2004. Effects of hydrodynamic dispersion on plume lengths for instantaneous bimolecular reactions. Adv. Water Resour. Res. 27, 803-813.

Huang, W.E., Oswald, S.E., Lerner, D.N., Smith, C.C., Zheng, C., 2003. Dissolved oxygen imaging in a porous medium to investigate biodegradation in a plume with limited electron acceptor supply. Environ. Sci. Technol. 37, 1905-1911.

Hunt, B.W., 1978b. Dispersive sources in uniform groundwater flow, J. Hydrol. Div., Proc. Amer. Soc. Civil Eng., 104, 75-85.

Kao, C.M., Wang, C.C., 2000. Control of BTEX migration by intrinsic bioremediation at a gasoline spill site. Water Res.,13, 3413-3423.

Klenk, I.D., Grathwohl, P., 2002. Transverse vertical dispersion in groundwater and the capillary fringe. J. Contam. Hydrol. 58, 111-128.

Lerner, D.N., Bjerg, P., Datel, J., Gargini, A., Gratwohl, O., Hollinger, C., Morgan, P., Ptak, T., Schotting, R., Slenders, H., Thornton, S.F., 2005. CORONA

- Confidence in forecasting of natural attenuation as a risk-based groundwater remediation strategy, Final report of the EU research project EVK1-2001-00087. University of Sheffield, UK. 26 pages. Available from www.shef.ac.uk/corona.

Leij, F.J., Priesack, E., Schaap, M.G., 2000. Solute transport modeled with Green's functions with application to persistent solute sources. J. Cont. Hydrol., 41, 155-173.

Liedl, R., Valocchi, A.J., Dietrich, P., Grathwohl, P., 2005. The finiteness of steady-state plumes.

Mayer, K.U., Benner, S.G., Frind, E.O., Thornton, S.F., Lerner, D.N., 2001. Reactive transport modelling of processes controlling the distribution and natural attenuation of phenolic compounds in a deep sandstone aquifer. J. Contam. Hydrol. 53, 341-368.

Prommer, H., Davis, G.B., Barry, D.A., 2002. Modelling of physical and reactive processes during biodegradation of a hydrocarbon plume under transient groundwater flow conditions. J. Contam. Hydrol., 59, 113-131.

Prommer, H., Barry, D.A., Zheng, C., 2003. MODFLOW/MT3DMS-based reactive multicomponent transport modelling. J. Ground Water, 41(2), 247-257.

Suarez, M.P., Rifai, H.S., 2002. Evaluation of BTEX remediation by natural attenuation at a coastal facility. Ground Water Monitor. R. Winter, 62-77.

Thornton, S.F., Lerner, D.N., Banwart, S.A., 2001a. Assessing the natural attenuation of organic contaminants in aquifers using plume-scale electron and carbon balances: model development with analysis of uncertainty and parameter sensitivity. J. Contam. Hydrol., 53, 199-232.

Thornton, S.F., Quigley, S., Spence, M., Banwart, S.A., Bottrell, S., Lerner, D.N., 2001. Processes controlling the distribution and natural attenuation of phenolic compounds in a deep sandstone aquifer. J. Contam. Hydrol., 53, 233-267.

Wiedemeier, T.H., Rifai, H.S., Newell, C.J., Wilson, J.T., 1999. Natural Attenuation of Fuels and Chlorinated Solvents in the Subsurface. John Wiley.

Chapter 5

Effects of Biodegradation in the Fringe of Contaminant Plumes [3]

Abstract. In this paper, a two-dimensional biodegradation model is considered including simultaneous transport and biodegradation of organic contaminant, electron acceptor and, moreover, growth and decay of micro-organisms in a two-dimensional half plane. Three enhanced natural attenuation (ENA) problems are studied: Instantaneous planar source, continuous planar source, and line source ($y > 0$) injection of electron acceptor into a flow domain initially contaminated everywhere by a mobile organic contaminant species and filled with an immobile microbial species. In each case, injection of the electron acceptor leads to the development of a dispersive mixing zone between the zone where the biomass is activated and the inactive zone.

The base model consists of three coupled nonlinear partial differential equations. For the time-dependent cases, these three equations are reduced to an auxiliary linear equation with an explicit solution. The solution of this auxiliary problem is used to recast the three equations into two coupled equations. For stationary cases, the problem can be reduced further to a single PDE in terms of one of the dependent variables only, requiring a numerical solution.

Whilst transversal dispersion is the only controlling factor which determines overall lateral plume spreading, the width of the plume fringe where electron acceptor and electron donor populations co-exist is influenced strongly by microbial

[3] Ham, P.A.S., Schotting, R.J., Berentsen, C. In preparation for submission to *Advances in Water Resources Research.*

activity. Where there is sufficient microbial mass and growth rates are relatively large in comparison to microbial decay, complete degradation of the EA at the centre of the plume results in plume fringes becoming narrow. Apparent dispersion coefficients, which describe the steep concentration gradients between species are much smaller than effective values required to represent overall plume spreading. Understanding the connection between these values is of great importance at the field-scale, where microbial parameters are difficult to determine and plume attenuation capacity is often based on a representation of fringe characteristics.

5.1 Introduction

Natural Attenuation (NA) and Enhanced Natural Attenuation (ENA) are considered to be promising techniques for the remediation of contaminated soil and groundwater (Gutierrez-Neri *et al.*, In preparation). In particular, the mechanisms of (transverse) hydrodynamic dispersion and biodegradation determine whether a plume will grow, shrink or become stationary (Cirpka *et al.*, 1999). Therefore, within the context of NA, experimental and modelling work is divided into two distinctly different phases: the time-dependent or transient state and the stationary or steady-state.

The relevant NA processes take place in the 'transition zone' between a contaminant plume and surrounding subsurface environment. This zone is commonly referred to as the plume fringe. Dispersion results in a smearing of the biologically active zone (BAZ), which is created between the electron acceptor and contaminant fronts where all solutes are present. In a two- or three-dimensional domain, transverse dispersion is thought to be the controlling mechanism for aquifer remediation (Cirpka *et al.*, 1999; Klenk and Grathwohl, 2002), particulary when organic pollutants, e.g., petroleum hydrocarbons, are considered (Grathwohl *et al.*, 2000). Ham *et al.* (2004) confirm this is certainly the case for steady-state plume behavior, where solute mixing is assumed to occur only through hydrodynamic dispersion and reactions between solutes are considered instantaneous. The same paper demonstrates that longitudinal dispersion is only of importance during transient plume development, although other authors suggest longitudinal dispersion has little overall effect on mass removal rates (Borden & Bedient, 1986; Macquarrie & Sudicky, 1990).

Although it is often valid to assume biological reaction times be instantaneous

in comparison to transport times (Borden & Bedient, 1986; Huang *et al.*, 2003), this is frequently not the case, especially in the case of some enhanced remediation technologies (Koussis *et al.*, 2003). If biodegradation is controlled by kinetic processes instead, e.g., Lu *et al.* (1999); Essaid *et al.* (2000); Prommer et al. (2000), then the key question for NA is the rate at which contaminants can be degraded (Kremer & Sinke, 1999). Microbial activity is dependent on the bioavailability of all substrates (i.e. electron acceptor/donor, microbes and nutrients) and in general is limited by the lack of one of these compounds (Chu *et al.*, 2005). For such ENA applications, plume development becomes an interplay between dispersive mixing, causing plume expansion, and biodegradation, resulting in plume attenuation.

The competition between dispersive mixing and biodegradation is considered in one-dimension by Oya & Valocchi (1997), Oya & Valocchi (1998) and later by Keijzer *et al.* (2000). In those studies, transport and biodegradation of a contaminant and an electron acceptor, microbial growth and first-order microbial decay is simulated using a mathematical model consisting of three non-linear coupled partial differential equations, where microbial growth is described using the Michaelis-Menten model (Michaelis & Menten , 1913). Oya & Valocchi (1997) concluded that the subsequent travelling wave phenomenon results from interactions between the advective mixing and biodegradation processes although long-term contaminant removal rates are independent of dispersion parameters Oya & Valocchi (1998). Xin & Zhang (1998) simplified this approach by neglecting dispersion completely to yield a closed-form solution to approximate the travelling wave fronts of contaminant, electron acceptor and microbial mass. However, Keijzer *et al.* (2000) provides a semi-analytical solution to the mathematical model, which is less restrictive than that of Xin & Zhang (1998) and, when compared against a numerical solution (Keijzer *et al.*, 1998), almost perfectly approximates the travelling wave fronts. Cirpka & Valocchi (In press) present an analytical approach for a similar mixing controlled bioreactive transport problem in two-dimensions. However, that study considers only steady-state plume behavior where longitudinal dispersion can be assumed negligible.

This paper considers a two-dimensional extension of the problem originally proposed by Keijzer *et al.* (2000). Unlike Keijzer *et al.* (1998) the longitudinal dispersion term is not neglected in the governing equations, allowing both steady-state and time-dependent cases to be considered. Classical solution methods of this problem, as for example discussed by Sun (2002), can be infeasible. Therefore

the basic concept in this paper is the following: Instead of solving the coupled non-linear partial differential equations simultaneously, the equations are reduced to a more simple form to allow a sequential approach to solution. This provides an elegant solution method, which is computationally efficient and straightforward to execute.

5.2 The Mathematical Framework

The governing partial differential equation describing the fate of a reactive species k in three-dimensional transient incompressible flow is given by the advection-dispersion equation

$$\begin{aligned} \frac{\partial c^k}{\partial t}(\mathbf{x},t) &= \nabla \cdot (D \cdot \nabla c^k(\mathbf{x},t)) - v(\mathbf{x}) \cdot \nabla c^k(\mathbf{x},t) + R_{c^k}, \\ \mathbf{x} &= (x_1, x_2, x_3), \end{aligned} \tag{5.1}$$

where c is the concentration of species k, D is the hydrodynamic dispersion tensor, v is the effective pore water velocity through the medium and R_c is a reaction term.

The following assumptions (Oya & Valocchi, 1997; Keijzer *et al.*, 2000) are necessary to formulate a set of model equations from equation (5.1): Physical and biodegradation parameters (e.g. dispersivity, density, stoichiometric and half saturation coefficients) remain constant with respect to time and space; the microbial biofilm is immobile and microbes consume electron acceptor and degrade the electron donor at rates governed by Monod kinetics (Monod, 1949) following the Michaelis-Menten model (Michaelis & Menten , 1913); and the contaminant species is considered mobile and reversibly linearly sorbing. For simplicity, on the basis of the ratio of aquifer thickness to horizontal extent, it is assumed that flow is essentially horizontal and the aquifer can be modelled as a two-dimensional infinite domain (Bear & Bachmat, 1991). Therefore, the two-dimensional reactive transport of an electron acceptor C, a contaminant species G, and growth of microbes

M is written

$$\frac{\partial C}{\partial t} = D_l\frac{\partial^2 C}{\partial x^2} + D_t\frac{\partial^2 C}{\partial y^2} - v_x\frac{\partial C}{\partial x} - v_y\frac{\partial C}{\partial y} - m_C\frac{\partial M}{\partial t} - m_C d_m(M - M_{max}), \quad (5.2)$$

$$R\frac{\partial G}{\partial t} = D_l\frac{\partial^2 C}{\partial x^2} + D_t\frac{\partial^2 G}{\partial y^2} - v_x\frac{\partial G}{\partial x} - v_y\frac{\partial G}{\partial y} - m_G\frac{\partial M}{\partial t} - m_G d_m(M - M_{max}), \quad (5.3)$$

$$\frac{\partial M}{\partial t} = \mu_m\left[\frac{C}{k_C + C}\right]\left[\frac{G}{k_G + G}\right] M - d_m(M - M_{max}), \quad (5.4)$$

where R is a constant retardation factor governing the sorption/desorption of the contaminant species; D_l and D_t are the coefficients of longitudinal and transversal dispersion; μ_m and d_m are the maximum specific growth rate and decay rate; m_C and m_G are the ratios of electron acceptor and donor consumption rate to microbial growth rate; k_C and k_G are the half saturation constants for electron donor and acceptor.

Equations (5.2)-(5.4) are scaled using the dimensionless quantities

$$\begin{aligned} \bar{x} &= \frac{x}{L},\ \bar{t} = \frac{v_x t}{L},\ \bar{C} = \frac{C}{C_0},\ \bar{M} = \frac{M}{M_{max}},\ \bar{G} = \frac{G}{G_0}, \\ Pe^l &= \frac{v_x L}{D_l},\ Pe^t = \frac{v_x L}{D_t}, M_C = \frac{m_C M_{max}}{C_0},\ M_G = \frac{m_G M_{max}}{G_0}, \\ K_C &= \frac{k_C}{C_0},\ K_G = \frac{k_G}{G_0},\ L_\mu = \frac{\mu_m L}{v_x},\ L_d = \frac{d_m L}{v_x}, \end{aligned} \quad (5.5)$$

where L is a characteristic length scale. L_μ, L_d, Pe^l and Pe^t are the Damkolmer number, decay number and Peclet numbers in the longitudinal and transversal direction respectively. L_μ describes the rate of microbial growth over advection, L_d the rate of decay over advection and Pe^l and Pe^t the rate of advection over dispersion in the longitudinal and transverse directions. M_{max} is the maximum amount of microbial mass that can accumulate in the domain. Note that the dimensionless quantities, e.g. L_μ, L_d, etc., are defined with the velocity component in the x-direction.

The resulting set of dimensionless equations, after omitting the bar notation and assuming that convection in the y-direction is absent, i.e., uniform flow in the

x-direction, are written as

$$\frac{\partial C}{\partial t} = \frac{1}{Pe^l}\frac{\partial^2 C}{\partial x^2} + \frac{1}{Pe^t}\frac{\partial^2 C}{\partial y^2} - \frac{\partial C}{\partial x} - M_C\frac{\partial M}{\partial t} - M_C L_d(M-1), \quad (5.6)$$

$$R\frac{\partial G}{\partial t} = \frac{1}{Pe^l}\frac{\partial^2 G}{\partial x^2} + \frac{1}{Pe^t}\frac{\partial^2 G}{\partial y^2} - \frac{\partial G}{\partial x} - M_G\frac{\partial M}{\partial t} - M_G L_d(M-1), \quad (5.7)$$

$$\frac{\partial M}{\partial t} = L_\mu \left[\frac{C}{K_C + C}\right]\left[\frac{G}{K_G + G}\right] M - L_d(M-1), \quad (5.8)$$

which will be the starting point for further analysis.

5.3 ENA Model Scenarios

In this paper three ENA scenarios will be investigated: (i) Instantaneous (Figures 5.2) and, (ii) Continuous injection (Figures 5.4) over a planar source area and, (iii) Continuous line source injection ($y > 0$) (Figures 5.5) of an electron acceptor into a flow domain initially contaminated everywhere by a mobile organic contaminant species and filled with an immobile microbial species. For scenarios (i),(ii), a planar source provides the most realistic geometry for field-scale problems (Domenico & Schwartz, 1997). The initial conditions indicate that the electron acceptor concentration is the limiting biodegradation factor for each case presented.

5.3.1 Case 1: Instantaneous planar source

At a time $t = 0$, there is an instantaneous injection of electron acceptor across an area A of dimension $2a$ by $2a$, symmetrically distributed about the origin (0,0) (see Figure 5.1)). At $t > 0$ for $y \in \mathbf{R}$ there is a mass flux of contaminant and microbes at the inlet of the domain. A plume of electron acceptor develops which moves downstream in time and activates the microbial mass. Dispersion causes lateral and longitudinal spreading of the electron acceptor and consequently a decrease in the contaminant concentration per unit area in the BAZ.

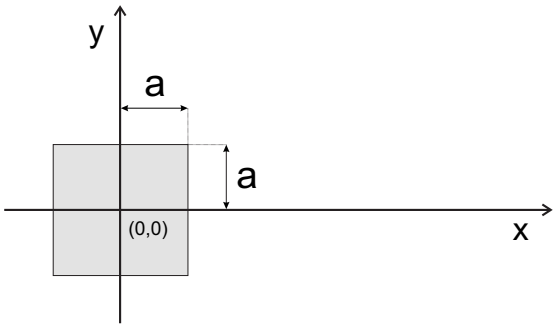

Figure 5.1: *Geometry of the planar source.*

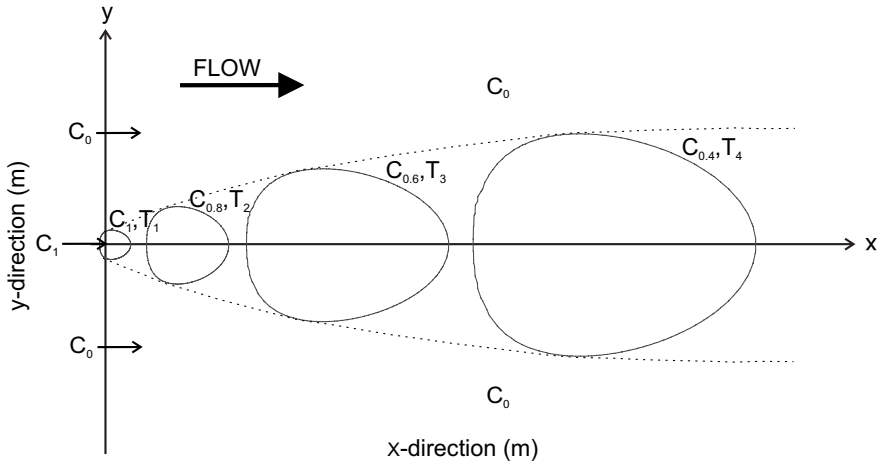

Figure 5.2: *Case 1: Instantaneous planar source injection of electron acceptor.*

Initial and boundary conditions

Equations (5.6-5.8) are subject to the initial conditions (IC)

$$\begin{aligned} C(x,y,0) &= C_0(x,y) = 0 \text{ for } -a > x > +a \text{ and } -a > y > +a \\ G(x,y,0) &= G_0(x,y) = 1 \text{ for all } (x,y) \in \mathbf{R}, \\ M(x,y,0) &= M_0(x,y) = 1 \text{ for all } (x,y) \in \mathbf{R}, \end{aligned} \tag{5.9}$$

Across the planar source, the electron acceptor is instantaneously injected, such that

$$C(x,y,t) = C_0(x,y,t) = 1 \text{ for } -a < x < +a \text{ and } -a < y < +a. \tag{5.10}$$

Mathematical analysis: The time-dependent case

Starting point for the analysis are the non-dimensional approximate equations (5.6)-(5.8), subject to (5.9-5.10). Multiplication of (5.6) by M_G and (5.7) by M_C, subtraction of the resulting equations and introduction of the parameter $\beta = M_C/M_G$ yields

$$\begin{aligned} \frac{\partial}{\partial t}\left[C - R\beta G\right] = \frac{1}{Pe^l} \quad & \frac{\partial^2}{\partial x^2}\left[C - \beta G\right] \\ & + \frac{1}{Pe^t}\frac{\partial^2}{\partial y^2}\left[C - \beta G\right] - \frac{\partial}{\partial x}\left[C - \beta G\right]. \end{aligned} \tag{5.11}$$

Disregarding contaminant retardation, which is a reasonable assumption for most organic contaminants, i.e. $R = 1$ in (5.11), allows the introduction of the new variable

$$w(x,y,t) = C(x,y,t) - \beta G(x,y,t). \tag{5.12}$$

After introduction of w, equation (5.11) reduces to

$$\frac{\partial w}{\partial t} = \frac{1}{Pe^l}\frac{\partial^2 w}{\partial x^2} + \frac{1}{Pe^t}\frac{\partial^2 w}{\partial y^2} - \frac{\partial w}{\partial x}, \tag{5.13}$$

subject to the IC (5.9)

$$w(x,y,0) = w_0(x,y) = -\beta \text{ for all } (x,y) \in \mathbf{R}. \tag{5.14}$$

Note that equation (5.13) describes two-dimensional displacement of a conservative tracer. Introducing the moving coordinate $s(x,y) = x - t$ such that $w(x,y,t) = w(s(x,t),y,t)$ yields

$$\frac{\partial w}{\partial t} = \frac{1}{Pe^l}\frac{\partial^2 w}{\partial s^2} + \frac{1}{Pe^t}\frac{\partial^2 w}{\partial y^2}, \tag{5.15}$$

where the initial condition, only when $C = 0$ and $G = 1$, is given by

$$w(s,y,0) = w_0(s,y) = -\beta \ \text{ for all } \ (s,y) \in \mathbf{R}. \tag{5.16}$$

Considering the case of an instantaneous injection of a mass M of tracer w over the planar area A, an explicit solution to problem (5.15), subject to the BC, follows from Hunt (1978) and is given by

$$\begin{aligned} w(s,y,t) = \frac{w_0}{4} &\left[erf\left(\frac{a-s}{2\sqrt{\frac{1}{Pe^l}t}}\right) + erf\left(\frac{a+s}{2\sqrt{\frac{1}{Pe^l}t}}\right)\right] \\ &\times \left[erf\left(\frac{a-y}{2\sqrt{\frac{1}{Pe^t}t}}\right) + erf\left(\frac{a+y}{2\sqrt{\frac{1}{Pe^t}t}}\right)\right] \quad -\beta, \end{aligned} \tag{5.17}$$

where

$$w_0 = \frac{M}{A} = \frac{M}{4a^2}. \tag{5.18}$$

Once the solution $w(x,y,t)$ is known, and thereby $C(x,y,t) = \beta G(x,y,t) + w(x,y,t)$, the result can be used to reduce equations (5.6)-(5.8) to two coupled PDE's in terms of G and M, yielding

$$\begin{aligned} \frac{\partial G}{\partial t} = \frac{1}{Pe^l}\frac{\partial^2 G}{\partial x^2} + \frac{1}{Pe^t} &\quad \frac{\partial^2 G}{\partial y^2} - \frac{\partial G}{\partial x} \\ &\quad -M_G L_\mu \left[\frac{\beta G + w}{K_C + \beta G + w}\right]\left[\frac{G}{K_G + G}\right] M, \end{aligned} \tag{5.19}$$

and

$$\frac{\partial M}{\partial t} = L_\mu \left[\frac{\beta G + w}{K_C + \beta G + w}\right]\left[\frac{G}{K_G + G}\right] M - L_d(M-1), \tag{5.20}$$

subject to the IC and BC for G and M, i.e. given by (5.9) and (5.10). Due to the nonlinear coupled character of the equations, we have to rely on numerical techniques to obtain the solution for G and M. Substitution of G into the definition of w, i.e. (5.30), immediately gives the solution for C.

5.3.2 Case 2: Continuous planar source

The continuous planar source follows the same principle as with the instantaneous model. However, in this case, it is required that the concentration across the source area be maintained at C_0. For the planar source, this can only be achieved by extending the source geometry to infinity in the $-x$ direction (Crank , 1964). In Domenico & Robbins (1985) this is called the *extended pulse approximation* and the geometry for the problem considered here is shown in Figure 5.3. Thus, for

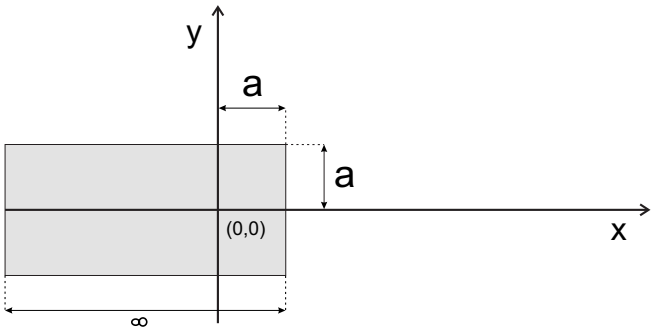

Figure 5.3: *Extended source geometry for continuous injection*

$t > 0$ there is an continuous injection of electron acceptor from the source area, and for $y \in \mathbf{R}$ there is a mass flux of contaminant and microbes at the inlet of the domain. This results in the formation of a steady-state plume of electron acceptor downstream of the source as $t \to \infty$. The contaminant concentration per unit area is lowest at the source, and increases the further downstream from the source, or further away from the plume centre line (x-direction), the observation point is.

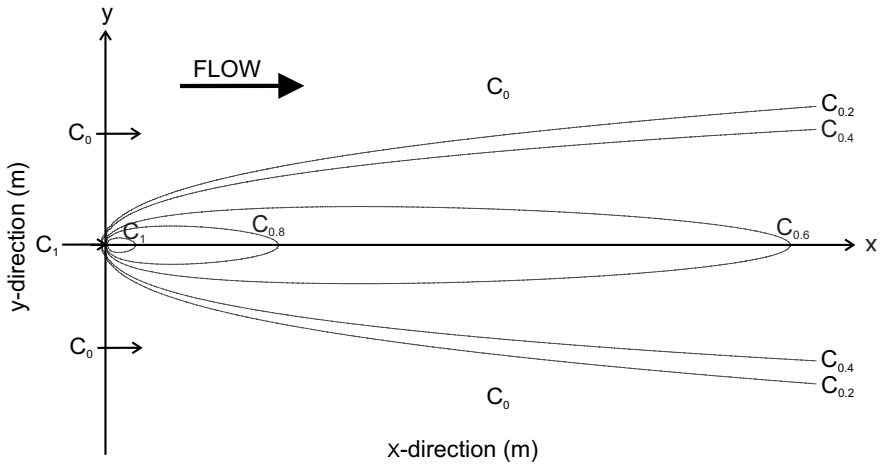

Figure 5.4: *Case 1: Continuous point source injection of electron acceptor (steady-state condition at $t = \infty$).*

Initial and boundary conditions

Similar to case 1, IC are given by

$$\begin{aligned} C(x,y,0) &= C_0(x,y) = 0 \text{ for } -\infty > x > +a \text{ and } -a > y > +a \\ G(x,y,0) &= G_0(x,y) = 1 \text{ for all } (x,y) \in \mathbf{R}, \\ M(x,y,0) &= M_0(x,y) = 1 \text{ for all } (x,y) \in \mathbf{R}. \end{aligned} \tag{5.21}$$

The contaminant is continuously injected over the extended source area, such that

$$C(x,y) = C_0(x,y) = 1 \text{ for } -\infty < x < +a \text{ and } -a < y < +a. \tag{5.22}$$

Mathematical analysis: The time-dependent case

The problem (5.6)-(5.8) can be solved using the same procedure as for Case 1, using the intermediate solution of equation (5.15), subject to the IC (5.21 - 5.22), where

$$w(s,y,0) = w_0(s,y) = -\beta \text{ for all } (s,y) \in \mathbf{R}. \tag{5.23}$$

An explicit solution for w(s,y,t), which describes the advection and dispersion of a tracer solute originating from a continuous source, follows from Domenico &

Robbins (1985) yielding

$$w(s,y,t) = \frac{w_0}{4} erfc \left(\frac{s}{2\sqrt{\frac{1}{Pe^l}t}} \right) \times \left[erf\left(\frac{a-y}{2\sqrt{\frac{1}{Pe^t}t}} \right) + erf\left(\frac{a+y}{2\sqrt{\frac{1}{Pe^t}t}} \right) \right] - \beta, \quad (5.24)$$

where

$$w_0 = \int_0^t \frac{M}{Q}\, dt, = \frac{M}{2a^2}. \quad (5.25)$$

and Q is the flow rate. Again, once the solution of $w(x,y,t)$ is known, the starting equations (5.6)-(5.8) reduce to (5.19) and (5.20).

The stationary case

If all terms containing a time-derivative are equated to zero in equations (5.6)-(5.8), we arrive at the stationary equations, given by

$$\frac{1}{Pe^l}\frac{\partial^2 C}{\partial x^2} + \frac{1}{Pe^t}\frac{\partial^2 C}{\partial y^2} - \frac{\partial C}{\partial x} - M_C L_d (M-1) = 0, \quad (5.26)$$

$$\frac{1}{Pe^l}\frac{\partial^2 G}{\partial x^2} + \frac{1}{Pe^t}\frac{\partial^2 G}{\partial y^2} - \frac{\partial G}{\partial x} - M_G L_d (M-1) = 0, \quad (5.27)$$

and

$$L_\mu \left[\frac{C}{K_C + C} \right] \left[\frac{G}{K_G + G} \right] \; M - L_d (M-1) = 0. \quad (5.28)$$

Note that (5.26) and (5.27) are linear PDE's, while (5.28) is an algebraic equation, relating M to C and G. The solution of the problems (5.26) and (5.27), subject to (5.21), can be constructed applying the procedure used for the time-dependent cases. Multiplication of (5.26) by M_G and (5.27) by M_C and subtraction the resulting equations yields

$$\frac{1}{Pe^l}\frac{\partial^2}{\partial x^2}[C - \beta G] + \frac{1}{Pe^t}\frac{\partial^2}{\partial y^2}[C - \beta G] - \frac{\partial}{\partial x}[C - \beta G] = 0. \quad (5.29)$$

Again this allows the introduction of the new variable

$$w(x, y, \infty) = C(x, y, \infty) - \beta G(x, y, \infty), \tag{5.30}$$

and the auxiliary problem takes the form

$$\frac{1}{Pe^l}\frac{\partial^2 w}{\partial x^2} + \frac{1}{Pe^t}\frac{\partial^2 w}{\partial y^2} - \frac{\partial w}{\partial x} = 0, \tag{5.31}$$

subject to

$$w(x, y, \infty) = w_0(s, y) = -\beta \text{ for all } (s, y) \in \mathbf{R}. \tag{5.32}$$

In the limit $t \to \infty$, the value of the complimentary error function in equation (5.24) approaches the value 2 and, as such, equation (5.24) reduces to the stationary distribution, given by

$$w(x, y, \infty) = \frac{w_0}{2} \cdot \left[erf\left(\frac{a - y}{2\sqrt{\frac{1}{Pe^t}x}}\right) + erf\left(\frac{a + y}{2\sqrt{\frac{1}{Pe^t}x}}\right)\right] - \beta. \tag{5.33}$$

Note that this expression (5.33) is independent of longitudinal dispersivity, which demonstrates that transversal dispersivity is the only governing dispersion parameter for the stationary distribution of the new parameter, w. Substitution of the result for $w(x, y, \infty)$ into (5.28), and rearranging terms gives

$$M = \frac{1}{1 - \gamma P(G(x, y))}, \tag{5.34}$$

where

$$P(G(x, y)) = \left[\frac{\beta G(x, y) + w(x, y)}{K_C + \beta G(x, y) + w(x, y)}\right] \left[\frac{G(x, y)}{K_G + G(x, y)}\right], \tag{5.35}$$

and $\gamma = L_\mu / L_d$. Combining (5.34) and (5.27) yields

$$\frac{1}{Pe^l}\frac{\partial^2 G}{\partial x^2} + \frac{1}{Pe^t}\frac{\partial^2 G}{\partial y^2} - \frac{\partial G}{\partial x} - M_G L_d \frac{\gamma P(G)}{1 - \gamma P(G)} = 0. \tag{5.36}$$

Note that $G = G(x, y)$ is the only dependent variable in equation (5.36). This problem (5.36) has to be solved numerically. Once a numerical approximation of the function $G(x, y)$ has been obtained, the corresponding distributions of $C(x, y)$ and $M(x, y)$ follow directly from (5.30) and (5.34), respectively.

5.3.3 Case 3: Continuous line source ($y \geq 0$)

At $t > 0$ for $y > 0$ there is a mass flux of electron acceptor and microbes at the inlet of the domain, whilst for $y < 0$ there is a mass flux of contaminant species and microbes. Here, a mixing zone forms between the the two species.

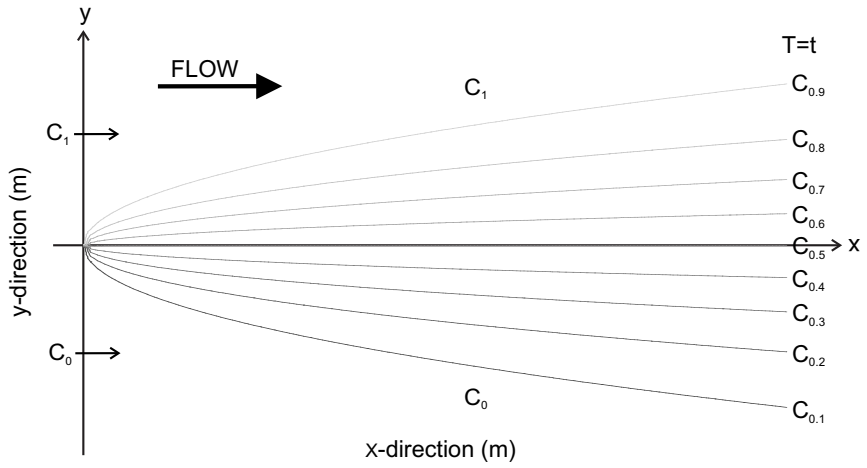

Figure 5.5: *Case 3: Continuous line ($y \geq 0$) source injection of electron acceptor (steady-state condition at $t = T$).*

Initial and boundary conditions

The following IC apply:

$$\begin{aligned} C(x, y, 0) &= C_0(x, y) = 0, \\ G(x, y, 0) &= G_0(x, y) = 1, \\ M(x, y, 0) &= M_0(x, y) = 1, \end{aligned} \tag{5.37}$$

for all $x > 0$ and $y \in \mathbf{R}$. The BC are given by

$$C(0, y, t) = 1, \;\; G(0, y, t) = 0 \;\text{ and }\; M(0, y, t) = 1 \;\text{ for }\; y > 0, \tag{5.38}$$

and

$$C(0, y, t) = 0, \;\; G(0, y, t) = 1 \;\text{ and }\; M(0, y, t) = 1 \;\text{ for }\; y < 0, \tag{5.39}$$

for $t > 0$.

Mathematical analysis: The time-dependent case

Again the same analysis follows as for the transient case in Scenarios 1 & 2. Equation (5.15) is subject to (5.38 and 5.39), yielding

$$w(0, y, t) = +1 \;\text{ for }\; y > 0 \;\text{ and }\; t \geq 0, \tag{5.40}$$

$$w(0, y, t) = -\beta \;\text{ for }\; y < 0 \;\text{ and }\; t \geq 0. \tag{5.41}$$

The analytical solution to (5.15) subject to (5.40 and 5.41), extended from the solution for a finite line source proposed by Domenico and Schwartz, reads

$$w(s, y, t) = -\beta + \frac{1}{4}(1 + \beta)\,\text{erfc}\left(\frac{s}{2\sqrt{\frac{1}{Pe^l}t}}\right)\left(1 + \,\text{erf}\left(\frac{y}{2\sqrt{\frac{1}{Pe^t}t}}\right)\right). \tag{5.42}$$

Once again, once the solution to $w(x, y, t)$ is known, the governing equations can be reduced to (5.6-**??**) and solved numerically.

The stationary case

The conditions at $x = 0$ for C and G are respectively given by

$$C(0, y) = C_0(y) = \begin{cases} 1 & \text{for} \quad y > 0, \\ 0 & \text{for} \quad y < 0. \end{cases} \tag{5.43}$$

and

$$G(0,y) = G_0(y) = \begin{cases} 0 & \text{for} \quad y > 0, \\ 1 & \text{for} \quad y < 0. \end{cases} \tag{5.44}$$

The solution of the problems (5.26), subject to (5.43), and (5.27), subject to (5.44), can be constructed applying the same procedure given for the continuous point source (stationary case). The auxiliary problem, subject to

$$\begin{aligned} w(0,y) &= w_0^-(y) = -\beta \ \text{ for } \ y < 0 \ \text{ and} \\ w(0,y) &= w_0^+(y) = 1 \ \text{ for } \ y > 0, \end{aligned} \tag{5.45}$$

can be solved in terms of an explicit solution given by

$$w(x,y,t) = -\beta + \frac{1}{4}(1+\beta)\left(1 + \ \text{erf}\left(\frac{y}{2\sqrt{\frac{1}{Pe^t}x}}\right)\right). \tag{5.46}$$

Again, expression (5.46) is independent of longitudinal dispersivity. Substitution of this result into (5.28), and rearranging terms yields the same set of equations as given by (5.34 - 5.36).

5.4 Results and Discussion

The numerical models developed for the three ENA scenarios present an elegant method of solving the original coupled PDE's. Whilst the initial and boundary conditions are obviously different for all three scenarios, the general solution presented for the time dependent cases is the same for all three models, and in the two cases (i.e., continuous injection) where a stationary case develops, the formulation of the resulting solution is also the same. Therefore, the difference between the models is only apparent in the intermediate solution of the new variable w, which is a conservative quantity equal to the concentrations of contaminant and electron acceptor present in the domain at a particular time. Since this quantity is conservative, it is possible to solve the linear PDE in terms of w using an appropriate analytical solution. In this study, the solutions from Domenico & Robbins (1985) for a pulse and continuous injection omitted from a planar source were used, although it would be possible to use other solutions.

5.4.1 Simplified solutions

Dispersion is assumed to be the only mixing mechanism in the ENA problems considered here. This mechanism establishes the contact between EA, ED and M. If $Pe^t \to 0$, then the model equations decouple, implying the absence of a mixing fringe. In that case, solutions become trivial. If $Pe^t > 0$, contact between EA and ED is established, and a BAZ is created. Note that in the limit $M_C \to 0$ and $M_G \to 0$, the equations for the EA and ED decouple. In that case, (independent) explicit solutions for C and G can be obtained in terms of error functions. In the limit $\beta \to 0$, which corresponds to $M_C \to 0$, while $M_G > 0$, the solution for the EA is explicitly given by $C(x, y, t) = w(x, y, t)$.

5.4.2 Model validation

A numerical code was developed in Matlab to simulate the three ENA scenarios. The coupled PDE's expressing flow and transport of the electron acceptors and donors, along with microbial growth were solved using a 3rd order Runge-Kutta scheme. In this section, results of the modelling exercise are presented and the limitations of the model are discussed. For the benefit of the reader, the results presented are given in dimensional notation.

The developed model was validated in two ways. Firstly it was tested against a purely numerical simulation of the three original coupled equations (5.2-5.4). It was evident from simulations for all ENA scenarios that, in order to provide an accurate solution, it is vital to include longitudinal dispersion in the model input parameters. If $\alpha_l \to 0$, then the front of the plume obviously becomes too sharp, and the model fails to converge to a solution at the front of the plume, which leads to oscillating concentrations in this zone. This effect cannot be reduced simply by refining the grid discretisation. However, it is not really seen as a limitation, since time dependent development of reactive plumes is dependent not only on transversal, but also longitudinal mixing (Ham *et al.*, 2004). These effects become negligible when considering steady-state plume behavior, so care must only be taken when transient plume development is of importance. Note also that some discrepancy exists between the full numerical solution and the model developed in this study close to the source area. Centreline concentrations ($y = 0$) of the EA, ED, microbial mass M and parameter w are presented in Figure 5.6, for Scenario 3 (continuous injection over a half plane) at time $t = 25$ *days* and the parameter

Parameter	Value
C_0	1mg/l
G_0	1mg/l
M_0	1mg/l
v_x	1m/d
α_t	0.1 m
α_l	1 - 1e^{-4} m
m_C	1
m_G	1
k_C	0.5 mg/l
k_G	0.5 mg/l
μ_m	0.25 day^{-1}
d_m	0.2 day^{-1}
Domain length	50 m
Domain width	15 m
d_x	0.25 m
d_y	0.25 m

Table 5.1: *Parameter values for model validation (first exercise).*

values listed in Table 5.1.

As a secondary test, the model was compared against results presented by Huang *et al.* (2003). In that study, aerobic microbial degradation of acetate injected from a planar source was investigated using high-resolution laboratory experiments. The experiments considered by Huang *et al.* (2003) were conducted under steady, horizontal flow conditions in a thin porous media of dimensions $156 \times 120 \times 3\ mm$, constructed from quartz plates and quartz sand enriched with acetate degrading bacteria. After an initial time-dependent phase, the continuous injection of ED over time results in a quasi-stationary condition after approximately a day, when the net influx of EA into the plume is equal to the net flux of ED being emitted from the source zone. The plume is quasi steady-state because the experiments were conducted over short distances and (due to the hydrological setup) short times, where microbial growth is rapid and microbial decay is, in comparison, not important. Parameter values for the Monod-kinetic reactions were obtained from batch reactions, whilst transversal and longitudinal dispersivites were derived from conservative (fluorescein tracer) experiments. These parameters were used as input values in the numerical model RT3D (Clement , 2002) to simulate

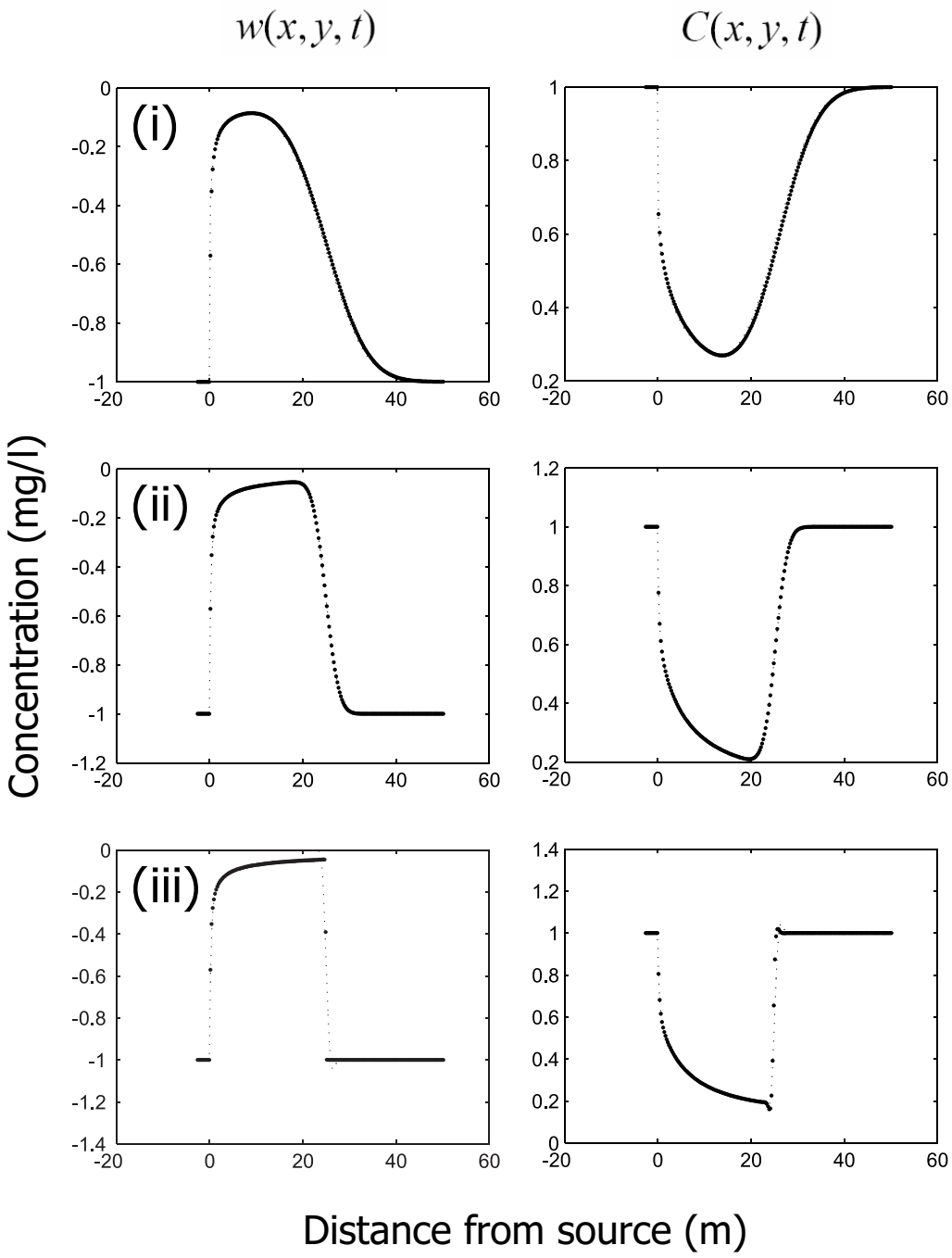

Figure 5.6: *Discrepancies between the developed model (points) and full numerical solution (dashed line) at t = 25 days for Scenario 3. Parameters as in Table 5.1 for* α_l *= (i) 1 m, (ii) 0.1 m, and (iii) 1e-4 m.*

Parameter	Value
C_0	1000mg/l
G_0	6.64mg/l
M_0	10mg/l
v_x	1.08m/day
α_t	1.64e^{-4} m
α_l	7.5e^{-4} m
D_mol	8.65e^{-5} m^2/day
m_C	1.22
m_G	3.13
k_C	0.01 mg/l
k_G	2.1 mg/l
μ_m	7.2 day^{-1}
Source size	8 mm
Domain length	120 mm
Domain width	156 mm
d_x	1 mm
d_y	1 mm

Table 5.2: *Parameter values used in the numerical simulations by Huang et al. (2003). Values are given in terms of the notation used in this article.*

the steady-state profiles of oxygen depletion transverse to the flow direction at a distance of 76mm downstream of the source. Through a sensitivity analysis, the numerical model provided an excellent comparison with experimental data.

The parameter values, given in Table 5.2, used in the numerical simulations by Huang *et al.* (2003) were used in the model developed in this study for the case of continuous injection from a planar source. A model domain of 200×120 mm (at a discretisation of $dx = 1$ mm, $dy = 1$ mm) was considered, slightly longer than in the simulated study to avoid boundary effects at the outflow end of the domain. The EA was injected over an 8 mm wide source. Note that in this experiment ED is injected into the domain initially containing EA. Figure 5.7 shows the EA profiles at a distance 76 mm downstream of the source zone after 1 day. There is an excellent comparison between numerical simulations by Huang *et al.* (2003) and the model presented in this study.

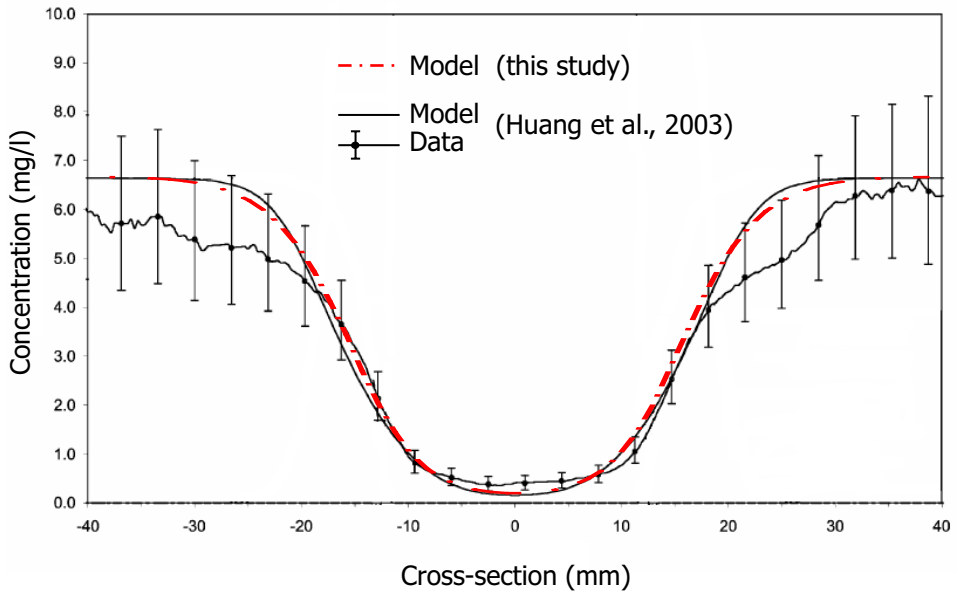

Figure 5.7: *Comparison of numerical model from this study with modelling and experimental data from Huang et al. (2003).*

5.4.3 Fringe width and microbial activity

The effects of microbial activity on plume attenuation were investigated using the conceptual model presented by Huang *et al.* (2003). That paper is one of the few studies which provide comprehensive data (especially parameter values for reaction-kinetics) for kinetic-controlled attenuation. This is preferable to field-scale data, e.g., MacQuarrie *et al.* (1990); Kindzelbach & Schafer (1991); Chen *et al.* (1992), where the assumptions of a homogeneous medium and steady-state uniform flow may not apply.

In particular, the focus of this investigation is to look at the mechanisms controlling the development of the steady-state plume fringe, where biological reactions take place. The plume fringe can be described as the zone between the contaminated and uncontaminated aquifer; in this model it is defined as the area from $C = 1$ to $C = 0$ or, alternatively, $G = 0$ to $G = 1$. In the steady-state mathematical models considered here, transversal dispersion is the primary mechanism leading to the development of a plume fringe, causing mixing of the EA and ED. In contrast, the effect of microbial activity works in opposition to the dilution of the EA concentrations, causing a 'sharpening' of the fringe and larger concentra-

tion gradients between EA and ED. That is, transversal mixing causes a widening of the fringe, whilst degradation increases depletion of the available EA. These combined effects can be termed as *effective dispersion* and is of great practical importance. In the case of Huang *et al.* (2003), an effective transversal dispersivity of $1.67e^{-4}$ m was needed to match the profiles from the experimental data, whilst the actual transversal dispersivity of the medium derived from conservative tracer experiments was only $5e^{-5}$ m. Since transversal dispersivity is a property of the porous medium, the effective value must be influenced by microbial activity.

The numerical model developed in this study was applied to the data from Huang *et al.* (2003) to investigate the governing attenuation processes controlling the width of the plume fringe. However, these investigations were conducted over longer time periods, to account for the effects of microbial decay and achieve steady-state plumes. Figure 5.8 demonstrates the effects of microbial activity on the width of the plume fringe, measured from the point within the plume where EA are almost completely consumed to the point outside the plume where EA concentrations are at a maximum. In all simulations the parameters listed in table 5.2 were adopted and only decay l_d was varied. Clearly, when microbial growth is significantly greater than microbial decay, the plume fringe narrows considerably. In the limit that $l_d \rightarrow 0$, the gradient of the plume fringe tends towards that given by a model assuming instantaneous reactions between EA and ED. For values of $l_d > \mu_m$, which is not physically realistic, there is no change in the size of the plume fringe since there is no net growth in microbial mass. Moreover, the overall extent of plume spreading, indicated by f in Figure 5.8), remains unchanged (approximately 37 mm) regardless of microbial activity because the maximum extent of plume spreading is controlled only by transversal dispersion.

5.4.4 Apparent transversal dispersion

The three curves in Figure 5.8 were obtained using a transversal dispersion coefficient of 1.8e^{-4} m^2/day and a molecular diffusion coefficient of 8.65e^{-5} m^2/day. However, it is also possible to reproduce the same gradients using an appropriate analytical solution for tracer transport, e.g., as suggested for a continuous planar source by Domenico & Robbins (1985). The transversal dispersion coefficient obtained from linear regression techniques is known as apparent transversal dispersion. Figure 5.9 shows the reduction in the apparent dispersion coefficient plotted against increased microbial activity for the same simulations. When the

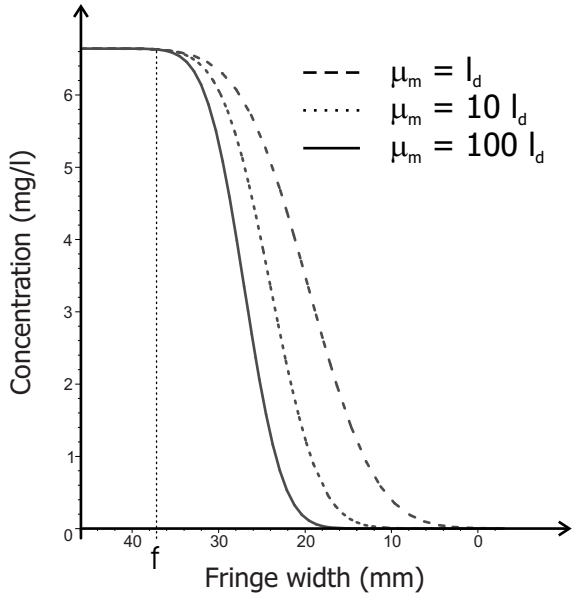

Figure 5.8: *Reduction of fringe width due to increased microbial activity.*

microbial decay rate is approximately 13 times smaller than microbial growth, the apparent dispersivity of the plume fringe is similar to the value derived from the conservative experiments, i.e., $\approx 5e^{-5}\ m$.

5.5 Conclusions

In this paper, a new method of solving the three nonlinear coupled PDE's for transport and mixing of contaminants (electron donors) and electron acceptors was presented. The assumption is that reactions between the EA and ED are kinetically controlled. The model developed is a two dimensional extension of the model presented by Keijzer *et al.* (2000), where microbial growth can be expressed mathematically as a Monod term and microbial decay, which occurs when either EA or ED concentrations are completely depleted, as a first order reaction. In this study, the domain was assumed to be homogeneous with steady, uniform flow in the $x-$direction. Three cases of enhanced natural remediation (ENA) were considered for the development of the mathematical model. These included (i) pulse, and (ii) continuous injection from a planar source, and (iii) continuous injection across a half plane, of EA into a domain initially containing only an ED

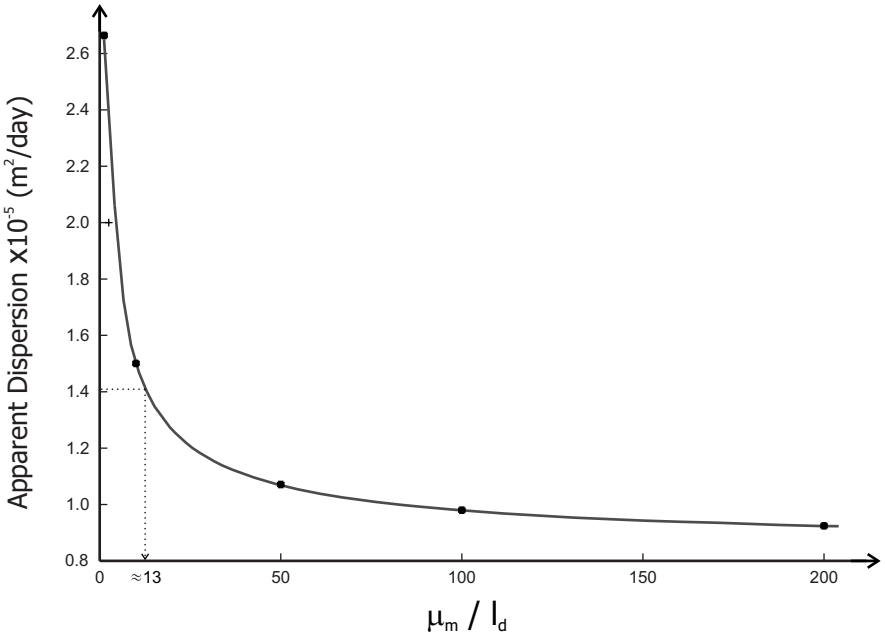

Figure 5.9: *Reduction of apparent dispersion coefficient as a result of increased microbial activity.*

.

and an immobile microbial mass M. In all the transient cases it was demonstrated that the initial three coupled equations can be reduced to two coupled nonlinear PDE's in terms of G and M through the introduction of a new variable $w(x, y, t)$, which is a conservative quantity combining the variables C and G and can be described explicitly. In the cases where a stationary solution arises, the equations can be further reduced to one equation in terms of the single variable G. In both cases the final equation(s) have to be solved numerically but the advantage of this procedure lies in the fact that the three coupled nonlinear PDE's do not have to be solved simultaneously, which provides an elegant method of solution for both transient and steady-state cases. This is the main advantage over, for example, the procedure presented by Cirpka & Valocchi (In press), which provides only steady-state solutions by assuming that longitudinal dispersion is not important in terms of stationary plume development. Of course, whilst the models developed here consider only cases of ENA, the model equations can be easily re-written to address appropriate NA scenarios as necessary.

The model developed in this study was validated against a purely numerical solution of the original three coupled PDE's. An excellent comparison was found, however, failure to include longitudinal dispersion results in oscillating concentrations developing at the leading edge of a migrating (transient) plume. Furthermore the model was tested against the quasi-stationary results presented by Huang *et al.* (2003), who considered kinetic controlled reactions between an EA and an ED in high resolution laboratory experiments. An excellent agreement was found between the numerical simulations presented in that paper and the model developed in this study. Furthermore, the conceptual model of Huang *et al.* (2003) was extended to larger time limits, where effects of microbial decay become important. Through numerical simulations, it was found that the width of a stationary plume fringe becomes increasingly narrower, due to the steep concentration gradients between EA and ED populations, as microbial activity is increased. Although microbial activity has no overall effect on the maximum lateral spreading of a plume, which is governed purely by transversal dispersion, the reduction in size of the plume fringe has large implications for remediation strategies.

This study demonstrates that apparent transversal dispersion coefficients, which describe only the gradient of the biologically active zone between EA and ED, can be much smaller than the effective dispersion coefficients used to predict the overall spreading of a groundwater plume. This is of practical importance in the field,

where often the focus of remediation is on the description of the characteristics of the plume fringe, where biological reactions take place. Since it is difficult to access microbial parameters at the field-scale, consideration of only apparent dispersivities can lead to under predictions in natural attenuation capacity of contaminant plumes. Therefore, understanding the link between apparent and effective dispersion mechanisms is paramount to describing plume migration where kinetically controlled reactions occur.

Bibliography

Bear, J., Bachmat, Y., 1991. Introduction to Modeling Phenomena of Transport in Porous Media. Kluwer Academic publishers, Dordrecht, The Netherlands.

Borden, R.C., Bedient, P.B., 1986. Transport of dissolved hydrocarbons influenced by oxygen-limited biodegradation 1. Theoretical Development. Water Resources Research (22), 1973-1982.

Carslaw and Jaeger (eds.), 1986. Conduction of Heat in Solids (Second Edition). Claredon Press, Oxford.

Chen, Y., Abriola, L.M., Alvarez, P.J.J., Anid, P.J., Vogel, T.M., 1992. Modeling transport and biodegradation of benzen and toluene in sandy aquifer material: Comparisons with experimental measurements. Water Resour. Res. 28(7), 1833-1847.

Chu, M., Kitanidis, P.K., McCarty, P.L., 2005. Modeling microbial reactions at the olume fringe subject to transverse mixing in porous media: When can the rates of microbial reaction be assumed instantaneous? Water Resour. Res. 41, W06002, doi:10.1029/2004WR003495.

Cirpka, O.A., Frind, E.O., Helmig, R., 1999. Numerical simulation of biodegradation controlled by transverse mixing. J. Contam. Hydrol. 40, 159-182.

Cirpka, O.A., Valocchi, A.J. Two-Dimensional Concentration Distribution for Mixing-Controlled Bioreactive Transport in Steady State. Submitted.

Clement, P.T. A modular computer code for simulating reactive multi-species transport in 3-dimensional groundwater aquifers. Technical Report PNNL-SA-28967, Battelle Pacific Northwest National Laboratory Research Report, Richlands, Washington, September 1997.

Crank, J., 1964 The mathematics of diffusion (Third Edition). Clarendon Press, Oxford.

Domenico P.A, Robbins, G.A., 1985. A new method of contaminant plume analysis. Groundwater 23, 476485.

Domenico, P.A., Schwartz, F.W., 1997. Physical and Chemical Hydrogeology (Second Edition). J. Wiley & Sons Inc, New York.

Essaid, H.I., I.M. Cozzarelli, R.P. Eganhouse, W.N. Herkelrath, B.A. Bekins, Delin, G.N., 2003. Inverse modeling ofBTEX dissolution and biodegradation at the Bemidji, MNcrude-oil spill site. J. Contam. Hydrol., 67, 269299.

Grathwohl, P., Klenk, I.D., Ederhardt, C., Maier, U., 2000. Steady state plumes: mechanisms of transverse mixing in aquifers. In C.D. Johnston: Contaminant Site Remediation: From Source Zones to Ecosystems, Proc. CRSC, Melbourne, Vic., 4-8 Dec., Centre for Groundwater Studies, CSIRO, Perth, Western Australia, 459-466.

Gutierrez-Neri, M., Ham, P.A.S., Schotting, R.J., Lerner, D. Article in preperation for submission to Ground Water.

Ham, P.A.S., Schotting, R.J., Prommer, H, Davis, G.B., 2004. Effects of hydrodynamic dispersion on plume lengths for instantaneous bimolecular reactions. Adv. Water Resour. Res. 27, 803-813.

Huang, W.E., Oswald, S.E., Lerner, D.N., Smith, C.C., Zheng, C., 2003. Dissolved oxygen imaging in a porous medium to investigate biodegradation in a plume with limited electron acceptor supply. Environ. Sci. Technol. 37, 1905-1911.

Hunt, B., 1978. Dispersive sources in uniform groundwater flow. J. Hydraul. Div., Proc. Am. Soc. Civ. Eng. 104, 75-85.

Keijzer, H., Zee, S.E.A.T.M. van der, Leijnse, A., 1998. Charachteristic regimes for in-situ bioremediation of aquifers by injecting water containing an electron acceptor, Computational Geosciences 2, 1-22.

Keijzer, H., Schotting, R.J., Zee, S.E.A.T.M. van der, 2000. Semi-analytical traveling wave solution of one-dimensional aquifer bioremediation. Communications on Applied Nonlinear Analysis 7, 1-20.

Kindzelbach, W., Schafer., J., 1991. Numerical modelling of natural and enhanced denitrification processes in aquifers. Water Resour. Res. 27(6), 1123-1135.

Klenk, I.D., Grathwohl, P, 2002. Transverse vertical dispersion in groundwater and the capillary fringe. J. Contam. Hydrol. 58, 111-128.

Koussis, A.D., Pesmajoglou, S., Syriopoulou, D., 2003. Modelling biodegradation of hydrocarbons: when is the use of the instantaneous reaction approximation justified? J. Contam. Hydrol. 60, 287-305.

Kremer, F.V., Sinke, A., 1999. Evaluation of Demonstrated and Emerging Technologies for the Treatment and Clean Up of Contaminated Land and Groundwater (Phase III), Special Session Monitored Natural Attenuation, NATO/CCMS Pilot Study, Report Number 236.

Lu, G., Clement, T.P., Zheng, C., Wiedemeier, T.H., 1999. Natural attenuation of BTEX compounds: Model development andfield-scale application. Ground Water 37(5), 707717.

Macquarrie, K.T.B., Sudicky, E.A., 1990. Simulation of biodegradable organic contaminants in groundwater 2. Plume behavior in uniform and random flow fields. Water Resour. Res. 26, 223-239.

MacQuarrie, K.T.B., Sudicky, A., Frind, E.O., 1990. Simulation of biodegradable organic contaminants in groundwater 1. Numerical formulation in principal directions. Water Resour. Res. 26(2), 207-222.

Michaelis, L., Menton, M.M.L., 1913. Die Kinetik der Invertinwerkung. Biochemische Zeitschrift 49.

Monod, J, 1949. The growth of bacterial cultures. Ann. Rev. of Microb. 3, 371-394.

Oya, S., Valocchi, A.J., 1997. Characterization of travelling waves and analytical estimation of pollutant removal in one-dimensional subsurface bioremediation modeling. Water Resources Research 33, 1117-1127.

Oya, S., Valocchi, A.J., 1998. Analytical approximation of biodegradation rate for in situ bioremediation of groundwater under ideal radial flow conditions. J. Cont. Hydrol. 31, 275-293.

Prommer, H., Barry, D.A., Davis, G.B., 2000. Numerical modelling for design and evaluation of groundwater remediation schemes. Ecological Modeling 128, 181-195.

Sun, N.Z., 2002. Modeling biodegradation processes in porous media by the finite cell method. Water Resour. Res. 38(3), doi:10.1029/2000WR000198.

Xin, J., Zhang, D., 1998. Stochastic analysis of biodegradation fronts in one-dimensional heterogeneous porous media. Adv. Water Resour. Res. 22, 103-116.

Chapter 6

Predictive Modelling of Dispersion Controlled Reactive Plumes at the Laboratory Scale [4]

Abstract. A model-based interpretation of laboratory scale experimental data is presented. Hydrolysis experiments carried out using thin glass tanks filled with glass beads to construct a hypothetical and inert, homogeneous porous medium were analysed using a 2D numerical model. A new empirical formula, based upon results for non-reactive (tracer) experiments is used to calculate transversal dispersivity values for a range of grain sizes and any flow velocities. Combined with effective diffusion coefficients calculated from Stokes-Einstein type equations, plume lengths arising from mixing between two solutes can be predicted accurately using numerical modelling techniques. Moreover, pH and ion concentration profiles lateral to the direction of flow of the mixing species can be determined at any given point downstream, without the need for result fitting. In our case, this approach does not lead to overpredictions of lateral mixing, as previously reported when using parameters derived from non-reactive tracer experiments to describe reactive solute transport.

[4] Ham, P.A.S., Olsson, Å.H., Prommer, H., Grathwohl, P., 2006. Accepted for publication in *Journal of Contaminant Hydrology.*

6.1 Introduction

In many cases, transversal hydrodynamic dispersion is thought to be the controlling mechanism for the attenuation of organic and other contaminants (Cirpka *et al.*, 1999; Grathwohl *et al.*, 2000). For example, the length of steady-state contaminant plumes of biodegradable, oxidisable organic compounds was found to be controlled by transversal mixing of electron acceptors, or growth limiting nutrients across the plume fringe (Grathwohl *et al.*, 2000; Ham *et al.*, 2004). In contrast, longitudinal dispersion was shown to only influence pre-steady-state, i.e. transient plume behaviour (Ham *et al.*, 2004), in particular at the downstream end of a developing plume (Cirpka *et al.*, In press).

Both transversal and, to an even greater extent, longitudinal dispersion have been reported to be scale-dependent mechanisms (Dykaar & Kitanidis, 1996; Kitanidis, 1994; Kapoor & Kitanidis, 1998; Sturman *et al.*, 1995) and dispersivity values employed to characterise, for example, plume behaviour, often reflects the scale of heterogeneity of the porous medium (Huang, 2002; Sturman *et al.*, 1995). Given the inherent difficulties of accurately quantifying the transversal dispersivity α_t at the field-scale, α_t has for simplicity in many practical cases been assumed to be a certain fraction (e.g., approximately one tenth (Grane & Gardner, 1961)) of the longitudinal dispersivity values, which at the plume-scale (Cirpka *et al.*, 1999) largely characterises macro-scale dispersion. However, when considering reactive solute transport, for example in the context of field-scale biodegradation problems, the relevant scale of mixing that controls overall reaction rates is the pore-scale (Bear, 1972; Cirpka *et al.*, 1999; Cirpka & Kitanidis, 2000). Consequently, if hydrodynamic dispersion coefficients that represent macro-scale dispersion are used to quantify the transport of reacting solutes, this results in an overestimation of mixing (Cirpka *et al.*, 1999) and therefore an overprediction of reaction rates.

To date, no modelling approach that could fully get around those scaling-issues has been proposed. To overcome this problem, several laboratory studies have been initiated in attempts to study transport and reactive processes at a fundamental level and under controlled conditions. For example, Gramling *et al.* (2002) studied the one-dimensional transport, mixing and reactions of $CuSO_4$ and $EDTA^{4-}$ in a translucent chamber filled with cryolite sand. They found that if they used previously derived dispersion coefficients (from non-reactive experiments) to predict reactive transport behaviour the concentrations of the formed $CuEDTA^{2-}$ were overestimated by up to 20%. Similarly, an earlier modelling study to in-

vestigate in-situ biorestoration of chlorinated aliphatics by Semprini & McCarty (1991), shows that reactive mixing was overestimated when dispersivity values from non-reactive tracer experiments were used in model simulations. Huang *et al.* (2003) also used tracer experiments to determine a value for α_t and modelled two-dimensional biodegradation of an acetate plume. In contrast however, experimental data could only be fitted when dispersivity values were increased by a factor of three for the reactive cases; the authors concluding that biomass blocking some pore spaces could increase the tortuosity of the medium.

The present paper reports the results from a series of laboratory scale tank experiments and the model-based interpretation of the experimental data. Since at the laboratory scale the role of molecular diffusion maybe as or even more important than mechanical transversal dispersion in influencing lateral plume development (Huang *et al.*, 2003), an accurate quantification of the process and its contribution to the mixing is essential for the interpretation of the experimental data. Therefore we also briefly review the theory of multi-component diffusion in the context of the experiments analysed here.

6.2 General Theory

The generalised form of the macroscopic advection-dispersion equation (ADE) for a tracer of concentration C, with units $[ML^{-3}]$ can be written

$$\frac{\partial C}{\partial t} + V \cdot \mathrm{grad}C = \mathrm{div}(D \cdot \mathrm{grad}C) \tag{6.1}$$

where t is the time, V is the mean pore velocity with units $[LT^{-1}]$ and D is the dispersion tensor with units $[L^2T^{-1}]$. Equation (6.1) is valid for steady-state flow only, i.e. $\nabla \cdot V = 0$. Depending on the role played by molecular diffusion D_m, the dispersion tensor D is usually assumed to be proportional to some power of the velocity between 1 and 2 (Bear, 1972; Scheidegger, 1957). In a homogeneous two-dimensional uniform flow field, where there is no sorption, the macroscopic ADE for a single species k can be written

$$\varepsilon \frac{\partial C(k)}{\partial t} + q_x \frac{\partial C(k)}{\partial x} - D_l \frac{\partial^2 C(k)}{\partial x^2} - D_t \frac{\partial^2 C(k)}{\partial y^2} + r^k = 0, \tag{6.2}$$

where ε is the porosity of the porous medium, C is the concentration of species k, q_x is the specific discharge, D_l and D_t are the longitudinal and transversal dispersion coefficients respectively, and r is a reaction (source/sink) term.

Classical form of the dispersion tensor

Classical dispersion theory based on the random capillary bundle concept (Aris, 1956; Bear & Bachmat, 1966; de Josselin de Jong, 1958; Fried and Combarnous , 1971; Taylor, 1953) suggests a dispersion equation similar to Fick's law, which takes into account both dispersive and diffusive mass fluxes (Shulka *et al.* , 2003). When there is appreciable transversal molecular diffusion, the transversal dispersion coefficient D_t is considered as the sum of the effective molecular diffusion coefficient D_m and the product of transversal dispersivity α_t and average linear velocity $v = q_x/\varepsilon$, i.e.

$$D_t = D_m + \alpha_t |v|, \tag{6.3}$$

where D_m is assumed constant for a given temperature. Some authors would argue that the Fickian dispersion model using dispersivities derived from conservative experiments is only valid at the laboratory scale (Dagan, 1988) and in the case of uniform flow through a homogeneous domain. Homogeneous here means that the spatial scale of any heterogeneity, physical or chemical, is small compared to the scale of the contaminant plume.

Transversal dispersivity of a porous medium

Transversal dispersivity is traditionally considered to be a characteristic of the porous medium. de Josselin de Jong (1958) quantified the hydrodynamic dispersion coefficient as

$$D_t = D_m + \frac{3}{16} d|v|, \tag{6.4}$$

where d is the characteristic grain size of the porous medium. This implies that transversal dispersivity is only a function of the grain size. Conversely, based on laboratory findings, both Klenk & Grathwohl (2002) and Huang (2002) have reported that at high flow rates, there is an apparent decrease of transverse dispersivity with average velocity. In recent experimental investigations, Olsson (2005)

demonstrates a non-linear increase of the dispersion coefficient D_t across a range of seepage velocities from 0.37 m/d to 164 m/d, using a sand and glass bead porous medium. The empirical expression

$$\frac{D_t}{D_{aq}} = \frac{D_m}{D_{aq}} + 0.26(Pe)^{0.74}, \tag{6.5}$$

was proposed, where D_{aq} is the aqueous diffusion coefficient and Pe is the Peclet number of molecular diffusion (Bear, 1972), equal to $|v|d/D_{aq}$. The expression (6.5) is valid for non-reactive tracers and comparison with existing data from literature demonstrates that the expression holds for all investigated Peclet numbers (from $Pe \approx 1$ to 6307).

Deriving a diffusion coefficient

Unlike mechanical dispersion, aqueous molecular diffusion is not a property of the porous medium (Bear, 1972; Cussler, 1997). Individual diffusion coefficients which describe the diffusion of a solute through a solvent can be calculated (theoretically or empirically), or alternatively measured experimentally. More complicated is the description of multi-component aqueous diffusion, where solutes mix dependent on aqueous concentration gradients and react together. In such cases, it is common to measure or derive a single, average diffusion coefficient for the reacting solutes and products (Cussler, 1997), whereas it might be more accurate to consider the diffusion of solutes, and the reactions which occur as a result, as separate (interactive) processes (Huang *et al.*, 2003).

Where multi-component systems are considered, the movement and any (chemical) interaction between diffusing compounds influence the relative rates of diffusion of those species (Cussler, 1997). It is therefore important to note, where a single average diffusion coefficient is calculated, that this is a weighted average of the diffusion coefficients of individual species interacting together. In such cases, the diffusion coefficient of an aqueous compound is controlled by the rate of diffusion of the slowest species that make up the compound (Coulson & Richardson, 1995; Cussler, 1997; Grathwohl, 1997; Wilke & Chang, 1955) and likewise, where different compounds diffuse and interact, the slower compound controls the diffusive process. In simple multi-component systems, where interacting solutes are considered dilute and no ternary effects arise because of coupling of ions, multi-component effects are minor and the system can be reduced to a binary diffusion

problem (Coulson & Richardson, 1995; Cussler, 1997).

In the case of dilute 1-1 electrolytes, the electrolyte diffusion coefficient can be obtained as a harmonic mean of the diffusion coefficients of the individual ions and, where there is electroneutrality, is obtained from (Cussler, 1997)

$$+j_1 = +j_2 = -D\nabla c_1 = -\left(\frac{2}{1/D_1 + 1/D_2}\right)\nabla c_1, \tag{6.6}$$

where j_i is the flux of ion i, D is the binary diffusion coefficient and D_i and c_i are the aqueous diffusion coefficients and concentrations of ion i respectively. The individual diffusion coefficients D_1 and D_2 can be taken from international critical tables (Rodebush and Rodebush , 1929) or alternatively calculated based on the theory of diffusion. The literature contains a number of existing theories, e.g. (Glasstone *et al.*, 1941; Sutherland, 1905), which are based on, or extensions of, the Stokes-Einstein equation (Stokes, 1950). Unfortunately the inaccurate nature of these theories has resulted in a number of empirical relations being proposed (Bird *et al.*, 1960). It is common that empirical formulae (King *et al.*, 1965; Scheibel, 1954; Wilke & Chang, 1955) be used in favour of those derived theoretically (Glasstone *et al.*, 1941; Stokes, 1950; Sutherland, 1905) to provide mathematical descriptions. However, depending on the description of the diffusion coefficient adopted, errors in excess of twenty percent from measured values can occur (Cussler, 1997; Reid *et al.*, 1977). Wilke & Chang (1955) propose a correlation of diffusion coefficients for very dilute solutions based on the Stokes-Einstein equation, which is usually good within $\pm 10\%$ (Bird *et al.*, 1960). The expression

$$D_{AB} = 7.4 \times 10^{-8} \cdot \frac{\psi_B {M_B}^{0.5} T}{\mu \tilde{V}_A^{0.6}}, \tag{6.7}$$

where D_{AB} is the diffusion coefficient in $cm^2\ s^{-1}$ for small concentrations of solute A in solvent B, ψ_B is the association parameter (2.6 for water (Wilke & Chang, 1955)), M_B is the molecular weight of solvent B, T is the absolute temperature in ^oK, μ is the viscosity of the solution in centipoises and $\tilde{V}_A$ is the molar volume of the solute A in $cm^3/g\text{-}mole^{-1}$. This expression can be used to easily estimate mass diffusivity for a dilute binary liquid mixture. The molar volume is defined as the volume occupied by one mole of substance. In this manner it is possible to derive a binary diffusion coefficient accounting directly for changes in temperature (and viscosity), without the need to consult International Critical Tables.

In porous media, diffusion of an aqueous species only occurs in the pore spaces. An effective diffusion coefficient is given by

$$D_{m(eff)} = D_{aq}.\frac{\varepsilon}{\tau_f}, \tag{6.8}$$

where $D_{m(eff)}$ is the effective diffusion coefficient in the interstitial pores, ε is the porosity and τ_f is the tortuosity, which accounts for the pore geometry. This definition means effective molecular diffusion coefficients are therefore a property of the porous medium. Bear (1972) defines tortuosity as $(l/l_e)^2$, the ratio of flow path length to sample length squared. Bear (1972), and later Dykhuizen & Casey (1989), have derived theoretical values for the factor of tortuosity in an isotropic porous medium, based on a number of geometrical assumptions. Other authors (Carman, 1937; Peterson, 1958; Wahyudi *et al.*, 2002) have found tortuosity values empirically for natural porous media. It is also of importance to note that some authors prefer to define tortuosity inversely to that defined by Bear (1972), i.e. $\tau_f = (l_e/l)^2$, in which case values of tortuosity are greater than 1. However, regardless of definition, it is unanimously agreed that the factor of tortuosity is difficult to calculate or determine experimentally, and often serves as a 'fitting' factor (Grathwohl, 1997). A more accurate representation of the effective diffusion coefficient is therefore obtained by relating the tortuosity to the porosity ε (which can be well approximated) of the porous medium (Grathwohl, 1997)

$$D_{m(eff)} = D_{aq}.\varepsilon^m; \text{ where } \varepsilon^m = \frac{\varepsilon}{\tau_f}. \tag{6.9}$$

In natural porous media, the exponent m in equation (6.9) is empirically derived. Boving & Grathwohl (2001) found values for m around 2 for sedimentary rocks whereas for unconsolidated sediments lower values are observed. For isotropic porous media made up of spherical particles, Bruggeman (1935) derived a theoretical value of 3/2.

6.3 Laboratory Data: Experimental Method & Data Analysis

Recent laboratory experiments (Olsson, 2005) considered non-reactive transport of tracer solutes but, more interestingly, transport of chemical species that mix

together. The experimental setup is described fully in Olsson (2005) and in part by Cirpka *et al.* (In press). Since the laboratory experiments provide the conceptual model for the numerical modelling exercise presented in this study, the setup is briefly outlined again here.

The experiments were conducted in acrylic glass tanks filled with silica glass beads of uniform grain diameter. The smaller tank, of dimensions 28.0 cm × 14.0 cm × 1.05 cm, was used initially for the non-reactive tracer experiments and subsequently for reactive experiments. A larger tank of dimensions 77.9 cm × 14.0 cm × 0.8 cm was also used for the reactive experiments so plume development over a larger length scale could be observed. Figure 6.1 shows a schematic of the experimental setup. Eleven inlet ports, 0.75 mm in diameter, spaced at 1.1 cm intervals were present at either end of the tank. Flow in the tanks was controlled using two pumps, operated at the same rate, located at the inlet and outlet ends of the tank. The experiments were conducted under saturated laminar flow conditions for four different grain sizes (G1: 0.25-0.5 mm; G2: 0.5-0.75 mm; G3 :1.0-1.5 mm; G4 :2.0-2.3 mm) and a range of seepage velocities. For all grain sizes the porosity was estimated to be ≈ 0.37, from experimental measurements.

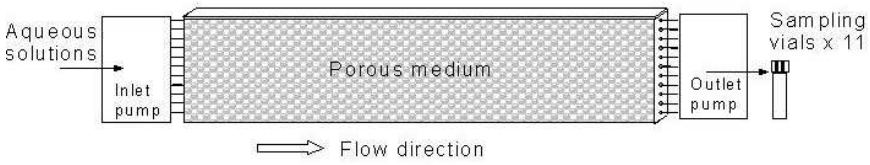

Figure 6.1: *Experimental setup, adapted from Olsson (2005)*

Non-reactive tracer experiments

In the non-reactive experiments, 1.33 $\times 10^{-5}$ mol/l of fluorescein was added to deionized water and injected continuously through the middle inlet port into the small tank, initially filled with only the deionized water. At steady-state (once fluorescein breakthrough had occurred at all outlet ports), concentrations of fluorescein were measured from samples collected at the outlet ports. Linear regression techniques were used to obtain D_t using the analytical solution for a continuous

planar source injection of a tracer solute (Domenico & Schwartz , 1990). There was a positive correlation between D_t and average velocity (Cirpka *et al.*, In press; Olsson, 2005), which was not linear and yielded a new empirical formula (6.5). Substituting (6.3) into (6.5) and rearranging yields

$$\alpha_t = 0.26 \left(\frac{|v|d}{D_{aq}} \right)^{0.74} D_{aq} \cdot \frac{1}{|v|}, \tag{6.10}$$

which clearly expresses apparent transversal dispersivity as a function of grain size d, average linear velocity v, and the aqueous diffusion coefficient D_{aq}. A value of $D_{aq} = 6.8 \times 10^{-10}\ m^2/s$ was taken for fluorescein (Huang, 2002). Assuming the porous matrix is isotropic, taking porosity of 0.37, and $m = 1.5$ (a value to be expected in loose packings according to Bruggeman (1935)) then rearranging (6.9) yields

$$\tau_f = \frac{0.37}{0.37^{1.5}} \approx 1.644. \tag{6.11}$$

Taking the inverse of this result, and substituting in (6.8) gives $D_{m(eff)} \approx 4.1 \times 10^{-10}\ m^2/s$. This value appears consistent with measured values for similar experiments reported in the literature (Huang, 2002; Seagren *et al.*, 1999b). Figure 6.2 shows the non-linear dependency (solid curves) of apparent transversal dispersivity on average velocity for the fluorescein tracer in four different grain sizes at 20^oC, as calculated from equation (6.10). It shows that in the limit $v \to 0$, $\alpha_t \to \infty$, as in this case molecular diffusion has sufficient time to mix over large lateral distances. For comparison, also plotted in Figure 6.2 is the corresponding function of α_t for grain 3 (dotted line), calculated using the formula (6.4) suggested by de Josselin de Jong (1958), which is dependent only on grain size. Clearly depending on the average velocity, these two methods can yield very different dispersivity values.

Reactive experiments

A series of experiments were performed where hydrolysis occurred as a result of mixing between dilute solutions of an acid (HCl) and a base ($NaOH$). At dilute concentrations in an unbuffered solution, both $NaOH$ and HCl completely dissociate into their respective ion constituents. Na^+ and Cl^- (known also as the spectator ions) behave as non-reactive tracers and do not form a neutral salt

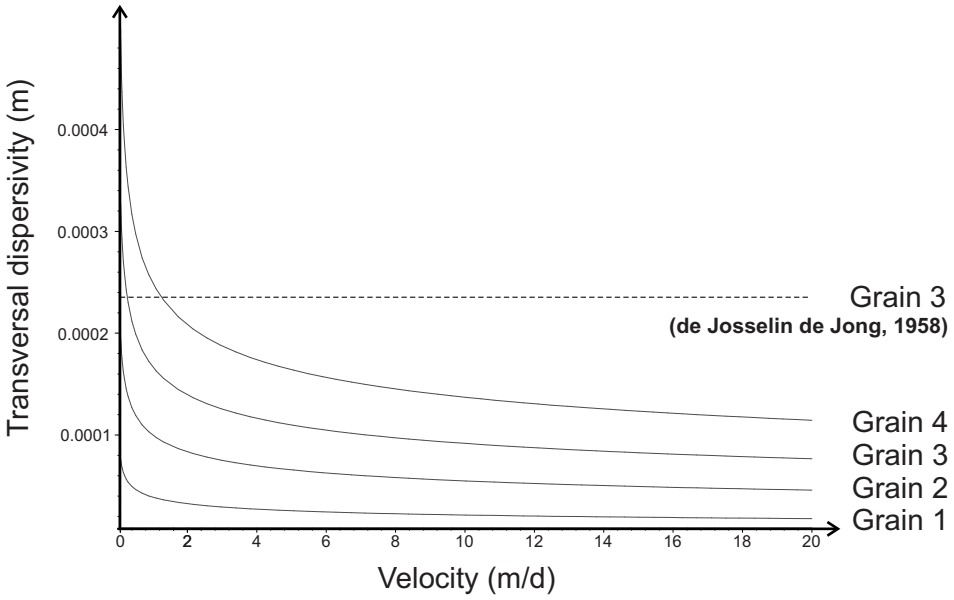

Figure 6.2: *Apparent transversal dispersivity as a function of average linear velocity for the fluorescein tracer species flowing through the four grain sizes at* 20^oC *(solid curves). Also,* α_t *for grain size 3, as proposed by de Josselin de Jong (1958), which is only a function of grain size (dotted line).*

precipitate ($NaCl$). Water is therefore the only product of the hydrolysis reaction considered here, which causes a change in the pH of the aqueous solution. The reaction considered takes the form

$$H_3O^+ + OH^- \rightarrow 2H_2O. \tag{6.12}$$

The experimental setup was such that $NaOH$ was injected continuously through the middle port of the experimental tank into a background solution of HCl. A pH indicator was added to both the background and to the injected solutions. Depending on the flow velocities and the grain size of the porous medium used, steady-state $NaOH$ plumes of different length developed in the initially HCl filled domain. Both solutions of $NaOH$ and HCl were prepared using deionized water and contained the pH indicator Bromophenol Blue or Methyl Orange at concentrations of $\approx 1.5 \times 10^{-6}$ mol/l. Titration experiments showed that a colour change would occur at pH $\approx$ 3.8, which made the zones of HCl and $NaOH$ clearly visible. In this way, measurements of plume length were taken for the different experiments. The use of pH indicators is widely documented in the literature, and at the concentrations reported here did not affect the acid-base reaction considered in this study. The bulk of the experiments were conducted at room temperature, which varied at maximum between 20 and 30 degrees Celsius during the experimental period. Plume lengths were measured for all the experiments undertaken and all data showed a positive correlation between plume length and average linear velocity. In addition, samples were taken at the outlet ports for some of the experiments, providing pH measurements and ion concentrations at the end of the tank.

It was assumed that the solution of $NaOH$ would diffuse through the resident HCl solution. Equations (6.7) and (6.9) were used to calculate diffusion coefficients in porous media over a temperature range. Since the concentrations of $NaOH$ and HCl used were very dilute, constant values of μ, ψ and density ρ for water were used. The value of μ_{water} decreases exponentially with temperature, and values were taken from Weast (1988-89) (p. F-40) together with values for the molecular weights of HCl and $NaOH$ (p. D-232,257). The change in the apparent transversal dispersion coefficient with velocity is represented graphically in Figure 6.3. The calculated molecular diffusion coefficients only vary between 1.214×10^{-4} m^2/d at 20^oC (full curves) and 1.577×10^{-4} m^2/d at 30^oC (dotted curves). At low flow velocities and especially in the case of the smaller grain sizes, molecular

diffusion accounts for a large proportion of the total hydrodynamic transversal dispersion.

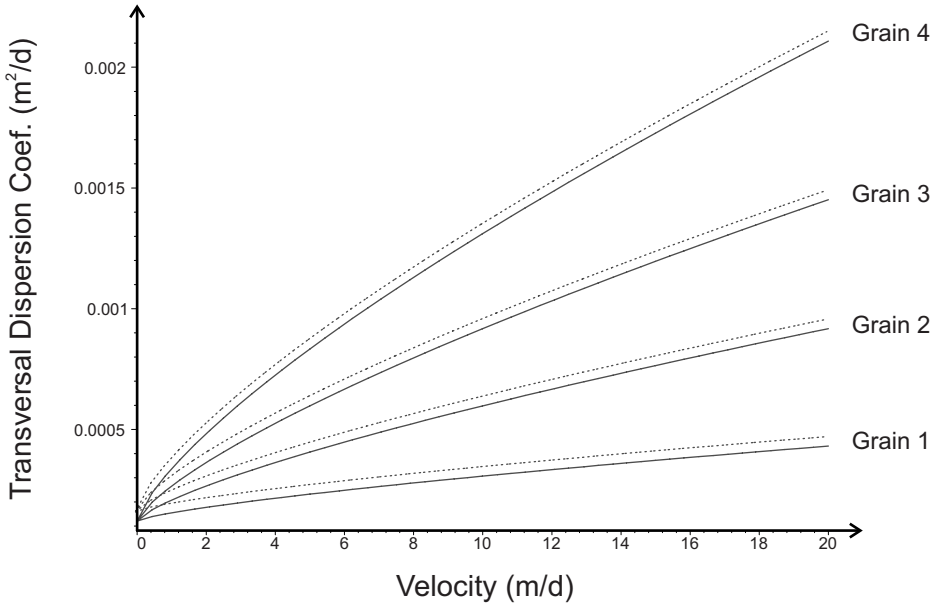

Figure 6.3: *Variation of D_t with flow velocity for a dilute solution of $NaOH$ in a dilute solution of HCl. Effective molecular diffusion coefficients differ between 1.214×10^{-4} m^2/d at 20^oC (solid curves) and 1.577×10^{-4} m^2/d at 30^oC (dotted curves).*

6.4 Numerical Modelling: Procedure

To analyse the data, tank experiments were simulated with the numerical model PHT3D (Prommer *et al.*, 2003), a verified reactive transport model. PHT3D combines the transport simulator MT3DMS (Zheng & Wang, 1999) with the geochemical code PHREEQC-2 (Parkhurst & Appelo, 1999) to model reactive transport in saturated porous media. Two (half-)model grids were constructed, representing the two different experimental tanks. The 'small' model consisted of 11644 grid cells and had an extension of 30 cm (in flow direction) by 7 cm, whilst the 'large' model was 80 cm in length and consisted of 14596 grid cells. In both models, a varying discretisation perpendicular to the flow Δy ($\Delta y_{min} = 0.0025\ m$, $\Delta y_{max} = 0.01\ m$) and a varying discretisation in the direction of the flow Δx ($\Delta x_{min} = 0.0001875\ m$, $\Delta x_{max} = 0.001325\ m$), was used. A steady-state flow field was induced in

the model using a *Neumann* boundary condition at the upstream boundary where the inlet ports were simulated as active cells ($\Delta y_{port} = 0.75\ mm$), spaced by inactive cells equivalent to the port spacing in the experimental tanks. Fixed head cells (*Dirichlet* boundary condition) were used at the downstream boundary where again the outlet ports were simulated in the same manner as the inlet ports. The TVD scheme (King *et al.*, 1965) was used to solve the advective transport problem and, depending on the average linear velocity required, the simulation time was selected such that steady-state concentration profiles were reached within the whole model domain.

Non-reactive modelling

PHT3D was run for non-reactive solute transport (advection and dispersion only) using seepage velocities and apparent α_t values from the conservative (fluorescein) experiments and an effective diffusion coefficient of $4.1 \times 10^{-10}\ m^2/s$ (Huang *et al.*, 2003; Olsson, 2005). Numerical results were compared against the concentration profiles obtained at the outlet end of the tank experiment for the fluorescein tracers (Olsson, 2005; Domenico & Schwartz , 1990). Figure 6.4 shows the results of the numerical model and sampled data for two tracer cases (0.68 m/d and 1.4 m/d) for grain size 1.

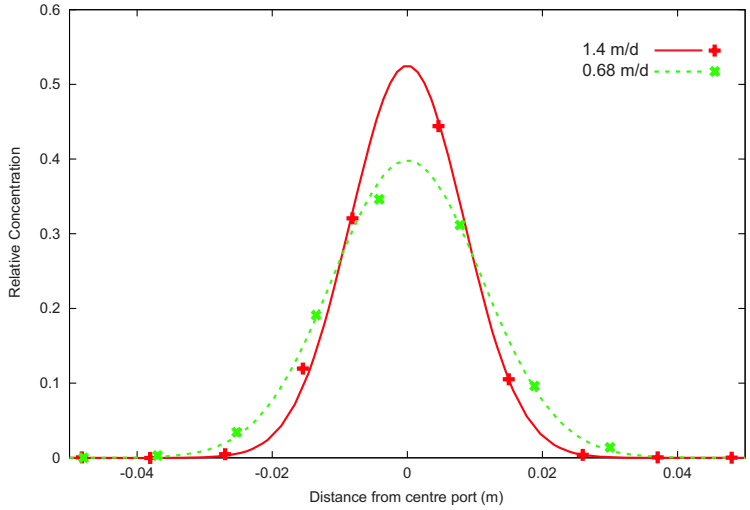

Figure 6.4: *Modelled (curves) and observed relative fluorescein concentrations (points) for two tracer experiments using grain size 1.*

Figure 6.4 clearly demonstrates the accuracy of the numerical model in predicting the experimental data. This model was used as the basis for the subsequent reactive modelling.

Reactive modelling

In the reactive study, values of apparent α_t (or apparent values of α_t at low and high flow velocities) were determined using equation (6.10) and used as input parameters in the reactive model. For each grain size, a selection of model simulations were performed where the velocity (and hence apparent α_t) varied. Simulations were carried out using different diffusion coefficients which correspond to the temperature range at which the experiments were carried out. The two different water compositions, i.e., the HCl and the $NaOH$ solution were simulated in the numerical model by transporting the respective total aqueous component concentrations of Cl and Na, while the pH was computed in the reaction step from a charge-balance condition.

6.5 Numerical Modelling: Results

Modelled and observed plume lengths are presented for the hydrolysis experiments in Figures 6.5 & 6.6, where the measured data has an error of $\pm$ 1 cm (Olsson, 2005). The model curves plotted were obtained from linear regression techniques, using results from model simulations conducted over the complete velocity range studied. Figure 6.5 shows the modelled and measured plume lengths for grains 1, 2 & 3, where 1 $mmol$ of $NaOH$ was injected into the ambient solution containing 10 $mmol$ of HCl. Figure 6.6 is a plot of the modelled and measured plume lengths for grains 3 & 4, where 2 $mmol$ of $NaOH$ was injected into the ambient solution. In general, there is good agreement between the modelled and measured plume lengths, with most observed data close to the simulated results. Only in the cases where observed plume lengths are very short, the model predicts plume lengths larger than those measured in the laboratory. This phenomenon seems more pronounced as the grain size increases and is attributed to the non-uniform velocity field which exists in very close proximity to the inlets of the tank but does not affect the rest of the experimental domain.

Figure 6.5 also illustrates the effect of temperature (and hence effective diffu-

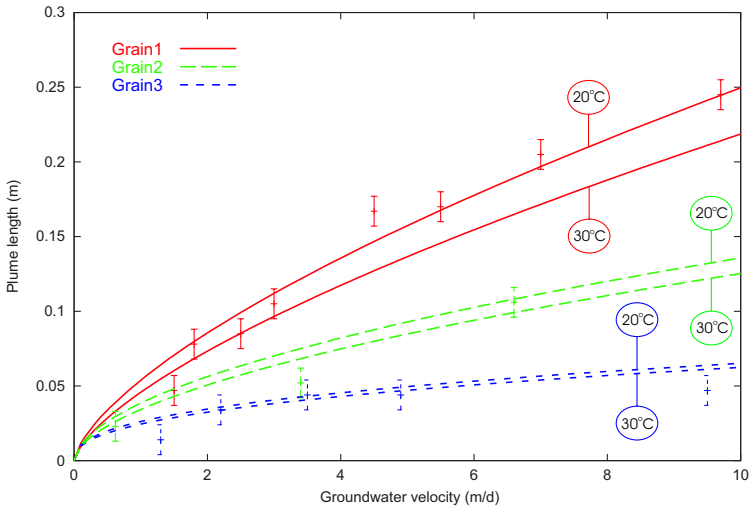

Figure 6.5: *Results predicted by the numerical model (curves) and observed plume lengths (points) against groundwater velocity for grains 1, 2 & 3 with injected $NaOH$ concentration of 1 mmol. Two model curves per grain size represent simulations at 20^oC and 30^oC. The experimental error is ± 1 cm. Predictions (curves) are done by pure forward modelling based on data from the conservative tracer.*

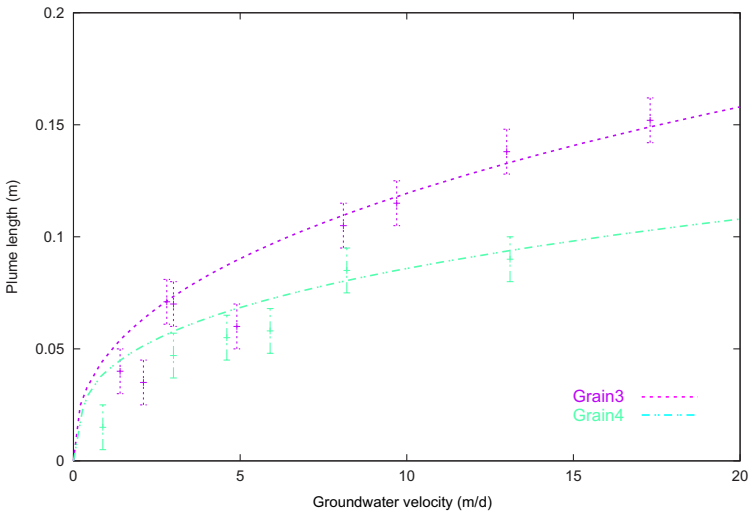

Figure 6.6: *Results predicted by the numerical model (curves) and observed plume lengths (points) against groundwater velocity for grains 3 & 4 with injected $NaOH$ concentration of 2 mmol. Model simulations are for 20^oC and the experimental error is ± 1 cm. Predictions (curves) are done by pure forward modelling based on data from the conservative tracer.*

sion coefficients) on the modelled plume lengths. The two model curves displayed for the three grain sizes corresponds to the two temperatures simulated. Unsurprisingly, the model predicts shorter plume lengths with increasing molecular diffusion. However, of more interest is the relative contribution of molecular diffusion in comparison to mechanical dispersion upon the lateral spreading of the simulated plumes. It is evident from Figure 6.5 that as grain size increases the contribution of molecular diffusion becomes less important. For this reason, only one model curve ($T = 20^oC$) is plotted for the two large grain sizes in Figure 6.6. Although Figure 6.2 shows an apparent decrease in transversal dispersivity with velocity, the mechanical dispersion term quickly becomes much more dominant than the molecular diffusion term as velocity and grain size increases. Only for low seepage velocities, and in particular small grain sizes, is the contribution of molecular diffusion greater than that of mechanical dispersion. The contributions of molecular diffusion and mechanical dispersion for the laboratory experiments considered in this study are shown graphically in Figure 6.7.

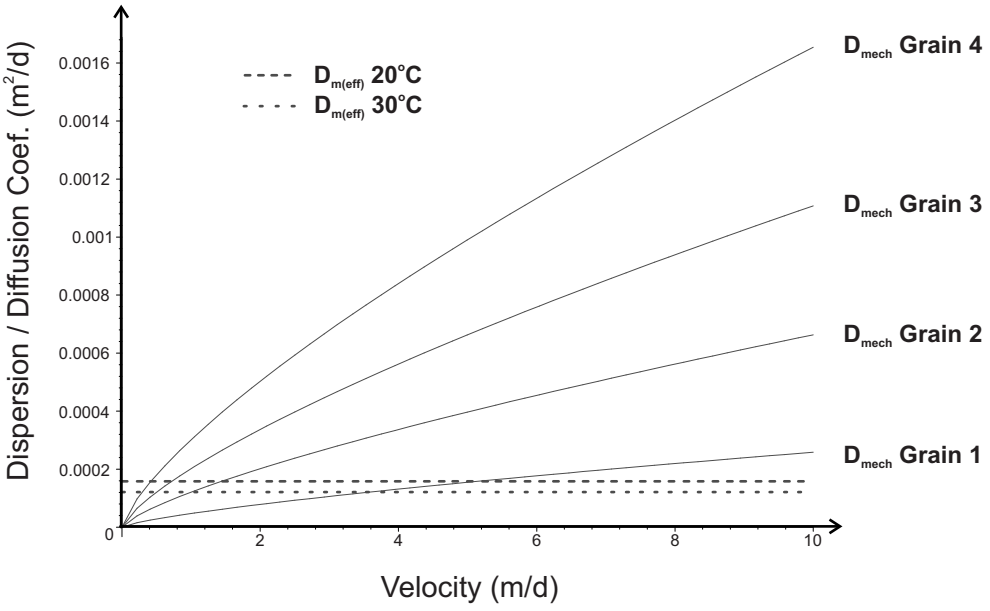

Figure 6.7: *Comparison of the magnitude of mechanical dispersion coefficient D_{mech} to the effective molecular diffusion coefficient $D_{m(eff)}$ for seepage velocities up to 10 m/d and all grain sizes.*

In some experiments, pH and ion concentrations were measured at the outlet end of the tank. There are a few cases where there is good agreement between

the modelled and measured plume lengths and also pH and ion concentration data are available for the same experiments. In these cases both modelled and observed pH and ion profiles appear to fit well together. Unsurprisingly, where the modelled and measured plume length did not match, the agreement between the ion and pH profiles was not as good. A selection of profiles are shown in Figure 6.8 for simulations conducted in grains 1, 3 & 4. No ion concentration or pH measurements were taken for experiments involving grain 2.

Figure 6.8a & 6.8b show modelled and measured relative concentrations of sodium and chloride respectively at the outlet end of the tank. Figure 6.8c illustrates the modelled and measured pH. Note that the background pH values (i.e. those furthest from the centre of the tank) for the profiles of the simulations shown are all slightly different. This is the because the background pH value of the each experiment was slightly different.

6.6 Discussion

In the present study apparent dispersivity values obtained in non-reactive (tracer) experiments were successfully used to predict plume lengths and concentration profiles of mixing solutes involved in hydrolysis reactions. This finding is in contrast to field (Semprini & McCarty, 1991) and partially lab (Gramling *et al.*, 2002) studies, which found that this procedure would lead to an overestimation of transversal mixing and therefore of reaction rates.

However, following, e.g., de Josselin de Jong (1958), the underlying assumption in those works was that the transversal dispersion coefficient increases linearly with the grain size of the porous medium, while the results from the laboratory experiments analysed here indicate this is not the case. Figure 6.2 shows an example of the apparent decrease in transversal dispersivity with pore velocity for the fluorescein tracer considered in this study, calculated from equation (6.10). Although this equation concludes that as the velocity goes to zero, α_t (slowly) goes to infinity it is important to remember that in the same limit the contribution of mechanical dispersion compared to diffusion is not significant anymore (as shown in Figure 6.7) and this apparent increase of α_t is not important. Figure 6.2 demonstrates that apparent transversal dispersivity values are highest when pore velocity is low, which is often the case for natural groundwater flows. This could explain why in the laboratory study by Huang *et al.* (2003), where the average linear velocity was

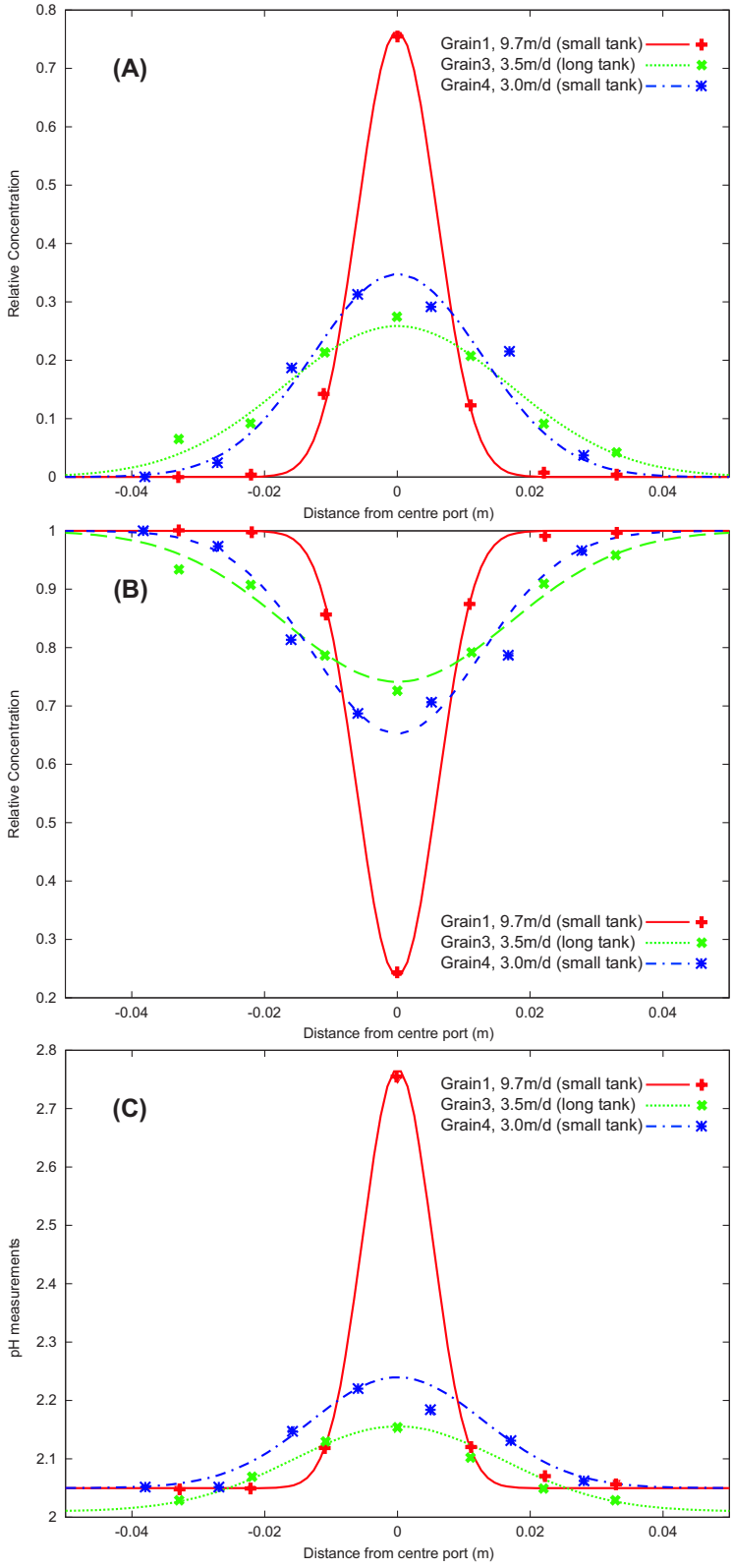

Figure 6.8: *Comparison of modelled results and experimental data for selected ion and pH profiles across the range of grain sizes: (a) sodium, (b) chloride and, (c) pH distributions at the outlet end of the tank. Curves are results predicted by the model and points indicate measured laboratory data.*

approximately 1 m/d, transversal dispersivity had to be increased to fit experimental data. In contrast, Gramling *et al.* (2002) would have needed to decrease dispersive mixing in order to prevent overpredictions in reactions during transport. The experiments in that study were conducted with high seepage velocities (> 10 m/d), which in the context of this study suggests that the dispersivity value was too large. Of course at very low groundwater velocities, molecular diffusion will still dominate the hydrodynamic dispersion mechanism. From equation (6.5), as $v \rightarrow 0$ then $D_t \rightarrow D_{aq}$.

While it is a significant result that this study provides a successful description of reactive transport at the laboratory scale, its immediate successful application to field-scale problems is not necessarily expected. This can be concluded from the fact that the transversal dispersivities required to match observed plume length at the field-scale (Cirpka & Kitanidis, 2000; Cirpka, 2002), while orders of magnitude below those found for longitudinal dispersivities, still appear to lie above the values found at the laboratory scale, as in the present experiments.

6.7 Summary and Conclusion

A model-based analysis (pure forward modelling) of laboratory scale experiments that examined the reactive transport of HCl and $NaOH$ in a homogeneous porous media for varying flow velocities and for varying grain sizes was presented. The study quantifies the controlling effect of hydrodynamic transversal dispersion and of effective molecular diffusion on the progress of the hydrolysis reactions at the plume fringes and therefore on plume length.

It was demonstrated that plume lengths along with pH measurements and ion concentration profiles of mixing solutes can be predicted numerically using data obtained from simple conservative (tracer) experiments and, most notably without fitting any model parameters. A new empirical formula (6.5) to calculate apparent transversal dispersion coefficients, based upon conservative laboratory experiments, was used in conjunction with an effective diffusion coefficient obtained from a Stokes-Einstein style equation (6.7) as input parameters for the reactive modelling.

Finally, the analysis reconfirms that at typical groundwater flow velocities molecular diffusion is an efficient mixing process that can not be neglected, however this mechanism is often overlooked in practice.

Bibliography

Aris, R., 1956. On the dispersion of a solute flowing through a tube. Proc. Roy. Soc. A. 235, 67-77.

Bear, J., 1972. Dynamics of fluids in porous media. American Elsevier, New York.

Bear, J., Bachmat, Y., 1966. Hydrodynamic dispersion in non-uniform flow through porous media taking into account density and viscosity differences. Technion Institute of Technology, Hydraulics Lab. P.N. 4/66, 308.

Bird, R.B., Stewart, W., Lightfoot, E., 1960. Transport Phenomena. John Wiley & Sons, New York.

Boving, T.B., Grathwohl, P., 2001. Tracer diffusion coefficients in sedimentary rocks: correlation to porosity and hydraulic conductivity. J. Contam. Hydrol. 53(1-2), 85-100.

Bruggeman, D.A.G., 1935. Berechnung verschiedener physikalischer konstanten von het-erogenen substanzen. Ann. Physik. 24, 636679.

Carman, P.C., 1937. Fluid flow through a granular bed. Transactions of the Institution of Chemical Engineers 15, 150-167.

Cirpka, O.A., Frind, E.O., Helmig, R., 1999. Numerical simulation of biodegradation controlled by transverse mixing. J. Contam. Hydrol. 40, 159-182.

Cirpka, O.A., Kitanidis, P.K., 2000. Characterization of mixing and dilution in heterogeneous aquifers by means of local temporal moments. Water Resour. Res. 36, 12211236.

Cirpka, O., 2002. Choice of dispersion coefficients in reactive transport calculations on smoothed fields. J. Contam. Hydrol. 58, 261282.

Cirpka, O.A., Olsson, Å.H., Qiongsong, J., Rahman, M.A., Grathwohl, P. Length of reactive plumes controlled by transverse dispersion. Ground Water.

Coulson, J.M., Richardson, J.F., 1995. Chemical Engineering Vol. 1 (4th Ed.): Fluid Flow, Heat Transfer and Mass Transfer. Pergamon.

Cussler, E.L., 1997. Diffusion: Mass Transfer in Fluid Systems (Second Edition). Cambridge University Press, Cambridge.

Dagan, G., 1988. Time-dependent macrodispersion for solute transport in anisotropic heterogeneous aquifers. Water Resour. Res. 24, 14911500.

de Josselin de Jong, G., 1958. Longitudinal and transverse diffusion in granular deposits. Transactions of the American Geophysical Union 39, 67-74.

Domenico P.A., Schwartz, P.A., 1990. Physical and Chemical Hydrogeology. John Wiley & Sons Inc., New York.

Dykaar, B.B., Kitanidis, P.K., 1996. Macrotransport of a biologically reacting solute through porous media. Water Resour. Res. 32(2), 307-320.

Dykhuizen, R.C., Casey, W.H., 1989. An analysis of solute diffusion in rocks. Geochimica et Cosmochimica Acta 53, 2797-2805.

Fried J.J., Combarnous, M.A., 1971. Dispersion in porous media. Adv. Hydrosci. 7, 169282.

Glasstone, S., 1941. Theory of Rate Processes. McGraw-Hill, New York.

Gramling, C.M., Harvey, C.F., Meigs, L.C., 2002. Reactive transport in porous media: a comparison of model prediction with laboratory visualization. Environ. Sci. Technol. 36, 2508-2514.

Grane, F.E., Gardner, G.H.F., 1961. Measurements of transverse dispersion in granular media. J. Chem. Eng. Data 6(2), 283-287.

Grathwohl P., 1997. Diffusion In Natural Porous Media Contaminant Transport, Sorption/Desorption and Dissolution Kinetics. Kluwer, Dordrecht.

Grathwohl, P., Klenk, I.D., Ederhardt, C., Maier, U., 2000. Steady state plumes: mechanisms of transverse mixing in aquifers. In C.D. Johnston: Contaminant Site Remediation: From Source Zones to Ecosystems, Proc. CRSC, Melbourne, Vic., 4-8 Dec., Centre for Groundwater Studies, CSIRO, Perth, Western Australia, pp.459-466.

Ham, P.A.S., Schotting, R.J., Prommer, H, Davis, G.B., 2004. Effects of hydrodynamic dispersion on plume lengths for instantaneous bimolecular reactions. Adv. Water Resour. Res. 27, 803-813.

Huang, W.E., 2002. The role of transverse mixing of electron acceptors and carbon substrates in natural attenuation. PhD thesis, University of Sheffield, Sheffield.

Huang, W.E., Oswald, S.E., Lerner, D.N., Smith, C.C., Zheng C., 2003. Dissolved oxygen imaging in a porous medium to investigate biodegradation in a plume with limited electron acceptor supply. Environ. Sci. Technol. 37, 1905-1911.

Kapoor, V., Kitanidis, P. K., 1998. Concentration fluctuations and dilution in aquifers. Water Resour. Res. 34(5), 11811193.

King, C.J., Hsueh, L., Mao, K-W., 1965. Liquid phase diffusion of non-electrolytes at high dilution. J. Chem. Eng. Data 10(4), 348-350.

Kitanidis, P. K., 1994. The concept of the dilution index. Water Resour. Res. 30(7), 20112026.

Klenk, I.D., Grathwohl, P, 2002. Transverse vertical dispersion in groundwater and the capillary fringe. J. Contam. Hydrol. 58, 111-128.

Olsson, Å.H., 2005. Investigation and modelling of dispersion-reaction processes in natural attenuation groundwater. PhD thesis, Eberhard-Karls Universität of Tübingen, Tübingen.

Parkhurst, D.L., Appelo, C.A.J., 1999. User's guide to PHREEQC (Version 2) - A computer program for speciation, batch-reaction, one-dimensional transport, and inverse geochemical calculations. U.S. Geological Survey Water-Resources Investigations Report 99-4259.

Perkins, T.K., Johnston, O.C., 1963. A review of diffusion and dispersion in porous media. J. Soc. Pet. Eng. 3, 7084.

Peterson, N.L., 1958. Diffusion in a pore of varying cross section. A.I.Ch.E. 4, 343345.

Prommer, H., Barry, D.A., Zheng, C., 2003. MODFLOW/MT3DMS-based reactive multicomponent transport modelling. Ground Water 41(2), 247-257.

Reid, R.C., Praunsnitz, J.M., Sherwood, T.K., 1977. The Properties of Gases and Liquids, Third Edition. McGraw-Hill, New York.

Robinson, R.A., Stokes, R.H., 1959. Electrolyte Solutions. Academic Press, New York.

in Rodebush and Rodebush (eds), 1929. Int. Critical Tables Vol. V. McGraw-Hill Book Co., New York.

Saffman, P.G., 1960. A theory of dispersion in a porous medium. Journal of Fluid Mechanics 6(3), 321349.

Scheibel, E.G., 1954. Liquid diffusivities. Ind. Eng. Chem. 46, 2007-2008.

Scheidegger, A.E., 1957. The Physics of Flow Through Porous Media. The Macmillan Company, New York.

Seagren, E.A., Rittmann, B.E., and Valocchi, A.J., 1999b. An experimental investigation of NAPL-pool dissolution enhancement by flushing. J. Contam. Hydrol. 37, 111-137.

Semprini, L., McCarty, P.L., 1991. Comparsion between model simulation on field results for in-situ biorestoration of chlorinated aliphatics: Part 1. Biostimulation of the methanotrophic bacteria. Ground Water 29(3), 365-374.

Shukla, M.K., Ellsworth, T.R., Hudson, R.J., Nielsen, D.R., 2003. Effect of water flux on solute velocity and dispersion. Soil Science Society of America Journal 67, 449-457.

Stokes, R.H., 1950. The diffusion coefficients of eight univalent electrolytes in aqueous solution at 25 C. J. Am. Chem. Soc. 72, 2243.

Sturman, P.J., Stewart, P.S., Cunningham, A.B., Bouwer, E.J., Wolfram, J.H., 1955. Engineering scale-up of in situ bioremediation processes: A review. J. Contam. Hydrol. 19, 171-203.

Sutherland, W., 1905. A dynamical theory of diffusion for non-electrolytes and the molecular mass of albumin. Philosophical Magazine 6(9), 781-785.

Taylor, G.I., 1953. Dispersion of solute matter in solvent flowing slowly through a tube. Proc. Roy. Soc. (London), Series A 219, 186-203.

Trefry, M.G., Ruan, F.P., McLaughlin, D., 2003. Numerical simulations of preasymptotic transport in heterogeneous porous media: Departures from the Gaussian limit. Water Resour. Res. 39(3), 10.1029/2001WR001101.

Wahyudi, I., Montillet, A., Khalifa, A.O.A., 2002. Darcy and post-Darcy flows within different sands. J. Hyd. Res. 4, 519-525.

Weast, R.C. (ed.), 1988-89. Handbook of Chemistry and Physics, 69th Edition. CRC Press Inc., Boca Raton, FL.

Wilke, C.R., Chang, P., 1955. Correlation of diffusion coefficients in dilute solutions. A.I.Ch.E. 1, 264-270.

Zheng, C., Wang, P.P., 1999. MT3DMS: A modular three-dimensional multispecies model for simulation of advection, dispersion and chemical reactions of contaminants in groundwater systems; documentation and user's guide. Contract Report SERDP-99-1, U.S. Army Engineer Research and Development Center, Vicksburg, MS.

Chapter 7

Three-dimensional Modelling of a Petroleum Hydrocarbon Contaminated Field Site in Western Australia [5]

Abstract. A three-dimensional analytical solution was used to determine longitudinal, transversal horizontal and transversal vertical dispersivities of non-reactive petroleum hydrocarbon compounds at a field site in Western Australia. These values were used to predict steady-state profiles and the plume length of a (reactive) toluene plume which, through data analyses, was demonstrated to be the major BTEX compound to be attenuated. Results demonstrate that this procedure yields accurate estimates of both non-reactive and reactive plume characteristics when compared to field measurements form a range of multi-port sampling devices located approximately along the centreline and transects of the plume. The length of the toluene plume was approximately 250 m, which corresponds well to previous analyses of the same field data. This article is an application-based study, and demonstrates the applicability of analytical modelling techniques to high resolution field-scale data is demonstrated, where some simplifying hydrogeochemical assumptions are valid. In this way, preliminary estimates of the natural attenuation capacity of contaminated aquifers at the field-scale can be easily and quickly obtained.

[5] Ham, P.A.S., Prommer, H.

7.1 Introduction

Mathematical modelling has become an increasingly important tool to assist in analysing natural attenuation and understanding environmental systems (Cirpka *et al.*, 1999; Mayer *et al.*, 2000; Prommer *et al.*, 2002). To this means, a range of analytical and numerical models exist, that when combined with field data, enable the prediction of the fate of contaminated groundwater plumes (Barry *et al.*, 2002). Of course both these modelling techniques have advantages and disadvantages. Typically, analytical models use simplifying assumptions about an environmental system in order to yield quick-to-implement explicit expressions to quantify fate and transport. For instance, under the assumptions of steady-state groundwater flow, isotropic and homogeneous hydraulic parameters, Ham *et al.* (2004) provide estimates of steady-state plume lengths for a two-dimensional continuous point source and solutes undergoing instantaneous fringe reaction. In comparison, numerical models are better suited to cases when geological conditions are highly heterogeneous, or the natural attenuation process involves complex chemical/biological interactions (Prommer *et al.*, 2002), however they generally require a deeper knowledge of the processes being modelled.

Analytical modelling is a useful technique to provide first estimates of plume characteristics (e.g. plume lengths, concentration profiles) and may act as a precursor to a more detailed numerical modelling exercise. Such models are therefore an important part in the formulation and assessment of an MNA framework (Lerner *et al.*, 2005). In this article, a modified version of the analytical model described by Ham *et al.* (2004) is applied to high resolution field-scale data to provide estimates of steady-state hydrocarbon plume lengths and plume characteristics. The application-based methodology described in the following sections, demonstrates how analytical models provide useful tools for engineers to make preliminary analysis of the attenuation capacity of contaminated aquifers.

7.2 Hydrogeology and Geochemistry of the Field Site

The field site is situated in the Metropolitan district of Perth, Western Australia, and forms part of the Bassendean Sand aquifer, comprising medium-fine grained bleached quartz sands. The aquifer is between $7m$ to $12m$ thick at the location in question and is underlain by a clay aquitard (Barber *et al.*, 1991; Davis *et al.*,

1999; Prommer *et al.*, 1999). The groundwater flow velocity is estimated to be between 100 and 170 m/yr, and seasonally the water table fluctuates by up to 1.8 m (Davis *et al.*, 1999; Prommer *et al.*, 1999).

A leaking underground fuel storage tank from a petrol station resulted in a contaminant plume, consisting of mainly BTEX compounds to develop in the underlying geological formation and groundwater. The development of this plume has been monitored periodically from 1991 until 1998 using up to 18 multilevel sampling (MLS) boreholes, and the data collected and analysed is the subject of previous papers by Thierrin *et al.* (1993), Davis *et al.* (1999) and Prommer *et al.* (1999). In the first paper by Davis *et al.* (1999), a detailed description of the contamination was presented and an analytical model was used to determine biodegradation rates of the BTEX compounds. The background geochemistry of the site was shown to be generally anaerobic with, in particular, very low nitrate concentrations (Gerritse *et al.*, 1990). Therefore, data analysis indicates that toluene degrades at the field site under sulphate reducing conditions, resulting in a quasi stationary toluene plume, whilst benzene does not appear to degrade or degrades very slowly.

Figure 7.1 shows contour plots for the benzene and toluene plumes resulting from concentration measurements at the site during August 1994 and August 1996, taken from Davis *et al.* (1999). The contours were constructed based upon the maximum concentrations measured at the sampling boreholes, i.e. a cross section of the plume in the vertical $z-$direction. The comparison between the contourplots for 1994 and 1996 demonstrate the approximate steady-state nature of the BTEX plume. Note also the location of the multi-port sampling boreholes. In 1994, there were 11 boreholes (MP1-MP12), located mainly along the length of the contaminant plume. MP10 was removed when the storage tank was excavated in 1991 but evidence would suggest that the source remained as entrapped NAPL close to the water table or the capillary zone which is seasonally inundated by the water table (Davis *et al.*, 1999). The BTEX concentrations at the source maybe therefore somewhat depleted in terms of the original estimates. By 1996 a further 6 multi-ports had been installed (MP13-MP19) in order to gain more detailed information across the width of the plume. In the work by Prommer *et al.* (1999), a two-dimensional numerical model was employed to investigate the role of ferric iron minerals as electron acceptors but in this case it was demonstrated that they are not important in terms of the aquifer's attenuation capacity. Both Davis *et*

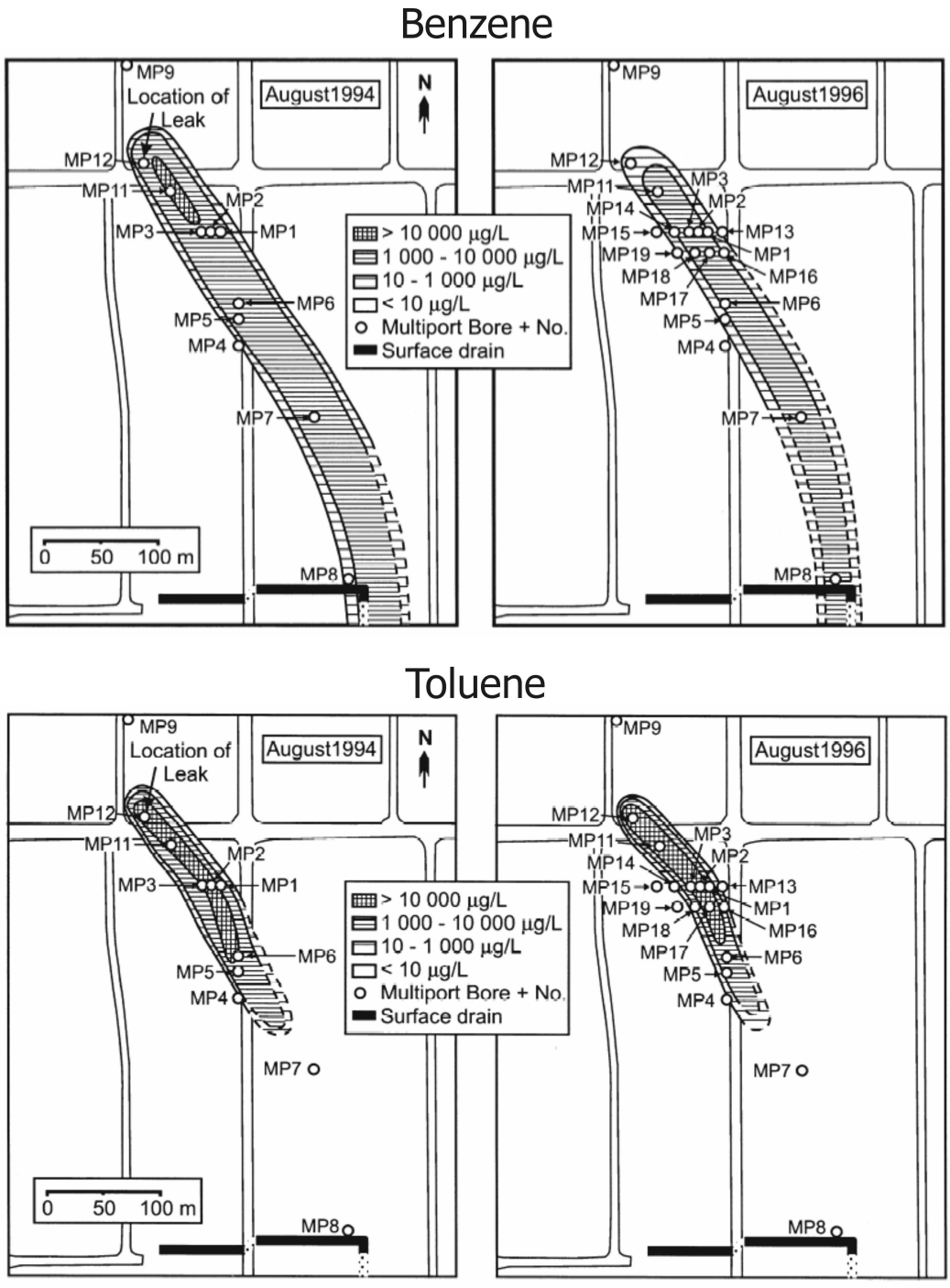

Figure 7.1: *Concentration contourplots of Benzene (top) and Toluene (below) for August 1994 and August 1996 determined from field measurements (Davis* et al.*, 1999).*

al. (1999) and Prommer *et al.* (1999) therefore suggest that sulphate provides the major part of the oxidation capacity of the uncontaminated aquifer, and therefore acts as the principle electron acceptor in the biodegradation of toluene at this site.

7.3 Modelling Approach

In this study, the analytical model presented by Ham *et al.* (2004) will be applied to the field study outlined above. The purpose of this is to demonstrate how simple engineering tools can be applied to field sites to obtain quick estimates of plume characteristics and the natural attenuation capacity of an aquifer. Of course, the unique hydrogeochemical situation of the field study considered here makes it an ideal test case and there maybe many examples where analytical modelling techniques are not applicable. In this study, the objective is to demonstrate how non-reactive data (benzene is chosen in this case) can be used to estimate reactive plume characteristics, i.e., the length and MP profiles of the toluene plume.

7.3.1 Assumptions

The basic modelling approach here is founded primarily on the assumption that the BTEX plume can be assumed quasi steady-state. The plume is termed quasi stationary because strong seasonal precipitation trends cause the BTEX plume to move up and down with the rising and falling of the water table and to move sideways due to changing flow directions, however field measurements have demonstrated that there is no significant change in species concentrations as a result. This is demonstrated in Figure 7.1, where it can be seen that data from August 1994 and August 1996 yield similar contourplots.

The concept of applying the analytical model is also based on the principal that non-reactive plume characteristics can be used to predict the migration of reactive plume species. The BTEX plume is therefore assumed to consist of non-reactive and reactive hydrocarbons. Benzene can be considered to behave as a conservative tracer, as there is no strong evidence to suggest depletion of this compounds due to biodegradation (Thierrin *et al.*, 1993; Prommer *et al.*, 1999). In contrast, toluene, ethylbenzene and xylene are assumed to be reactive compounds; degraded by sulphate and as such have definable plume lengths within the sampling boundaries of the field site. However, toluene concentrations at the source by far exceed those

of xylene and ethylbenzene and the sulphate reducing conditions favour toluene degradation over xylene and ethylbenzene. Therefore, in this case, biodegradation is only considered to occur between one electron acceptor (sulphate) and one electron donor (toluene). This reaction is assumed to be fast and as such can be considered instantaneous in nature.

Furthermore, it is assumed that boreholes MP12-11-3-6-7-8, are located approximately along the centreline of the BTEX plume; the source located close to MP12, whilst MP15-14-3-2-1-13 and MP19-18-17-16 form two horizontal transects across the plume width, 80 m and 100 m downstream of the source, respectively.

7.3.2 Solution method

A three-dimensional extension to the steady-state analytical solution presented by Ham *et al.* (2004) was developed. Following the same methodology outlined in that paper (Chapter 3 of this thesis), one easily obtains the non-reactive solution for the benzene plume, which takes the form

$$C_{benzene}(x,y,z,\infty) = \frac{F}{\sqrt{\beta\gamma}} e^{\frac{x}{2}} K_0 \left(\frac{1}{2} \sqrt{\left(x^2 + \frac{y^2}{\beta} + \frac{z^2}{\gamma} \right)} \right), \tag{7.1}$$

where

$$F = \frac{nC_0Q}{4\pi q_o {\alpha_l}^2}, \tag{7.2}$$

$C_{benzene}$ is the total aqueous concentration of benzene present in the domain, n is the porosity, C_0 is the initial benzene concentration, Q is the injection flow rate of benzene, q_0 is the average flow velocity, α_l, α_{th} and α_{tv} are the longitudinal and transverse horizontal and vertical dispersivities respectively and β and γ provide the ratios of α_{th} and α_{tv} to α_l. Equation (7.2) was used to fit the measured benzene concentration profiles along the centreline and transects of the plume, using data from August 1994 (Figure 7.2) and 1996 (Figure 7.3). This process involves a sensitivity analysis where α_l, α_{th} and α_{tv} are the primary variables to be fitted. The initial concentrations of benzene and toluene at the source was estimated from the profiles for MP12/11, which showed the highest BTEX and background electron acceptor concentration levels. Porosity and flow velocity was taken as 0.28 and 0.48 m/d (Davis *et al.*, 1999). The injection flow rate of benzene and

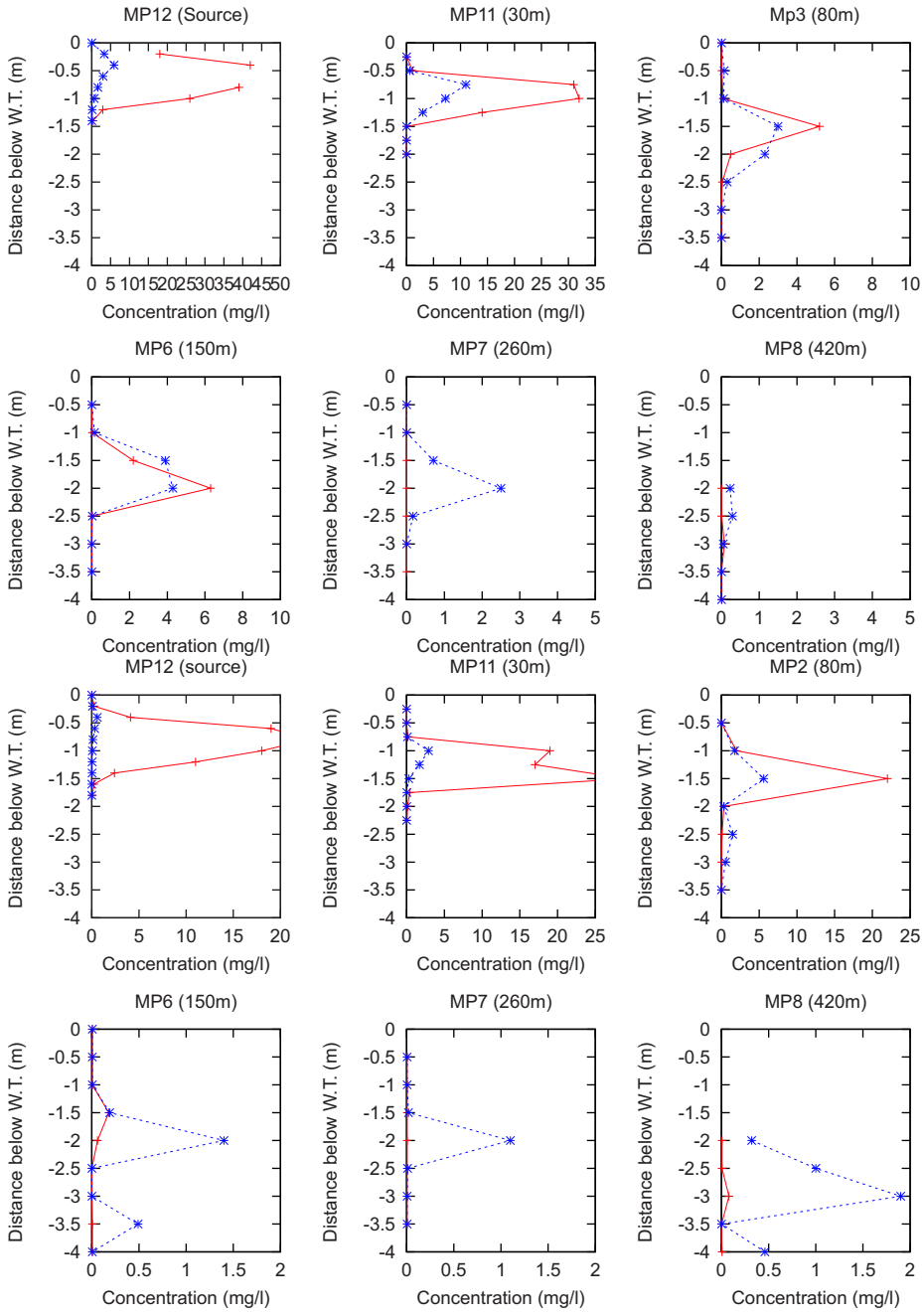

Figure 7.2: *Concentration profiles of benzene and toluene along the plume centreline for August 1994 (top) and for August 1996 (below). Dotted lines and full lines indicate the concentrations of benzene and toluene respectively, whilst the symbols indicate the sampling points.*

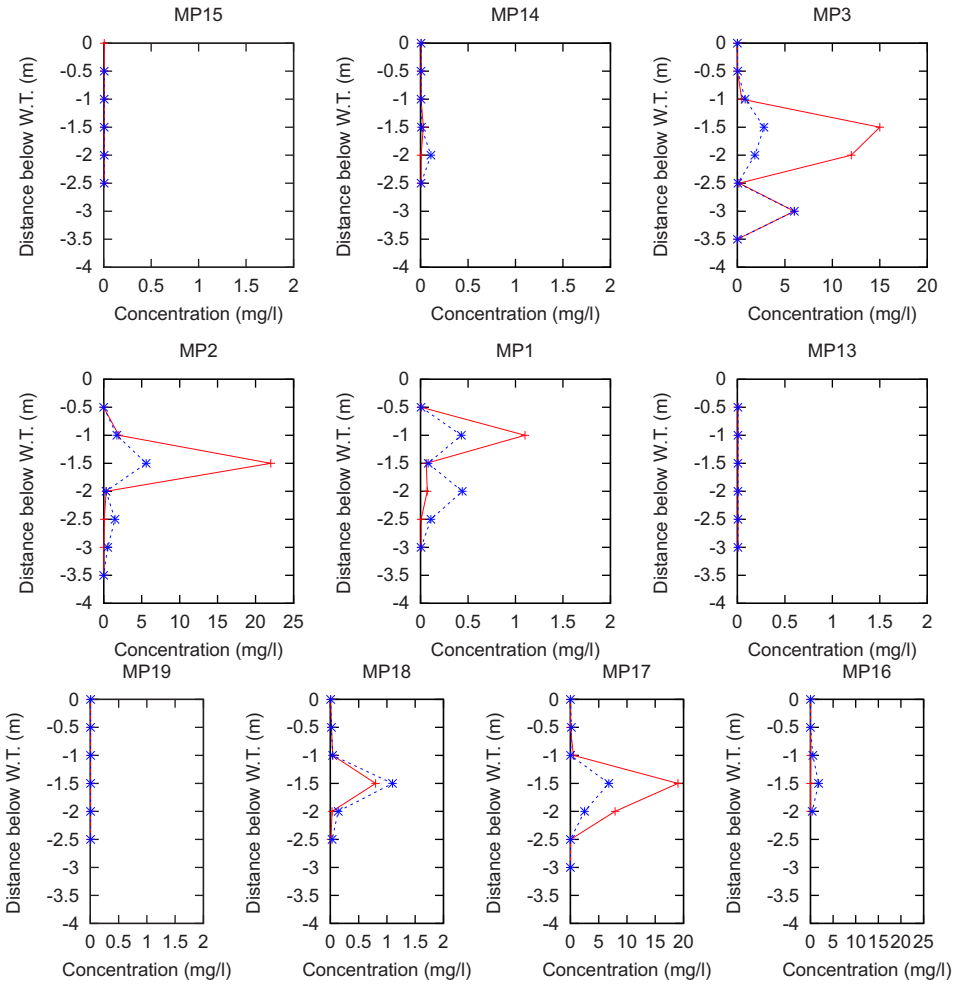

Figure 7.3: *Concentration profiles of benzene and toluene along the plume transects (80m and 100m downstream) for August 1996. Dotted lines and full lines indicate the concentrations of benzene and toluene respectively, whilst the symbols indicate the sampling points.*

toluene is equal to 0.48 m^3/d (see Ham *et al.* (2004)). Once a fit was achieved, the parameter values were applied to the case of the reactive toluene plume. The equation which describes toluene degradation under sulfate-reducing conditions (Davis *et al.*, 1999; Prommer *et al.*, 2002), is

$$C_7H_8 + 4.5{SO_4}^{2-} + 3H_2O + 2H^+ \rightarrow 7{HCO_3}^- + 4.5H_2S. \tag{7.3}$$

Equation (7.3) implies 4.5 moles of sulphate are required to degrade one mole of toluene. Note that equation (7.3) describes the stoichiometry of toluene and sulphate in moles, and when working in mg/l it is necessary to account for the molecular weights of the individual compounds. Therefore, the equation which expresses the concentration of toluene after reaction with sulphate reads

$$C_{toluene}(x,y,z,\infty) = \frac{F}{\sqrt{\beta\gamma}} e^{\frac{x}{2}} K_0 \left(\frac{1}{2} \sqrt{\left(x^2 + \frac{y^2}{\beta} + \frac{z^2}{\gamma} \right)} \right) - \frac{C_{sulphate}(x,y,z,\infty)}{4.5} \tag{7.4}$$

where $C_{sulphate}/4.5 = 28\ mg/l$. The maximum sulphate concentration at the source was taken from Prommer *et al.* (1999). The maximum plume length $L(x)$ of the toluene plume, located along the centreline, can then be calculated by solving

$$C_{toluene}(L(x),0,0,\infty) = \frac{F}{\sqrt{\beta\gamma}} e^{\frac{L(x)}{2}} K_0 \left(\frac{1}{2} \sqrt{\left(L(x)^2 + \frac{y^2}{\beta} + \frac{z^2}{\gamma} \right)} \right) - 28. \tag{7.5}$$

This yields a plume length and corresponding profiles, which were compared against measured data.

7.4 Results

7.4.1 Benzene plume

Equation (7.2) was used to fit the concentration profiles from the non-reactive BTEX compounds obtained from field measurements, using the centreline and transects of the plume, for August 1994 and 1996. The parameter values used in the model fitting can be found in Section 7.3.2. Through manual calibration, values for longitudinal, transverse horizontal and vertical dispersivity were determined. Preference was given to fitting the maximum concentrations obtained at

the multi-ports, with consideration of the values shown in Figure 7.2. Although it was assumed that the multi-ports were on the plume centreline, in reality this is unlikely. Therefore a fit was considered good if all the maximum concentrations at the multi-ports were equal to, or less than the predicted concentrations. The fitted dispersivity values were $\alpha_l = 1m$, $\alpha_t = 25cm$ and $\alpha_v = 2mm$. The benzene concentration at the source was assumed to be 11 mg/l (see profiles for MP11 in Figure 7.2), which indicates a reduction in the source concentrations in comparison with the original estimate of 36 mg/l (Davis *et al.*, 1999) prior to the removal of the storage tank in 1991. The resulting benzene plume is long and thin in shape and easily exceeds 420 m in length (where the farthest most multi-port sampling device was located). At this point, and based on the 10 $\mu g/l$ detection limit of the multi-port devices, the plume is approximately 75 m wide and 5 m in depth. Qualitatively speaking, this forms a good comparison to the data presented in Figures 7.1,7.2 & 7.3. Figure 7.4 and 7.5 show the change in calculated and measured concentrations along the centreline for both 1994 and 1996 and across the two transects of the plume in 1996 respectively. Note that all the measured benzene data are equal to or below the modelled values. In the case of the transects, the calculated plume was "shifted" slightly to better fit the measured data, which would indeed suggest that the multi-ports located along the plume centreline were not exactly located at the centre of the plume.

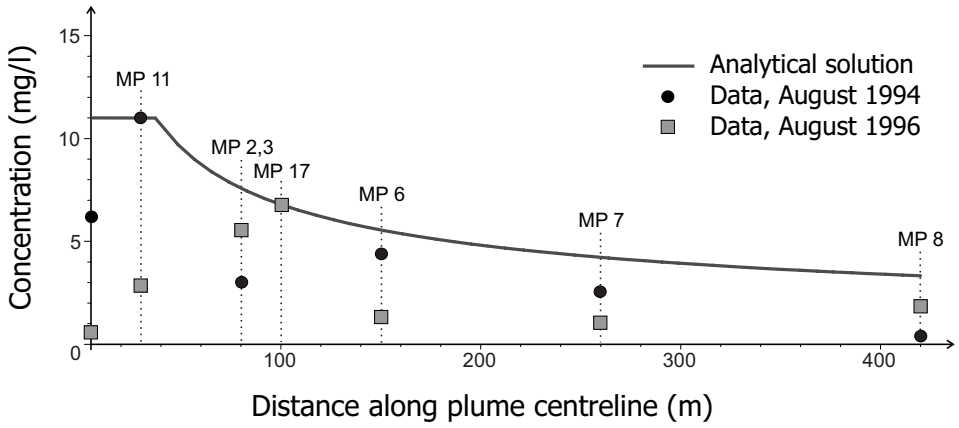

Figure 7.4: *Centreline concentrations for benzene as predicted by the model and data from August 1994 and 1996.*

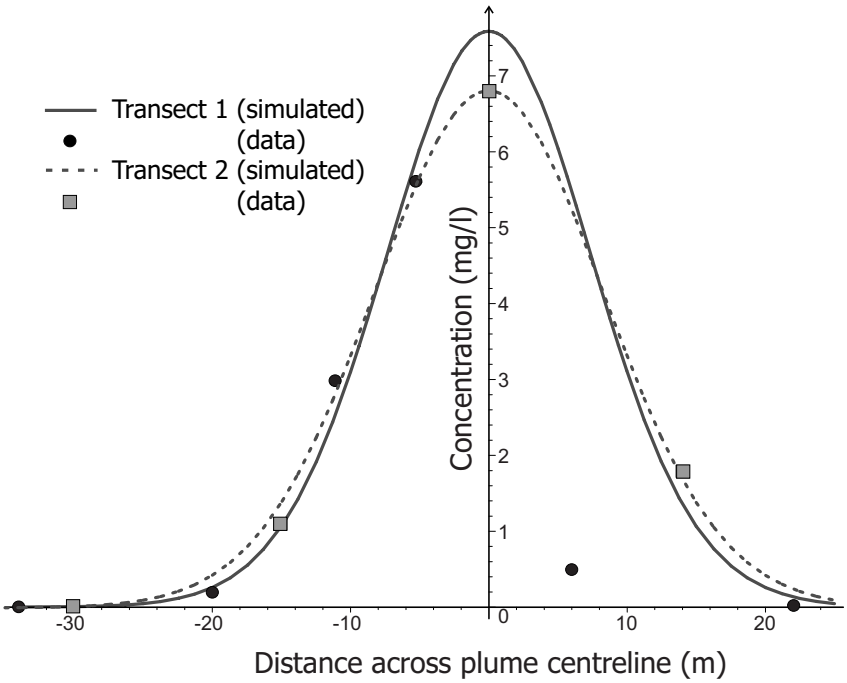

Figure 7.5: *Concentrations for benzene at transect 1 & 2 (80 and 100 m downstream of the source respectively) as predicted by the model and data from August 1994 and 1996.*

7.4.2 Toluene plume

The length of the reactive toluene plume, and the characteristics of that plume, were predicted from equation (7.5) and compared against measured data. The dispersivity values obtained from fitting the benzene plume data were applied and the initial concentration of toluene was taken as 70 mg/l, which can be determined from the profiles at MP12 in Figures 7.2 and 7.3 and is slightly less than the initial estimates prior to the removal of the storage tank. The solution to equation (7.5) yields a plume length of approximately 250 m, which would be within the range suggested by Davis *et al.* (1999). Again, the general shape and dimensions of the plume compared well with the original data analysis of Davis *et al.* (1999), as shown in Figures 7.1, 7.2 and 7.3. The toluene plume had a maximum width of approximately 20 m, and was no more than 1.5 m in depth. Figures 7.6 and 7.7 show the change in calculated and measured concentrations along the centreline for both 1994 and 1996 and across the two transects of the toluene plume in 1996 respectively. This comparison between the modelled and measured values appears to be generally good.

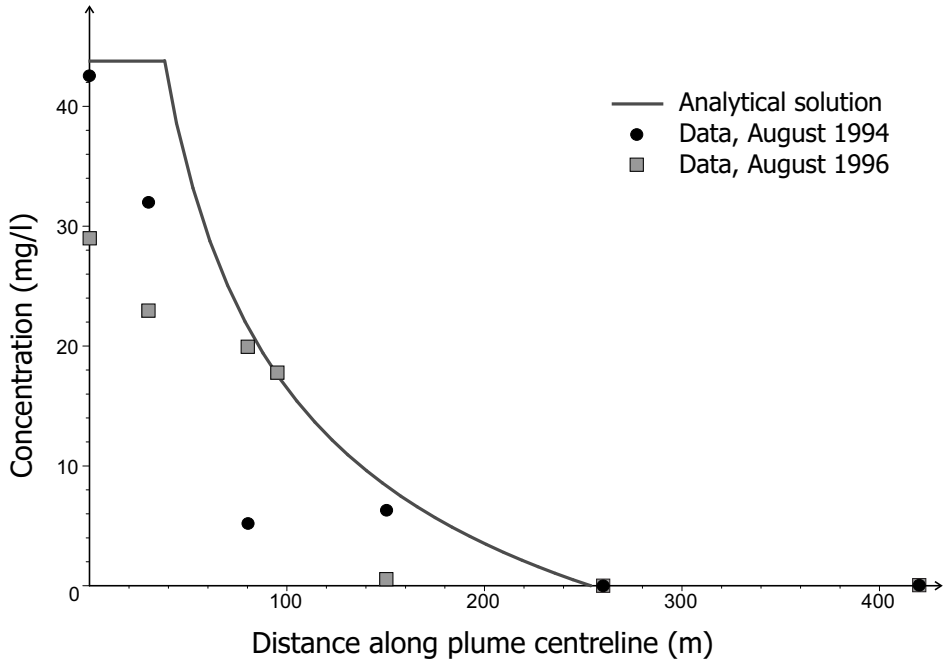

Figure 7.6: *Centreline concentrations for toluene as predicted by the model and data from August 1994 and 1996.*

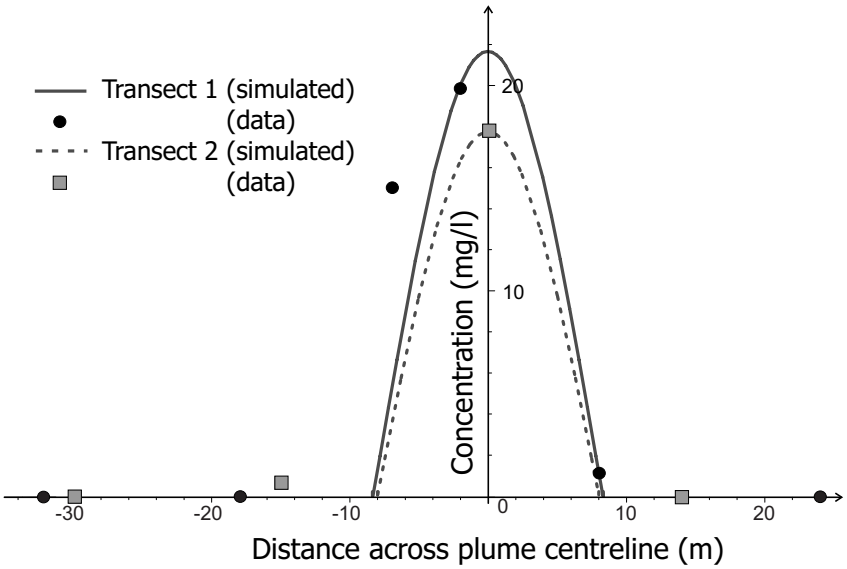

Figure 7.7: *Concentrations for toluene at transect 1 & 2 (80 and 100 m downstream of the source respectively) as predicted by the model and data from August 1994 and 1996.*

7.5 Discussion and Conclusions

The modelling approach used in this study demonstrates how a simple analytical model can be applied to a case of field-scale natural attenuation. In this article, data from a well defined site located in the Metropolitan borough of Perth, Western Australia, was chosen as a test case where a hydrocarbon groundwater plume, consisting of BTEX compounds leaked from an underground fuel storage tank. Previous studies analysed data from up to 18 multi-port sampling devices located across the length and breadth of the plume. There was no evidence to suggest that benzene was biodegrading and concentrations above acceptable levels were detected at all multi-ports along the length of the field site. Toluene however was observed to degrade where the principle electron acceptor was sulphate, and measurements over time suggested that a quasi stationary finite plume developed of around 250 m in length.

A three-dimensional extension of the analytical model developed by Ham *et al.* (2004) was applied to the field data. The modelling approach was based on the assumption that the reaction between toluene and sulphate could be considered instantaneous, and therefore the data from the conservative hydrocarbon

compounds could be used to predict the characteristics of the reactive toluene plume. Centreline benzene concentrations obtained from 6 multi-port devices in August 1994 and 1996, along with data obtained from 9 multi-ports which formed two plume transects in August 1996, were used to derive values for longitudinal, transversal horizontal and transversal vertical dispersivity. These values were $\alpha_l = 1m$, $\alpha_t = 25cm$ and $\alpha_v = 2mm$. Due to the large volume of high resolution data, the fitting procedure adopted assumed that measured concentrations could not exceed those predicted by the analytical model, which may not be valid at other field sites. In turn, the profiles for the toluene plume were calculated based using the dispersivity values for the benzene plume. Both concentrations along the plume centreline and transects could be well predicted, and the length of the toluene plume was calculated to be approximately 250 m, which is in good agreement with previous studies using the same data. The reader should note that the transversal dispersivities obtained by this method are average values which appear to reproduce field data measurements well, however these values may not accurately reflect local scale dispersion mechanisms.

This article demonstrates that cases of field-scale attenuation can be accurately predicted using the analytical approach developed by Ham *et al.* (2004). In the field case used in this study, the hydrology of the site was relatively simple, i.e., it was assumed that flow was steady and uniform. Moreover, the geochemistry of the hydrocarbon plume in question was also straightforward, i.e., one electron acceptor (sulphate) and one electron donor (toluene). However, it is possible to extend this approach to consider multiple electron acceptors and donors, using electron balances (e.g. Thornton *et al.* (2001a); Gutierrez-Neri *et al.* (in preparation)), so long as reactions can be considered to be instantaneous. Where these assumptions are not realistic then an analytical solution is unlikely to accurately predict actual plume characteristics and a more suitable model capable of simulating complex hydrogeochemistry should be applied. However, where these assumptions can be made, the analytical solution demonstrated through this application provides a straight forward engineering tool for preliminary estimates of the natural attenuation capacity of aquifers.

Bibliography

Barber, C., Davis, G.B., Thierrin, J., Bates, L., Patterson, B.M., Pribac, F., Gibbs, R., Power, T.R., Briegel, D., Lambert, M., Hosking, J., 1991. Final report for project on "Assessment of the impact of pollutants on groundwater beneath urban areas", July 1989 to June 1991. Technical refort, CSIRO Division of Water Resources.

Barry, D.A., Prommer, H., Miller, C.T., Engesgaard, P., Zheng, C., 2002. Modelling the fate of oxidizable organic contaminants in groundwater. Adv. Water Resources, 25, 899-937.

Cirpka, O.A., Frind, E.O., Helmig, R., 1999. Numerical simulation of biodegradation controlled by transverse mixing. J. Contam. Hydrol. 40, 159-182.

Davis, G.B., Barber, C., Power, T.R., Thierrin, J., Patterson, B.M., Rayner, J., Wu, Q., 1999. The variability and intrinsic remediation of a BTEX plume in anaerobic sulphate-rich groundwater. J. Contam. Hydrol. 36, 265-290.

Gerritse, R.G., Barber, C., Aderney, J.A., 1990. The impact of residential urban areas on groundwater quality: Swan Coastal Plain, Western Australia. Technical report CSIRO, Water Resources Series.

Gutierrez-Neri, M., Ham, P.A.S., Schotting, R.J., Lerner, D.L. Analytical modelling of fringe and core biodegradation in groundwater plumes. Article in preparation for submission to Ground Water.

Ham, P.A.S., Schotting, R.J., Prommer, H, Davis, G.B., 2004. Effects of hydrodynamic dispersion on plume lengths for instantaneous bimolecular reactions. Adv. Water Resour. Res. 27, 803-813.

Mayer, K.U., Benner, S.G., Frind, E.O., Thornton, S.F., Lerner, D.N., 2001. Reactive transport modelling of processes controlling the distribution and natural attenuation of phenolic compounds in a deep sandstone aquifer. J. Contam. Hydrol. 53, 341368.

Prommer, H., Davis, G.B., Barry, D.A., 1999. Geochemical changes during biodegradation of petroleum hydrocarbons: field investigations and biogeochemical modelling. Organic Geochemistry 30, 423-435.

Prommer, H., Davis, G.B., Barry, D.A., 2002. Modelling of physical and reactive processes during biodegradation of a hydrocarbon plume under transient groundwater flow conditions. J. Cont. Hydrol., 59, 113-131.

Lerner, D.N., Bjerg, P., Daterl, J., Gargini, A., Gratwohl, O., Hollinger, C., Morgan, P., Ptak, T., Schotting, R., Slenders, H., Thornton, S.F., 2005. CORONA - Confidence in forecasting of natural attenuation as a risk-based groundwater remediation strategy, Final report of the EU research project EVK1-2001-00087. University of Sheffield, UK. pages. Available from www.shef.ac.uk/corona.

Thierrin, J., Davis, G.B., Barber, C., Patterson, B.M., Pribac, F., Power, T.R., Lambert, M., 1993. Natural degradation rates of BTEX compounds and naphthalene in a sulphate reducing groundwater environment. Hydrol. Sci. J. 38(4), 309-322.

Thornton, S.F., Lerner, D.N. and Banwart, S.A., 2001a. Assessing the natural attenuation of organic contaminants in aquifers using plume-scale electron and carbon balances: model development with analysis of uncertainty and parameter sensitivity. J. Contam. Hydrol. 53, 199-232.

Summary

In many cases concerning natural attenuation, hydrodynamic transversal dispersion is the most important mechanism leading to the successful remediation of contaminated groundwater plumes. This is because transversal mixing controls the flux of electron acceptors, or growth limiting nutrients across the plume fringe. This thesis strengthens current knowledge and adds valuable insights into the interplay between transversal mixing and biological processes, which occur in the transition zone between fresh and polluted groundwater.

Following the Introduction in **Chapter 1**, **Chapter 2** reviewed the general theory behind the subject of this thesis, focussing on the relevance of hydrodynamic transversal dispersivity on controlling contaminated groundwater plumes. The origins of popular diffusion and dispersion theory were discussed, with an emphasis on reactive mixing and the importance of the scale effects on dispersion processes.

Chapter 3 used analytical techniques to explore the effects of longitudinal and transversal dispersivity on lengths of contaminant plumes where an instantaneous reaction occurs between two mixing solutes. A new two-dimensional analytical solution was presented to determine steady-state plume lengths and concentration distributions of two mixing solutes. It was demonstrated that in practical engineering limits, an approximation to this solution, resulting in an algebraic expression can be satisfactorily used to determine stationary plume lengths. This expression is dependent on a number of hydrogeological coefficients including transversal dispersivity but excluding longitudinal dispersivity, which as other researchers have previously suggested, conclusively proves that longitudinal dispersivity has no influence on the development of steady-state contaminant plumes. Using a numerical solution to the transient equation, it was demonstrated that longitudinal dispersion controls the transient plume behavior. If longitudinal dispersivity is much bigger than transversal dispersivity, then the time taken to reach steady-state plume development increases dramatically. The effects of sorption, solute stoichiometries

and transient behavior on plume development were also addressed.

Chapter 4 extended the analytical approach presented in the previous chapter to include core degradation processes along with reactions occurring at the plume fringe. Through the use of a well documented field study, it was demonstrated that the use of a 'combined' fringe-core degradation model is necessary to quantify plume lengths, where degradation is controlled not only by aerobic fringe reactions between electron donors and acceptors but also where anaerobic core degradation of an electron donor occurs. Moreover, a general framework for the application of analytical solutions to aid monitored natural attenuation studies was presented.

Chapter 5 further extended the findings in Chapter 3, this time to the case when reactions between mixing solutes are kinetically controlled. Three enhanced remediation scenarios, which are of practical importance, were considered. Mathematically, this problem pertains to a system of three coupled nonlinear partial differential equations (PDEs). A rigorous analysis showed, for the time-dependent cases, that these three PDEs can be reduced to an auxiliary linear PDE, which can be solved explicitly and used to recast the initial equations into two coupled PDEs. For the stationary cases, the problem reduces further to a single PDE in terms of one of the dependent variables only. In all cases, a numerical solution of the problem is required. This numerical model can be used to demonstrate the effects of microbial activity on the size of the fringe of a contaminant plume, where biological reactions between contaminant and electron acceptor take place. It was concluded that apparent transversal dispersion coefficients, which describe only the gradient of the plume fringe between EA and ED, can be much smaller than the effective dispersion coefficients used to predict the overall spreading of a groundwater plume.

In **Chapter 6** a model-based analysis (pure forward modelling) of laboratory scale experiments was presented. Non-reactive transport of conservative tracers and reactive transport of hydrochloric acid and sodium hydroxide in a homogeneous porous media for a range of flow velocities and grain sizes were considered. A new empirical formula to calculate apparent transversal dispersion coefficients, based upon conservative (tracer) laboratory experiments, was used in conjunction with an effective diffusion coefficient obtained from a Stokes-Einstein style equation as input parameters for the reactive modelling. This empirical formula suggests that at high velocities diffusion at the pore scale is too slow to allow complete mixing. Using this method it was possible to quantify the controlling effects

of hydrodynamic transversal dispersion and of effective molecular diffusion on the progress of the hydrolysis reactions at the plume fringes and therefore on plume length, which is otherwise impossible using classical descriptions of the transversal dispersion tensor.

Chapter 7 addressed a field-scale remediation problem at a former petrol station in Perth, Western Australia. A three-dimensional extension to the model presented in Chapter 3 was used to analyse the biodegradation of toluene hydrocarbons. Field data from 12 multi-port sampling devices was used to determine longitudinal and transversal (horizontal and vertical) dispersivities from data for the non-reactive benzene compound. In turn, these values were used to make predictions of the plume length and other plume characteristics for the reactive toluene compound. Concentration profiles of benzene and toluene along the centreline and transects of the plume correspond well with earlier data analyses. This modelling exercise demonstrated that, where high-resolution data is available, simple analytical models can be applied to give estimates of the natural attenuation capacity of aquifers, even at the field-scale.

Concluding Remarks

The findings of this thesis were made using mathematical techniques to study reactive solute transport in porous media and demonstrate ways in which reactive mixing processes can be determined from conservative plume characteristics. The ability to predict reactive mixing based on conservative quantities is important because often, as is certainly the case in experimental and field-scale analyses, conservative solute transport is easier to describe and parameterise than cases where reactions occur. Of course, some of these techniques are not without controversy and the results of this thesis do not provide the reader with one generic tool which is valid to access all cases where natural attenuation takes place.

The analytical solution presented in Chapter 3 (which was extended in Chapter 4) and applied in Chapter 7 proves conclusively that transversal, and not longitudinal, dispersion is the controlling dispersion mechanism in cases of natural attenuation. The methodology is based on a number of limiting assumptions. Most important is the fact that the resulting equations are only valid for the stationary case and where reactions between mixing solutes can be assumed instantaneous. In this way, it must be the responsibility of the reader to determine whether or not

these equations can adequately represent mixing processes at the site in question. In cases where reactions are kinetically controlled, then the numerical techniques presented in Chapter 5 may provide an elegant alternative to analyse reactive solute mixing.

However, Chapter 5 also raises an interesting question relating to the values of apparent and effective dispersivities. At large time scales the plume fringe becomes very narrow, resulting in steep concentration gradients between electron acceptors and donors. These gradients can be represented by values of apparent transversal dispersivity which are much smaller than the effective values needed to describe overall plume dispersion. In this way, apparent dispersivities decrease as a result of biodegradation processes, which is not unrealistic given that biological activity competes against dispersion to control plume spreading. Understanding the relationship between apparent and effective values is important, since failure to do so can result in incorrect predictions of the natural attenuation capacity of an aquifer. For example, using concentration measurements across a plume fringe to obtain dispersivities may not be sufficient to model the complete migration of a contaminant plume.

Most controversially, Chapter 6 considers modelling studies of laboratory experiments, which suggest that transversal dispersivity is dependent not only on the grain size of the porous medium but also on the average linear velocity. This outcome challenges the classical description of the transversal dispersion tensor and may confuse the reader when not put in context. At high flow rates that might be of more significance to some enhanced remediation strategies, transversal dispersivity is velocity dependent. This implies that there is incomplete solute mixing and as a result, transversal dispersivity decreases with velocity. At lower flow rates, which more closely reflect natural groundwater movement, this effect is much less pronounced so there is less deviation between dispersivity values obtained from classical and non-classical descriptions of the dispersion tensor.

The methodologies presented in this thesis further current scientific knowledge of transverse dispersion mechanisms. However, they are not only of importance in terms of scientific research but, as was demonstrated through application-based studies, can also provide some useful tools to engineers for the assessment of groundwater remediation.

Philip A.S. Ham

Samenvatting

Transversale dispersie is, als het om natuurlijke afbraak gaat, in veel gevallen het belangrijkste mechanisme dat beschouwd moet worden bij een succesvolle behandeling van verontreinigd grondwater. Transversaal mengen bepaalt namelijk de stroming van elektronacceptors, ofwel de groeiremmende nutriënten langs de rand van de verontreinigingspluim. Dit proefschrift levert een waardevolle bijdrage aan inzichten op het snijvlak van transversale menging en biologische processen die optreden in de overgangszone tussen zoet en verontreinigd grondwater, en bovendien wordt bestaande kennis verdiept.

Na de introductie in hoofdstuk 1, is in hoofdstuk 2 een review gegeven van de algemene theorie betreffende het onderwerp van dit proefschrift, waarbij de nadruk ligt op de rol van de transversale dispersiviteit bij het beheersen van verontreinigingspluimen. De oorsprong van algemene diffusie-en-dispersietheorie is behandeld, waar vooral aandacht is geweest voor reactieve menging en het belang van schaaleffecten bij dispersieprocessen.

In hoofdstuk 3 zijn analytische technieken gebruikt om het effect te bestuderen van zowel longitudinale als transversale dispersieparameters op de lengte van een pluim waarbij een instantane reactie optreedt tussen twee mengstoffen. Een nieuwe tweedimensionale analytische oplossing is gepresenteerd waarmee stationaire pluimlengtes en concentratieverdelingen van twee mengstoffen bepaald kunnen worden. Een benadering van deze oplossing kan in praktische toepassingen goed gebruikt worden om pluimlengtes te bepalen. De vergelijking van deze benadering hangt van een aantal hydrogeologische coëfficiënten af, waaronder de transversale dispersiviteit, maar meestal niet van de longitudinale dispersiviteit, hetgeen door andere onderzoekers is aangegrepen om te stellen dat de longitudinale dispersiviteit geen invloed heeft op de ontwikkeling van stationaire verontreinigingspluimen. Gebruikmakend van een numerieke oplossing van de tijdsafhankelijke vergelijking, is aangetoond dat juist longitudinale dispersie het gedrag van de pluim bepaalt.

Als longitudinale dispersiviteit veel groter wordt genomen dan transversale dispersiviteit, dan neemt de tijd, benodigd voor de ontwikkeling van een pluim, om een stationaire toestand te bereiken, enorm toe. In dit hoofdstuk zijn tevens effecten als sorptie, de stoichiometrieën van de opgeloste stoffen en tijdsafhankelijk pluimgedrag bestudeerd.

De analytische benadering van het voorafgaande is in hoofdstuk 4 uitgebreid naar afbraakprocessen in het centrum en aan de rand van de pluim. Door middel van een goed gedocumenteerde veldstudie is aangetoond dat het noodzakelijk is een gecombineerd rand-centrum afbraakmodel te gebruiken om pluimlengtes te bepalen, waarbij de afbraak niet alleen door aërobische randreacties tussen elektrondonors-en-acceptors wordt bepaald, maar ook op plaatsen waar anaërobische dispersie van de pluimkern van een elektrondonor plaatsvindt. Bovendien wordt in dit hoofdstuk een algemeen raamwerk gegeven voor de toepassing van analytische oplossingen die gebruikt kunnen worden bij studies naar gecontroleerde natuurlijke afbraak.

Ook in hoofdstuk 5 worden de bevindingen van hoofdstuk 3 verder uitgewerkt, in dit geval waar het de kinetisch gecontroleerde reacties tussen de mengoplossingen betreft. Drie saneringsscenario's zijn behandeld, die van praktisch belang zijn. Wiskundig gezien vertaalt dit probleem zich in een stelsel van drie gekoppelde niet-lineaire partiële differentiaalvergelijkingen. Een rigoureuze analyse laat zien dat, voor de tijdsafhankelijke gevallen, het stelsel gereduceerd kan worden tot één lineaire partiële differentiaalvergelijking, die in expliciete termen opgelost kan worden en vervolgens gebruikt kan worden om de oorspronkelijke vergelijkingen om te zetten in twee gekoppelde differentiaalvergelijkingen. Voor de stationaire gevallen wordt het probleem gereduceerd tot één enkele differentiaalvergelijking die slechts afhankelijk is van één van de variabelen. Overigens is in alle gevallen een numerieke oplossing nodig. Dit numerieke model kan gebruikt worden om de effecten te laten zien van bacteriologische activiteit op de grootte van de overgangszone van een verontreinigingspluim, waar biologische reacties tussen de verontreinigde stof en de elektronacceptor plaatsvinden. Er is vastgesteld dat de schijnbare transversale dispersiecoëfficiënt, die slechts de gradiënt van de overgangszone tussen elektronacceptor-en-donor beschrijft, veel kleiner kan zijn dan de effectieve dispersiecoëfficiënten die de totale spreiding van een grondwaterpluim voorspellen.

In hoofdstuk 6 wordt een analyse op modelbasis gegeven van schaalexperi-

menten in een laboratorium. Niet-reactief transport van conservatieve tracers en reactief transport van zoutzuur en natriumhydroxide in een homogeen poreus medium voor verschillende stromingssnelheden en korrelgroottes zijn behandeld. Een nieuwe empirische uitdrukking om schijnbare transversale dispersiecoëfficiënten, gebaseerd op laboratoriumexperimenten aan conservatieve tracers, te berekenen, is gepresenteerd. Deze formule is samen met een effectieve diffusiecoëfficiënt - verkregen met een Stokes-Einsteinachtige vergelijking - gebruikt als input voor het reactieve model. De vorm van de empirische formule lijkt te suggereren dat voor hoge snelheden, diffusie op de porieschaal te langzaam is om voor complete menging te zorgen. Met deze methode is het mogelijk gebleken om de effecten van transversale dispersie en effectieve moleculaire diffusie op de hydrolysereacties aan de pluimrand te kwantificeren, en daarmee de invloed op de pluimlengte, hetgeen anders onmogelijk is, gebruikmakend van klassieke beschrijvingen van de transversale dispersietensor.

Hoofdstuk 7 behandelt een saneringsprobleem bij een voormalig benzinestation in Perth, in het westen van Australië. Een driedimensionale uitbreiding van het model, zoals dat in hoofdstuk 3 is gepresenteerd, is gebruikt om de biologische afbraak van tolueen te analyseren. Data van veldexperimenten zijn gebruikt om longitudinale en transversale dispersiviteiten te bepalen uit gegevens voor het niet-reactieve benzeen. Deze data op hun beurt, zijn gebruikt om lengte en andere karakteristieke eigenschappen van de pluim te voorspellen. Concentratieprofielen van benzeen en tolueen in de lengte-en-breedterichting van de pluim komen goed overeen met resultaten van eerdere data-analyses. Deze modeloefening demonstreert dat, wanneer gedetailleerde data beschikbaar zijn, eenvoudige analytische modellen gebruikt kunnen worden om schattingen te geven van de natuurlijke afbraakcapaciteit van aquifers, zelfs op de veldschaal.

De uitkomsten van dit proefschrift zijn verkregen met wiskundige technieken om reactief transport van opgeloste stoffen in poreuze media te bestuderen en om de manieren te laten zien hoe eigenschappen van reactieve mengprocessen bepaald kunnen worden met behulp van pluimkarakteristieken. Deze methodologieën zijn niet alleen van belang vanuit het oogpunt van wetenschappelijk onderzoek, maar, zoals is gedemonstreerd met toepassingsgerichte voorbeelden, ze bieden ook enkele, zeer nuttige hulpmiddelen voor ingenieurs bij aquifersanering.

Philip A.S. Ham

Curriculum Vitae

Philip A.S. Ham was born on the 27th October, 1978 in Rochdale, United Kingdom. He attended Bacup and Rawtenstall Grammar School until 1997, before perusing further education at The University of Edinburgh. In June 2001, after earlier completing his Master's thesis on the subject of natural attenuation of hydrocarbon plumes, he graduated with an MEng (1:1) in Civil and Environmental Engineering. In October of the same year he moved to The Netherlands to take up the position of PhD research assistant on an NWO funded project entitled 'Mixing Processes in Enhanced and Natural Attenuation'. He spent the first two years as a member of the Hydrology and Ecology Group, Faculty of Civil Engineering and Technical Geosciences at Delft University of Technology. However, after the relocation of the research group to which he was attached, his PhD research was completed in March 2006 at the Environmental Hydrogeology research group, Faculty of Earthsciences at the University of Utrecht. This thesis is a testament to those years of scientific research.

Dankwoord

De laatste vier jaar van mijn leven zijn tot nu toe de meest plezierige jaren van mijn leven geweest en, wetenschappelijk gezien, ook de meest inspirerende. Vandaar dat ik een aantal mensen graag nog even op deze plek willen bedanken.

Mijn co-promotor, Ruud. Jij hebt mij vanaf het begin gestimuleerd. Zonder jouw steun had ik nooit kunnen promoveren. Bovendien ben jij een goede vriend geworden. Dit laatste geldt ook voor je vrouw Kitty, natuurlijk. Ik denk met veel plezier terug aan de talloze avonden in Rotterdam - de beste stad ter wereld! - die ik met plezier in jullie gezelschap heb doorgebracht. Majid, mijn promotor, hartelijk bedankt. Jouw kritische blik heeft altijd vruchtbare discussies opgeleverd. Henning, you have always been an 'unofficial' supervisor and I know I'll never be able to compensate you for all your input and communications over the years. Many thanks for my extended summers in Perth, especially the Ricard evenings! David Lerner, Peter Grathwohl, Asa Olsson, Greg Davis, many thanks for your consistent interest and contributions to my research. Cas Berentsen - wat jij niet van MATLAB weet, wil je eigenlijk niet weten! Mariene - por añadirle toda una nueva dimensión a mi trabajo.

En laat ik ook de rest van mijn collega's niet vergeten die ik de afgelopen vier jaar heb leren kennen! 'The one and only' Sam. Na slechts vier weken in Nederland had je mij al de tekst van "Oh Oh Den Haag" geleerd. Dat was toen al een slechte teken! Nipje...? En ook natuurlijk Birgitta, Anke Jannie, Johan (a.k.a. Crapstanzo), Bert-Rik, Saeed, Marian, Simona, Henk, Roberta & Ueli, met wie ik veel heb meegemaakt de laatste jaren. Allemaal ken ik jullie als directe collega's, sommigen als medereizigers naar verschillende conferenties en workshops en de meesten beschouw ik ook als vrienden.

Natuurlijk was dit project nooit mogelijk geweest zonder de financiële steun van NWO en het zeer gewaardeerde inhoudelijk advies van de commissieleden van TRIAS. Onder andere wil ik graag Helenius Rogaar, Theo Saat, Peter Raats,

Timo Heimovaara en Toon Leijnse bedanken voor hun interesse en betrokkenheid bij mijn onderzoek.

I should also like to mention my family for their support, especially my parents. Lesley, you have provided me with an education, in the broadest sense, to which I owe you a debt of gratitude. Dave, you have given me the character which enables me to see opportunities where others see none. Thank you.

En verder wil ik natuurlijk alle (zomer)bewoners van de Westbroekse Binnenweg 10 bedanken! Jullie zijn inmiddels bijna familie geworden! Ik heb ruim twee jaar echt met en van jullie genoten, vooral s'avonds, buiten met een drankje (vaak werd het een fles!). Jullie vragen altijd hoe het met "het grondwater gaat". Ik moet eerlijk zeggen: ik heb echt geen flauw idee... maar het water is heerlijk, vooral eind augustus om een uur of twee s'avonds en zonder kleren! Allemaal bedankt en graag tot gauw.